Investigation of the role of microRNAs in Spinocerebellar Ataxia type 3

Dissertation

zur

Erlangung des Doktorgrades (Dr. rer. nat.)

der

Mathematisch-Naturwissenschaftlichen Fakultät

der

Rheinischen Friedrich-Wilhelms-Universität Bonn

vorgelegt von

Rohit Nalavade

aus

Pune, Indien

Bonn, 2015

Angefertigt mit Genehmigung der Mathematisch-Naturwissenschaftlichen Fakultät der
Rheinischen Friedrich-Wilhelms-Universität Bonn

1. Gutachter: PD Dr. Bernd Evert

2. Gutachter: Prof. Dr. Jörg Höhfeld

Tag der Promotion: 20.10.2015

Erscheinungsjahr: 2015

Declaration

I hereby confirm that this dissertation is my own work. It was written independently without the help of aid unless stated otherwise. Any concepts, data taken from other sources have been indicated as such. This work has never before been submitted to any University. I have not applied for a Doctoral procedure before.

An Eides statt versichere ich, dass die vorgelegte Arbeit - abgesehen von den ausdrücklich bezeichneten Hilfsmitteln - persönlich, selbständig und ohne Benutzung anderer als der angegebenen Hilfsmittel angefertigt wurde, die aus anderen Quellen direkt oder indirekt übernommenen Daten und Konzepte unter Angabe der Quelle kenntlich gemacht sind, die vorgelegte Arbeit oder ähnliche Arbeiten nicht bereits anderweitig als Dissertation eingereicht worden ist bzw. sind, kein früherer Promotionsversuch unternommen worden ist, für die inhaltlich-materielle Erstellung der vorgelegten Arbeit keine fremde Hilfe, insbesondere keine entgeltliche Hilfe von Vermittlungs- bzw. Beratungsdiensten (Promotionsberater oder andere Personen) in Anspruch genommen wurde sowie keinerlei Dritte vom Doktoranden unmittelbar oder mittelbar geldwerte Leistungen für Tätigkeiten erhalten haben, die im Zusammenhang mit dem Inhalt der vorgelegten Arbeit stehen.

Ort, Datum Unterschrift

Acknowledgements

This thesis would not have been possible without the support and help of several people. First and foremost I want to thank my two supervisors PD Dr. Bernd Evert and Dr. Sybille Krauss for giving me the opportunity to work in their laboratories. It was great working with both of them and I really learnt a lot about science and also outside science from them. Both always had time for discussions regarding experiments and advice on the way forward. They trusted me and were always patient with me. I would like to thank Prof. Höhfeld for consenting to be my second referee and Prof. Haas and PD Dr. Eichert for agreeing to be part of my thesis committee. Also, I would like to thank Prof. Nicotera for creating an ideal research environment with great infrastructure at DZNE Bonn.

I would like to thank my lab mates for their constant support, help and for making our lab such a fun place to work. Thanks to Stephanie, who from my first day in the lab has always helped me and taught me several techniques. A special thanks to Frank for teaching me mouse related techniques and along with Nadine and Judith for the discussions and tips during progress reports. Separate thanks to Nadine for ferrying me back to the lab after our journal clubs. Also, I would like to thank our collaborators in the Institute of Reconstructive Neurobiology, especially Dr. Michael Peitz and Johannes Jungverdorben for providing me material for experiments and Dr. Stefan Bonn at DZNE, Göttingen for conducting the gene and miRNA expression profiles. I also worked on occasions closely with other labs and facilities in DZNE and hence thanks to members of the work groups Jackson, Tamguney, Fuhrmann, Bano, Fava who helped me with the use of equipment in their labs. I would like to thank Clemens, Melvin and Devon for their help with analysis of profiling data, Kevin for help with the microscope, Julia for her guidance with mouse related work and Christoph for his help with the microscopy images. I really appreciate the help provided by Nancy with administrative issues and the IT Dept. for IT support. I would also like to thank Dr. Peter Breuer and other members of the Neurobiology workgroup in the University clinic Bonn for their help. I would like to thank my parents who constantly supported me although I was half a globe away from them. Finally I would like to thank Tulika for always being there for me. Being a biologist herself, she was able to understand the ups and downs of lab life and was always at hand to help me through difficult times.

Summary

Spinocerebellar Ataxia Type 3 (SCA3) is an inherited, neurodegenerative disorder belonging to the group of polyglutamine repeat disorders. It is caused by CAG repeat expansions in the *ATXN3* gene leading to expanded polyglutamine repeats in the ATXN3 protein. The expanded ATXN3 protein forms intranuclear inclusions in neuronal cells ultimately leading to neuronal death. MicroRNAs are endogenously produced, small, non-coding RNAs that play a role in post-transcriptional regulation of gene expression. MicroRNA mediated regulation of gene expression is associated with several processes such as the development of organisms, maintenance of homeostasis as well as with several human disorders such as cancer and neurodegenerative diseases.

The present study demonstrates the ability of specific microRNAs to target the expression of the proteins ATXN3, MID1 and DNAJB1 which play important roles in the pathogenic mechanisms in SCA3. The microRNAs hsa-miR-32 and hsa-miR-181c were found to target and reduce ATXN3 expression, while hsa-miR-216a-5p, hsa-miR-374a-5p, hsa-miR-542a-3p target and reduce the expression of MID1. Profiling of gene and microRNA expression in iPSC-derived neurons from SCA3 patients and controls revealed that in SCA3 neurons, hsa-miR-370 and hsa-miR-543 that target the expression of the neuroprotective DNAJB1 chaperone are upregulated, while the target DNAJB1 mRNA and protein are downregulated. Similarly, DNAJB1 mRNA level was found to be downregulated in a transgenic SCA3 mouse model suggesting that the miRNA mediated reduction in the neuroprotective DNAJB1 might contribute to the pathogenesis observed in SCA3.

These results demonstrate the two sided role of microRNAs in the pathogenesis of SCA3 by targeting the expression of neurotoxic proteins such as ATXN3, MID1 as well as neuroprotective proteins such as DNAJB1. The findings of this study might contribute towards miRNA based therapeutic strategies such as enhancing miRNA targeting of neurotoxic proteins and preventing miRNA targeting of neuroprotective proteins.

Abbreviations

3’ UTR	3’ untranslated region
5’UTR	5’ untranslated region
ALS	amyotrophic lateral sclerosis
AR	androgen receptor
ATP	adenosine triphosphate
ATXN1	ataxin 1 protein
ATXN3	ataxin 3 gene
ATXN3	ataxin 3 protein
C.elegans	*Caenorhabditis elegans*
CBP	CREB-binding protein
CMV promoter	cytomegalovirus promoter
DM1	myotonic dystrophy type 1
DMEM	Dulbecco’s modified Eagle medium
DMSO	dimethyl sulfoxide
DNA	deoxyribonucleic acid
DNAJB1	DnaJ (Hsp40) homolog, subfamily B, member 1
Drosophila	*Drosophila melanogaster*
E.coli	*Escherichia coli*
eIF4B	eukaryotic translation initiation factor 4B
EYA	eyes absent protein
FBS	fetal bovine serum
FDR	false discovery rate
FMR1	fragile X mental retardation 1
FXTAS	fragile X-associated tremor/ataxia syndrome
GO	gene ontology
HD	huntington’s disease
HRP	horse radish peroxidase
hsa-miRNA	homo sapiens-miRNA
HSP	heat shock protein

HTT	huntingtin gene
IB	immunoblotting
IF	immunofluorescence
iPSC	induced pluripotent stem cell
kDa	kilo Dalton
LB	lysogeny broth
LSM	laser scanning microscopy
Lys	lysine
MID1	midline 1
miRISC	microRNA associated RNA induced silencing complex
miRNA	microRNA
MJD	Machado Joseph Disease
mRNA	messenger RNA
mTOR	mechanistic target of rapamycin
NI	intranuclear inclusions
nt	nucleotides
PCR	polymerase chain reaction
PFA	paraformaldehyde
PolyQ diseases	polyglutamine diseases
PP2A	protein phosphatase 2
pre-miRNA	precursor miRNA
pri-miRNA	primary miRNA
PVDF	polyvinylidene fluoride
REST	RE1 silencing transcription factor
RNA	ribonucleic acid
RNA-seq	RNA sequencing
RNAi	RNA interference
S6K	ribosomal protein S6 kinase
SCA1	spinocerebellar ataxia type 1
SCA3	spinocerebellar ataxia type 3
SDS PAGE	sodium dodecyl sulfate polyacrylamide electrophoresis
SOD1	superoxide dismutase 1, soluble
TBP	TATA-binding protein

UIM	ubiquitin interacting motif
V	volt
WC match	Watson-Crick match
YAC	yeast artificial chromosome
μG	microgram
μL	microliter

Table of Contents

Section 2.2 Methods

Chapter 3 Results

3.1 miRNA targeting of ATXN3

3.2 miRNAs targeting Midline 1 (MID1)

3.3 Analysis of differentially expressed miRNAs in iPSC-derived SCA3 neurons

Chapter 4 Discussion

Chapter 1 Introduction

1.1 Trinucleotide repeat disorders

Trinucleotide repeat disorders are a class of inherited, neurological disorders characterized by expansions of trinucleotide repeats. With 16 disorders, they form the largest group of inherited neurodegenerative diseases. The trinucleotide expansions are unstable and studies have shown that the number of trinucleotide repeats might increase in successive generations (Fu et al, 1991). These mutations are therefore termed as 'dynamic' mutations. Since the severity of symptoms and the age of onset are dependent on the number of trinucleotide repeats, the instability of the repeats explains the variability of the symptoms and the age of onset (Orr & Zoghbi, 2007). The exact trinucleotide sequence that is expanded and the pathogenic mechanism vary amongst the trinucleotide disorders. For example CTG expansions in the DMPK gene cause Myotonic Dystrophy type 1 (DM1) where the expanded mRNA mediates the pathogenicity (Mankodi et al, 2002). CGG expansions in the FMR1 gene cause Fragile X syndrome (FXTAS) where the pathogenesis is mediated by an inability of the FMR1 gene to be expressed into FMRP protein (Pieretti et al, 1991). Relevant to this study are the CAG repeat disorders where the expanded polyglutamine chain coded by CAG repeat expansions mediates the pathogenesis.

1.2 Polyglutamine repeat diseases

Polyglutamine (PolyQ) diseases are a subset of the trinucleotide repeat disorders where expansions of the trinucleotide repeat CAG occur in the coding regions of various genes. Since CAG codes for the amino acid glutamine, these diseases are characterized by expanded glutamine repeats in the mutant proteins. Except for the presence of polyglutamine repeats, these proteins are unrelated (La Spada et al, 1994; Zoghbi & Orr, 2000).

A hallmark of all these diseases is the formation of intraneuronal inclusions, which primarily include the expanded polyglutamine proteins, but in which several other proteins such as ubiquitin and components of the proteasome are sequestered (Davies et al, 1998; Ross, 1997; Rubinsztein et al, 1999). The neurons that develop intraneuronal inclusions

vary between the different polyglutamine diseases; this results in a pattern of atrophy that is unique for each polyglutamine disease, and also explains the differential symptoms seen in each disease. The exact mechanism through which the presence of these mutant proteins leads to neuronal death is not yet known. Several mechanisms such as proteolytic cleavage of the mutant protein, shuttling of the mutant protein to the nucleus and its subsequent aggregation, failure to clear the mutant protein as well as mitochondrial dysfunction have been shown to contribute to the observed neuronal death (Weber et al, 2014). As of now there are nine polyglutamine diseases known. **Table 1.1** gives an overview of the genes mutated, the resultant proteins and the CAG repeat expansions associated with each polyglutamine disorder. Amongst the polyglutamine diseases one of the best studied is the most prevalent of the inherited ataxias, the Spinocerebellar Ataxia type 3 (SCA3) that is also the disorder studied in this project.

Disease	Gene	Protein	CAG repeats in	
			Wild type	Mutant
Spinocerebellar Ataxia type 1 (SCA1)	*ATXN1*	Ataxin 1	8-44	39-83
Spinocerebellar Ataxia type 2 (SCA2)	*ATXN2*	Ataxin 2	13-31	32-79
Spinocerebellar Ataxia type 3 (SCA3)	*ATXN3*	Ataxin 3	12-40	55-84
Spinocerebellar Ataxia type 6 (SCA6)	$CACNA1_A$	α-voltage dependent calcium channel subunit	4-18	19-33
Spinocerebellar Ataxia type 7 (SCA7)	*ATXN7*	Ataxin 7	4-35	37-306
Spinocerebellar Ataxia type 17 (SCA17)	*TBP*	TATA-binding protein	25-44	47-63
Huntington's Disease (HD)	*HTT*	Huntingtin	6-35	36-121
Spinal-bulbar muscular atrophy (SBMA)	*AR*	Androgen receptor	10-36	38-62
Dentatorubral-pallidoluysian atrophy (DRPLA)	*ATN1*	Atrophin 1	7-23	47-55

Table 1.1: An overview of the nine polyglutamine diseases. Listed above are the mutant genes and the resultant proteins alongside the CAG repeats associated with wild type and mutant alleles.

1.3 Spinocerebellar Ataxia type 3 (SCA3)

SCA3 is also known as Machado Joseph disease (MJD), named after Portuguese families originating from the Azores islands in whose members the symptoms of the disease were first described. Initially MJD and SCA3 were thought of as two different diseases with similar symptoms. It was only when the genetic locus of both these inherited diseases was discovered to be located in the same region of chromosome 14 that consensus was reached that both these diseases constitute a single disorder encompassing a rather heterogeneous group of symptoms (Kawaguchi et al, 1994; Stevanin et al, 1994; Twist et al, 1995). After initial studies in descendants from Portuguese ancestry, in the middle of the 1990s SCA3 was increasingly described in patients from several countries such as Japan, China, and Germany etc. thus widening the scope of its study (Schols et al, 1996; Soong et al, 1997; Takiyama et al, 1995). In several regions of the world SCA3 is the most prevalent of the dominant spinocerebellar ataxias (Schols et al, 1996; Trott et al, 2006; Watanabe et al, 1998).

The symptoms of SCA3 are heterogeneous, with deficits of the cerebellar, pyramidal, extrapyramidal systems seen to various degrees. The most common associated symptoms include cerebellar ataxia, opthalmoplegia (paralysis of eye muscles), bulging eyes, dystonia, incontinence, weight loss and involuntary contractions of the facial muscles. Owing to the heterogeneity, the symptoms have been grouped into 4 subgroups to aid in diagnosis. The type of symptoms and the age of onset are correlated to the number of CAG repeats in the expanded *ATXN3* gene, with the mean age of onset around 36 years (Durr et al, 1996; Riess et al, 2008).

The neuropathology of SCA3 is associated with degeneration and atrophy in the cerebellum, thalamus, parts of the midbrain, pons, medulla oblongata and basal ganglia. The neuronal loss affects the nuclei of oculomotor, vestibular, somatomotor and ingestion-related loops (Durr et al, 1996; Rub et al, 2013; Seidel et al, 2012b).

1.4 *ATXN3* gene

The *ATXN3* gene is present on chromosome 14 in humans. Its sequence is evolutionarily conserved as sequences homologous to human *ATXN3* have been found in the animal genomes such as mouse, rat, *Drosophila*, *C.elegans* as well as the plant genomes of *A.thaliana* and rice (Albrecht et al, 2003). The *ATXN3* gene has 11 exons and the *ATXN3* mRNA has several splice variants (Ichikawa et al, 2001) (**Fig 1.1**). In humans, healthy individuals have up to 44 CAG repeats in the *ATXN3* gene whereas SCA3 patients have between 52-86 CAG repeats. Individuals with 45-51 CAG repeats might or might not develop the disease, a phenomenon known as incomplete penetrance. Individuals with CAG repeats more than 55 definitely develop SCA3 (Todd & Paulson, 2010).

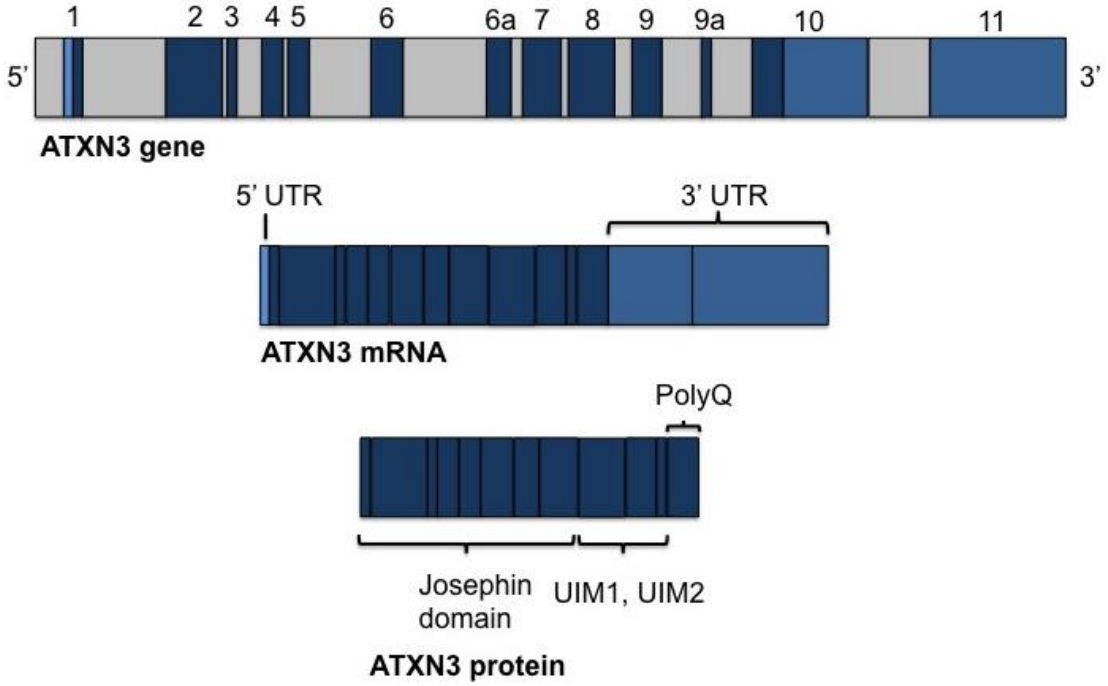

Figure 1.1: Structure of the *ATXN3* gene, mRNA and protein. Exons are denoted in dark blue, introns in grey and the untranslated regions in light blue. As seen in (a) the *ATXN3* gene is composed of a total of 11 exons interspersed by introns that are omitted in the *ATXN3* mRNA (b). The initial 7 exons code for the Josephin domain in the ATXN3 protein, the rest of the exons code for the C-terminal domain with the polyQ chain encoded by the 10^{th} exon (c).

1.5 ATXN3 protein

The ATXN3 protein is encoded by the *ATXN3* gene. In humans ATXN3 is expressed throughout the body primarily as a cytoplasmic protein, although it is also present in the nucleus and the mitochondria to some extent. It is widely expressed in the brain, even in areas which are unaffected by SCA3 (Paulson et al, 1997a) (Trottier et al, 1998). The wild type ATXN3 has a molecular weight of 42 kDa, whereas the molecular weight of the mutant protein is increased considerably due to the expanded polyglutamine chain. Structural studies have elucidated that ATXN3 is made up of a globular N-terminal domain known as the Josephin domain and an unstructured C-terminal domain that contains the polyglutamine repeat tract (Masino et al, 2003) (**Fig 1.1**). The Josephin domain has two ubiquitin binding sites and has ubiquitin protease activity (Chow et al, 2004; Nicastro et al, 2009) whereas the C-terminal domain has ubiquitin interacting motifs (UIMs) which define the specificity of the Josephin domain to cleave ubiquitin chains having linkages at Lys^{63} (Winborn et al, 2008).

ATXN3 functions as a ubiquitin protease and binds to poly-ubiquitylated proteins especially ones with four or more ubiquitins in chain through a specific domain known as the Ubiquitin Interacting Motif (UIM) (Burnett et al, 2003; Chai et al, 2004; Donaldson et al, 2003; Doss-Pepe et al, 2003). Analysis of the structure of the Josephin domain also revealed that ATXN3 belongs to the family of papain-like cysteine proteases (Nicastro et al, 2005). Besides, ATXN3 has been shown to interact with chromatin via histone binding and function as a transcriptional co-repressor, whereby it controls the transcription of several genes including genes coding for cell surface-associated proteins (Evert et al, 2006; Evert et al, 2003; Li et al, 2002).

The cell toxicity mediated by expanded ATXN3 is triggered by its proteolytic cleavage to form an aggregate prone fragment; a phenomenon seen in several polyQ disorders and called the toxic fragment hypothesis (Wellington et al, 1998). The expanded ATXN3 is cleaved by calcium dependent calpain proteases to form an aggregation prone C-terminal fragment containing the expanded polyglutamine stretch that is enough to induce aggregation and cell toxicity (Haacke et al, 2006; Haacke et al, 2007; Ikeda et al, 1996). The expanded ATXN3 fragment forms intranuclear inclusions (NIs) in neurons in affected brain regions in which several other proteins are recruited and sequestered including the full-length ATXN3 (Paulson et al, 1997b; Schmidt et al, 1998). Other proteins shown to be

recruited into the NIs are polyglutamine repeat containing proteins such as the TATA-binding protein (TBP), Eyes Absent (EYA) protein in a *Drosophila* model of SCA3 (Perez et al, 1998), several proteins that bind to ATXN3 such as the transcriptional co-activator CREB-binding protein (CBP) (McCampbell et al, 2000), human homolog of the yeast DNA repair protein HHR23 (Wang et al, 2000) as well as the 26 proteasome (Chai et al, 1999b) and ubiquitin (Schmidt et al, 1998). This recruitment and sequestration of proteins might be accompanied with a partial or complete loss of their function thereby contributing to the cell toxicity. Since the inclusions are formed only in the nucleus, the localization of the expanded ATXN3 to the nucleus is key to the aggregation-mediated toxicity (Bichelmeier et al, 2007). Other studies have documented the involvement of a variety of mechanisms and pathways that might mediate toxicity in SCA3. These include the downregulation of autophagy (Menzies et al, 2010; Nascimento-Ferreira et al, 2011), oxidative stress leading to mitochondrial dysfunction (Tsai et al, 2004; Yu et al, 2009), inflammation (Evert et al, 2001).

It is worth mentioning that although the main body of research has shown that aggregates mediate toxicity in polyQ diseases, there is also evidence on the contrary, i.e. the oligomeric fractions of the polyQ proteins mediate toxicity whereas aggregate formation serves to limit the amount of oligomers in the cells (Arrasate et al, 2004; Lajoie & Snapp, 2010; Leitman et al, 2013). The question of whether oligomeric fraction or the aggregates form the basis of toxicity in SCA3 is as yet still open to debate.

Several animal models have been established to study the molecular mechanism, pathogenesis and phenotypic effects of the expression of expanded ATXN3, either full length or just the pathogenic, aggregate prone fragment. Owing to the conservation of basic cellular pathways and mechanisms, transgenic *Drosophila* and *C.elegans* expressing the expanded human ATXN3 transgene have been instrumental in understanding the pathogenic mechanisms associated with SCA3 (Teixeira-Castro et al, 2011; Warrick et al, 1998). A number of transgenic mouse models have been shown to exhibit phenotypic effects such as gait abnormalities and progressive ataxia, along with cerebellar neurodegeneration and the presence of intranuclear inclusions (Cemal et al, 2002; Chou et al, 2008; Ikeda et al, 1996). A conditional knockout model of SCA3 transgenic mice exhibited a progressive neurological phenotype, which could be reversed by turning off the expression of mutant ATXN3 in early stages of the disease (Boy et al, 2009). Alternately, SCA3 models created by injecting lentiviral vectors expressing the expanded

ATXN3 into either rats or mice also exhibited the hallmarks of SCA3, i.e. formation of intranuclear inclusions and progressive neuronal cell loss (Alves et al, 2008; Nobrega et al, 2013). A recent development is the preparation of iPSCs (Induced Pluripotent Stem Cells) from fibroblasts from SCA3 patients. Neurons derived from these iPSCs exhibit the formation of aggregates following calpain-mediated cleavage induced by glutamate excitation (Koch et al, 2011).

Research into deciphering the molecular mechanisms of SCA3 and other polyQ diseases revealed the role of several proteins in the pathogenesis and disease progression of these diseases. Two of these proteins: namely the chaperone DNAJB1 (HSP40) and the CAG repeat mRNA interacting protein MID1, are also a part of the current study.

1.6 DNAJB1

Molecular chaperones are proteins that play an important role in maintaining protein homeostasis in the cell by aiding the process of proper folding of proteins and thereby preventing the accumulation of misfolded proteins and protein aggregates in the cell. One of the earliest publications to define this category of proteins, defines molecular chaperones as "proteins whose role is to mediate the folding of certain other polypeptides and, in some instances, their assembly into oligomeric structures, but which are not components of these final structures" (Ellis & Hemmingsen, 1989). Importance of the role of chaperones in maintaining proteostasis can be gauged from the fact that homologues of the chaperone proteins can be found in archaebacteria, eubacteria as well as eukaryotes with partial conservation of gene sequences across the evolutionary ladder (Bardwell & Craig, 1984). An important group of chaperones are heat shock proteins (HSPs), which were initially discovered to be expressed in response to heat shock (Lindquist, 1986). Gradually it was found that a.) HSPs are expressed in response to other stresses apart from heat stress (Lanks, 1986; Whelan & Hightower, 1985) and b.) certain HSPs are also expressed under non-stress conditions (Ingolia & Craig, 1982). Amongst the HSPs, an important group are the Heat Shock Protein 70 (HSP70) proteins, named so due to their size, which is approximately 70 kDa. HSP70 proteins mediate the refolding of proteins in eukaryotes, while their bacterial counterpart, the protein DnaK, which bears a partial sequence similarity to HSP70 mediates protein refolding in bacteria (Bardwell & Craig, 1984). Certain members of the HSP70 group are expressed in response to stress, whereas

some such as Hsc70 are expressed constitutively under non stress conditions (Ingolia & Craig, 1982). The HSP70 proteins however are not able to refold proteins alone. In 1990 Ohtsuka and colleagues described for the first time a 40 kDa protein, which was expressed in cells along with HSP70 in response to stress (Ohtsuka et al, 1990). Further studies elucidated that this protein, named HSP40 or HDJ-1 since it bears a partial sequence similarity to the bacterial DnaJ chaperone, is a mammalian homologue of the Dnaj whose association with the DnaK in bacteria is essential for the chaperone function of DnaK (Hattori et al, 1992; Ohtsuka, 1993; Raabe & Manley, 1991). Proof of the co-chaperone function of HDJ-1 was found when it was discovered that it physically interacts with HSP70 and in the presence of ATP this complex is able to refold a substrate, which is normally a misfolded protein or an unfolded protein intermediate (Freeman & Morimoto, 1996; Freeman et al, 1995; Sugito et al, 1995). The HSP70-HSP40 machinery was found to be active in the nucleus as well as the cytoplasm (Michels et al, 1997). Subsequently it was found that HDJ-1 is just one of several HSP40 proteins which comprise the DNAJ group of co-chaperones, characterized by the presence of a 'J-domain' through which they interact with the HSP70 chaperones. Although studies have shown that several members of the DNAJ family potentially play a role in the aggregation of polyglutamine expanded proteins, one member, DNAJB1 has been of particular interest since a majority of studies have found it to be the dominant member of the DNAJ family associated with polyglutamine aggregates in cells.

1.7 DNAJB1 in polyglutamine diseases

The phenomenon of aggregation is seen in several diseases where mutations in genes render the mutated proteins unable to fold in the appropriate way. In many cases these aggregates contain not only the misfolded protein but also other interacting proteins and components of the proteasome machinery such as ubiquitin, subunits of the proteasome and chaperones, which try to clear these aggregates (Chai et al, 1999b; Schmidt et al, 1998). The HSP70-HSP40 chaperones have been found to be co-localized with protein aggregates seen in several inherited disorders such as the mutant SOD1 aggregates in familial ALS (Takeuchi et al, 2002), mutant transcription factor Hoxd13 with poly-alanine repeat expansions (Albrecht et al, 2004) as well as mutant proteins with polyglutamine

repeats such as androgen receptor (AR) (Bailey et al, 2002), ATXN1 (Cummings et al, 1998), ATXN3 (Chai et al, 1999a) and huntingtin (Muchowski et al, 2000).

Although some studies have implicated other members of the DNAJ family as the co-chaperones associated with HSP70 during interactions with polyglutamine mediated aggregates, the majority of the studies have exhibited that the DNAJB1 is the active HSP40 co-chaperone that binds to HSP70 in such interactions. The HSP70-HSP40 chaperones seem to bind to polyQ aggregates and prevent the propagation of the fibril like detergent insoluble aggregates, forming detergent soluble amorphous aggregates that are also less toxic (Muchowski et al, 2000). Several cell culture studies have shown that the overexpression of the DNAJB1 chaperone suppresses polyQ aggregate formation and the associated cell toxicity (Chai et al, 1999a; Jana et al, 2000). The underlying mechanism is thought to be that the DNAJB1 recognizes and binds to the misfolded polyQ protein and attempts to refold it in such a way that it is recognized by the HSP70. HSP70 then binds to the protein and, in an ATP dependent reaction converts it into a less toxic form that can be degraded (Lotz et al, 2010; Rujano et al, 2007). The yeast homologue of DNAJB1, Sis1p is sequestered by polyQ-expanded proteins, thus rendering it unable to perform its function of binding and transporting misfolded proteins to the nucleus for proteasomal degradation. As a result the misfolded proteins form toxic, cytoplasmic aggregates (Park et al, 2013). A similar phenomenon was observed in neurons from SCA3 patients where DNAJB1 co-localized with the intranuclear inclusions and was markedly decreased from the cytoplasm (Seidel et al, 2012a). Along with other HSP40 chaperones it was found that the differential expression of DNAJB1 seems to play a role in the CAG independent age of onset of symptoms in SCA3 patients (Zijlstra et al, 2010).

1.8 MID1

The MID1 protein encoded by the *MID1* gene is an E3 ubiquitin ligase (Quaderi et al, 1997; Trockenbacher et al, 2001). It associates with microtubules and has been shown to bind and regulate the activity of several proteins as well as mRNAs, including CAG repeat mRNAs (Krauss et al, 2013; Schweiger et al, 1999). MID1 binds to Protein Phosphatase 2A (PP2Ac) via its alpha-4 subunit and regulates its activity by mediating its degradation by the proteasome (Liu et al, 2001; Trockenbacher et al, 2001). Since the protein mTOR Kinase is a target of PP2A, MID1 indirectly also regulates the activity of mTOR (Liu et al,

2011). PP2A and mTOR together regulate mRNA translation in cells by regulating the phosphorylation of proteins such as ribosomal S6 kinase (S6K), which further targets proteins important for translation such as elongation factor 4B (elF4B) and ribosomal S6 (Holz et al, 2005). Further proof that MID1 plays a crucial role in translation regulation is provided by findings that MID1 binds to proteins associated with mRNA transport and translation as well as mRNAs, which have a specific motif known as a MIDAS motif (Aranda-Orgilles et al, 2011; Aranda-Orgilles et al, 2008). Thus it forms a ribonucleoprotein complex at the microtubules and mediates the translation of specific mRNAs at the microtubules. This mechanism suggests that MID1 might play a crucial role in neurons, where translation in axons would probably be preceded by mRNA transport along the microtubules. Apart from these findings, which exhibit the importance of MID1 in translation, the most important finding relevant to this study is the one that MID1 along with PP2A and S6K is able to bind to the CAG repeat region of HTT mRNA in a repeat-length dependent manner. This binding has an effect on augmenting the translation of the CAG repeat RNA into the HTT protein with expanded polyglutamine repeats (Krauss et al, 2013). Also, a recent study has elucidated that MID1 binds to the AR mRNA at the CAG repeats and that the overexpression of MID1 leads to increased levels of the AR protein while the levels of AR mRNA remain unchanged (Kohler et al, 2014). **Figure 1.2** gives an overview of the role of MID1 in mRNA translation via the various mechanisms described above.

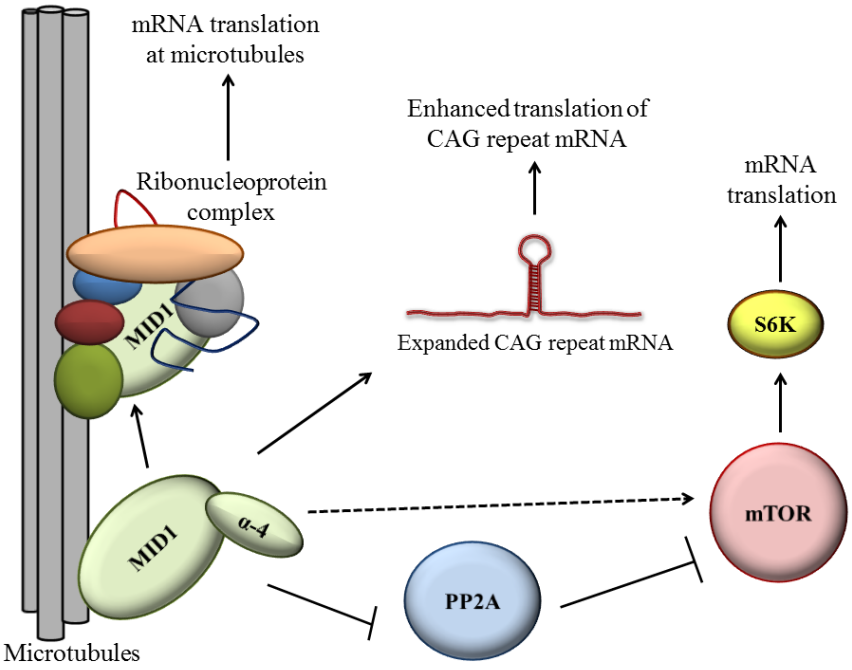

Figure 1.2: Various mechanisms through which MID1 protein enhances mRNA translation. MID1 binds and regulates PP2A through its α-4 subunit, thereby indirectly enhancing mTOR activity leading to increased mRNA translation. MID1 binds to expanded CAG repeat RNAs leading to enhancement of their translation and forms a ribonucleoprotein complex at the microtubules enhancing mRNA translation at the microtubules.

In SCA3, a crucial aspect in disease progression and neuronal death is the level of expression of the mutant ATXN3, apart from other proteins involved: including DNAJB1 and MID1. An important mechanism in cells to regulate protein expression is the RNA interference machinery, of which microRNAs (miRNAs) form a vital part. miRNAs might play a role in SCA3 pathogenesis, and therefore are worth giving attention to.

1.9 MicroRNAs

It was in the last decade of the 20th century after Andrew Fire and colleagues first published their results documenting the presence of double stranded RNA being able to interfere with the expression of genes in *C.elegans* (Fire et al, 1998) that the field of RNA interference came alive. Soon, Hamilton and colleagues proved that antisense RNAs

regulating gene expression are also present in plants (Hamilton & Baulcombe, 1999) while Tuschl et al. observed RNA interference mediated by double stranded RNAs in *Drosophila* (Tuschl et al, 1999). It was soon discovered that RNA interference is mediated by a ribonucleoprotein complex that includes short RNAs which confer specificity for the target mRNA (Elbashir et al, 2001; Hammond et al, 2000; Zamore et al, 2000)

MicroRNAs are endogenously produced, non-coding RNAs that are a part of the RNA interference machinery of the cell (Lagos-Quintana et al, 2001). miRNAs share partial sequence complementarity with their 'target' sequences present on mRNAs, mostly in the 3' untranslated region (3'UTR) of the mRNAs (Lai, 2002). miRNAs in association with a protein complex known as the miRISC (miRNA associated RNA Induced Silencing Complex) bind to the above mentioned complementary sequences on their 'target' mRNAs. This binding either blocks the translation of the mRNA or leads to its degradation (Hutvagner & Zamore, 2002); in either way regulating the expression of the protein coded by the target mRNA. miRNAs have been found to play important roles in plants (Palatnik et al, 2003; Reinhart et al, 2002), *C.elegans* (Lau et al, 2001; Lee & Ambros, 2001; Lim et al, 2003), *Drosophila* (Xu et al, 2003) and in mammals (Chen et al, 2004; Lagos-Quintana et al, 2002). miRNAs are estimated to target upto 30% genes in the human genome (Lewis et al, 2005). As such miRNAs have been shown to play crucial roles in several important pathways in the development of organisms (Houbaviy et al, 2003; Krichevsky et al, 2003; Lim et al, 2003; Pasquinelli & Ruvkun, 2002; Sempere et al, 2004) as well as in several important diseases such as cancer, heart disease, neurodegenerative diseases etc. An indication of their importance in translational regulation can be found from the fact that miRNA sequences and their binding sites on the mRNAs are evolutionarily conserved. miRNAs are transcribed from miRNA coding genes as well as from introns into several hundred nucleotide long primary miRNA transcripts in the cell nucleus (Lee et al, 2002) (**Fig 1.3**). These transcripts serve as templates for the RNAses Drosha and its cofactor Pasha, which cleave these transcripts into premature 70-80 nucleotide long miRNAs (pre-miRNAs) (Lee et al, 2003). The pre-miRs are exported from the nucleus into the cytoplasm via the exportin complex (Lund et al, 2004; Yi et al, 2003). In the cytoplasm, the pre-miRNAs are further cleaved by the RNAse Dicer to form a duplex of miRNAs (Bernstein et al, 2001). Of this duplex, one strand (the guide strand) eventually associates with miRISC and plays a role in translational repression of mRNAs. The other strand (passenger strand or * strand) has a far less probability of being

associated with the miRISC complex (Schwarz et al, 2003). miRNA binding sites on the target mRNAs are mostly situated in the 3' untranslated region (3' UTR). However, recent research seems to suggest that miRNA recognition and binding sites are also present in the 5' untranslated region (5' UTR) as well as in the coding region (Duursma et al, 2008; Forman et al, 2008; Lytle et al, 2007).

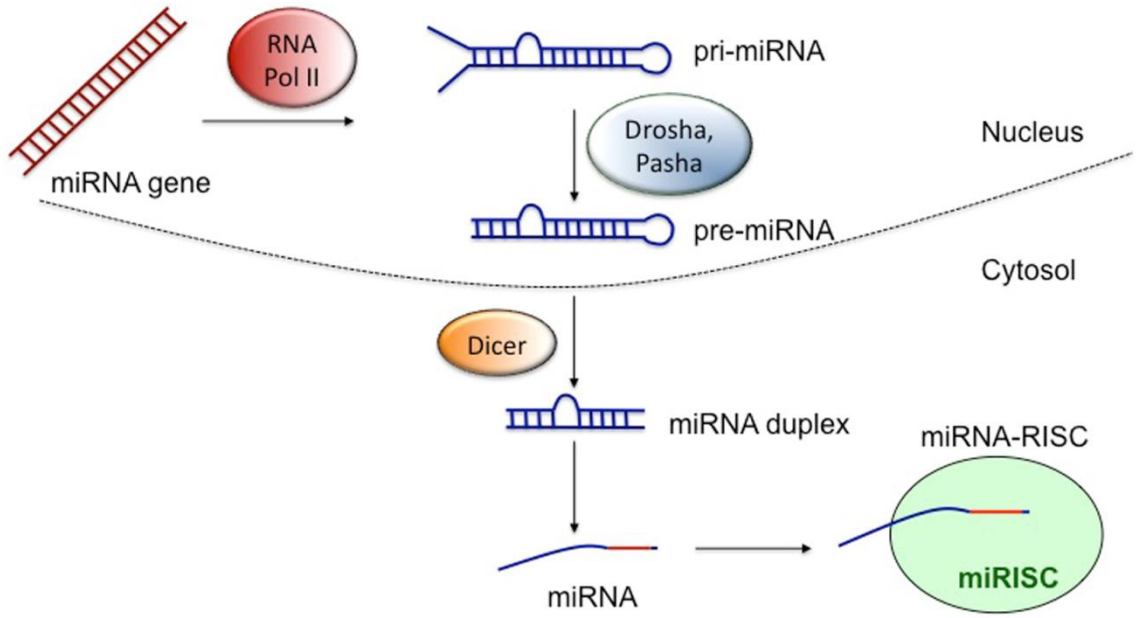

Figure 1.3: Schematic showing the miRNA biogenesis pathway. Primary miRNAs are transcribed in the nucleus by RNA polymerase II. Upon cleavage by Drosha/Pasha the precursor miRNAs are exported to the cytosol where further cleavage by Dicer leaves the miRNA duplex. The guide strand associates with the RISC complex to participate in translation repression.

1.10 MicroRNAs in neurodegenerative diseases

Several studies have shown that miRNAs play an important role in maintaining the homeostasis of neurons over time and modulations in miRNA levels and pathways also contribute towards the effects of aging in the brain. For example, it was seen that the ablation of the enzyme Dicer (important for miRNA maturation) in Purkinje cells in mice led to a gradual decrease in levels of certain miRNAs accompanied by development of ataxia and eventually Purkinje neuron death (Schaefer et al, 2007). Experiments in

Drosophila uncovered that a miRNA, the miR-34 is essential for a normal lifespan and prevents untimely ageing (Liu et al, 2012). Various miRNAs have also been shown to play a role in the pathogenesis of neurodegenerative diseases such as Alzheimer's disease (Lehmann et al, 2012; Wong et al, 2013), Friedreich Ataxia (Mahishi et al, 2012), Fragile X Associated Tremor/Ataxia Syndrome (FXTAS) (Tan et al, 2012; Zongaro et al, 2013). With regards to the involvement of miRNAs in polyglutamine diseases, most of the research as yet has been in Huntington's disease. Studies in mouse, primate models of HD, as well as HD patients exhibited altered expression of miRNAs and proteins that are either involved in miRNA pathways or are probable targets of the altered miRNAs (Jin et al, 2012; Kocerha et al, 2014; Lee et al, 2011). Many of these miRNAs are regulated by the transcriptional repressor REST, which is activated in HD (Johnson et al, 2008; Marti et al, 2010; Packer et al, 2008). An altered expression of miRNAs and its role in toxicity has also been seen in models of SCA1 (Lee et al, 2008; Persengiev et al, 2011; Rodriguez-Lebron et al, 2013). Not much has as yet been published regarding the role of miRNAs in SCA3. In a Drosophila model of SCA3, it was seen that hampered miRNA processing brought about by mutation of the Dicer enzyme enhances toxicity associated with the expression of mutant ATXN3. A miRNA named Bantam was also found to be vital to prevent degeneration (Bilen et al, 2006).

Aims of the thesis

SCA3 is an inherited disorder caused by CAG repeat expansions in the *ATXN3* gene, leading to expanded polyglutamine repeats in the ATXN3 protein coded by this gene. The expression of the expanded ATXN3 protein leads to neurotoxicity via several mechanisms involving the soluble form as well as the intraneuronal aggregates formed by the mutant ATXN3 protein. miRNAs are endogenously produced, non-coding RNAs that play an important role in post-translational gene regulation via the RNA interference (RNAi) mechanism. miRNAs in association with specific protein complexes block the translation or degrade mRNAs by binding at specific target sites mostly on the 3'UTR of the mRNA. miRNAs play an important role in maintaining homeostasis and response to stress and disease. On the other hand, dysregulation of miRNAs has been shown to be associated with several human disorders.

This study aimed at elucidating the role of miRNAs in SCA3 where the expanded ATXN3 protein triggers the involvement of multiple proteins and pathways in pathogenesis. miRNAs might be differentially expressed in SCA3 cells in response to the metabolic stress and protein aggregates to downregulate the expression of mutant ATXN3 and other neurotoxic proteins such as MID1 which has been shown to augment the translation of mRNAs with expanded CAG repeats. With this consideration, ATXN3 and MID1 were chosen as candidate neurotoxic proteins to analyse the ability of miRNAs to target their expression. The aim here was to find miRNAs that bind at specific sites on the 3'UTR of ATXN3 and MID1 mRNAs and to validate the ability of these miRNAs to regulate the mRNA and protein expression of ATXN3 and MID1 in human cell lines. Another aim of this study was to elucidate miRNA targeting of gene expression relevant to SCA3 pathogenesis using iPSC-derived neurons from SCA3 patients and controls. For this purpose, gene expression and miRNA expression profiles from iPSC-derived neurons were analysed to choose relevant candidate proteins that might be targeted by miRNAs. Finally, the study aimed at validation of miRNA targeting of the chosen candidate in terms of specific binding, regulation of candidate mRNA and protein expression in human cell lines.

Chapter 2 Materials and Methods

Section 2.1 Materials

2.1.1 List of consumables

0.1-5 mL Combitips: Eppendorf Research

1.5 mL/2 mL safe lock tubes: Sarstedt

10-1000 µL pipette tips: Nerbeplus

100/250 mL conical flasks

15 mL/20 mL Screw cap centrifuge tubes: VWR International

5/10/25/50 mL serological pipettes: Sarstedt

8 well glass chamber slide: Lab Tek II, NUNC (154534)

96-well reaction plate: Applied Biosystems (4306737)

Disposable hypodermic needle (0.60*30 mm): 100 Sterican, Braun Medical AG

Filter paper: Bio Rad (cat: 1703969)

Glass plates (Short/1.0mm spacer): Mini Protean System

Pasteur pipettes: Carl Roth GmbH

Petri plates

PVDF membrane: Roche Diagnostics GmbH (Ref: 03010040001)

Syringe, 5 mL: Braun Medical AG

Tissue culture flask: TPP 75 cm^2 (90075)/150 cm^2 (90150)

Tissue culture test plate (12 well): TPP (92012)

2.1.2 List of Devices

0.2-1000 µL Pipettes: Eppendorf Research

Agarose gel electrophoresis chamber: Sub-Cell GT (Bio Rad)

Agarose Gel/Immunoblot imaging system: Stella (Raytest)

Automatic pipette: Multipette stream (Eppendorf)

Bacterial culture shaker/incubator: Kuhner Shaker X (Lab Therm)

Bacterial plates incubator: Binder

Cell analysis system: CASY (Innovatis)

Centrifuge for 1.5/2 mL tubes: Heraeus Fresco 21 (Thermo Scientific)

Centrifuge for 15/50 mL tubes: Heraeus Multifuge X3R (Thermo Scientific)

CO_2 incubator: Heracell 240i (Thermo Scientific)

Confocal Laser Scanning microscope: LSM 700 (Zeiss)

Fluorometer: Qubit (Life Technologies)

Heating block: Thermomixer comfort (Eppendorf)

Ice machine: Ziegra Labor

Laminar Airflow hood: Mars Safety Class 2 (Scanlaf)

Light microscope: Primovert (Zeiss)

Luminescence signal plate reader: Envision Plate reader (Perkin Elmer)

Microwave oven: NN-SD450W (Panasonic)

PCR Cycler: DNA Engine Dyad (Bio Rad)

pH meter: SevenEasy (Mettler Toledo)

Powerpack: Powerpac Universal (Bio Rad)

Real-time PCR cycler: 7900HT Fast Real-time PCR systems (Applied BioSystems)

Roller Mixer: Stuart SRT6

SDS PAGE Blotter: Trans Blot Semi dry Transfer cell (Bio Rad)

SDS PAGE chamber: Mini Protean Tetra System (Bio-Rad)

Sonicator: Bandelin Sonoplus

Ultra Violet Trans illuminator: TL-2000 (Ultra Violet Products)

Vortex mixer: Vortex Genie 2 (Scientific Industries Inc)

Water Bath: Type 1083 (GFL)

Water purification system: Purelab Option-Q (Elga)

Weighing balance: Type 572 (Kern and Sohn GmbH)

2.1.3 List of chemicals

Chemical	Manufacturer (Catalogue no.)
2-Mercaptoethanol	Sigma Life Science (63689-100ML-F)
Acetic acid	Sigma Aldrich (A6283-500ML)
Acrylamide-bis 30% (37.5:1)	Merck KGaA (1.00639.1000)
Adenosine 5’ triphosphate disodium salt hydrate	Aldrich Chemistry (A26209-5G)
Agar	Sigma Aldrich (05040-1KG)
Agarose	peqGOLD (35.1020)
Albumin, IgG free	Carl Roth GmbH (3737.3)

Ammonium Persulphate (APS)	Sigma (A 3678.100G)
Bromophenol Blue	Sigma Aldrich (B8026-25G)
Coelenterazine	p.j.k. GmbH (260350)
Coenzyme A, sodium salt hydrate	Sigma (C4780)
DL-Dithiothreitol	Sigma Life Science (43815-5G)
D-Luciferin sodium salt	p.j.k. GmbH (269149)
DNA ladder 1 kb	Thermo Scientific GeneRuler (SM0313)
DNA ladder 100 bp	Thermo Scientific GeneRuler (SM0243)
DNA loading dye (6x)	Fermentas (R0611)
Dulbecco's Modified Eagle Medium (DMEM) + GlutaMAX	Gibco (21885-025 500ML)
Dulbecco's Phosphate Buffered Saline (DPBS)	Gibco (14190-094)
Ethylene Diamine TetraAcetic acid (EDTA)	Sigma Aldrich GmbH (03610.1KG)
Fluoroshield mounting medium with DAPI	Sigma (F6057)
Foetal bovine serum	PAN Biotech (1502-P122011)
Gel Red nucleic acid stain	Biotium (41003)
Glycine	Carl Roth GmbH (3790.3)
Hydrochloric acid (HCl) 32%	Carl Roth GmbH (P074.1)
Hydrogen Peroxide (H2O2)	Sigma Aldrich (95299-500ML)
LB broth powder	Sigma Life Science (L7658-1KG)
Luminol	Aldrich Chemistry (123072)
Magnesium sulphate heptahydrate ($MgSO_4.7H_2O$)	Sigma Aldrich (13142-1KG)
Methanol	Carl Roth GmbH (4627.2)
Opti-MEM	Gibco (31985-070)
Passive Lysis Buffer (5x)	Promega (E1941)
p-Coumaric Acid	Sigma Life Sciences (C9008-25G)
Penicillin-Streptomycin	Gibco (15140-122 100ML)
Protein Standard ladder	Bio Rad Precision Plus Kaleidoscope (161-0375)
Roti-Phenol	Carl Roth GmbH (0038.2)

Sodium Chloride (NaCl)	Sigma (S30.14-5KG)
Sodium Dodecyl Sulphate (SDS) 20% solution in H_2O	Sigma Life Science (05030-1L-F)
TEMED	Carl Roth GmbH (2367.1)
Tricine	Sigma Life Science (T0377-1KG)
Tris (hydroxymethyl) aminomethane	Sigma Aldrich (252859-500G)
Trypsin-EDTA	Gibco (25300-054 100ML)
Tryptone	Carl Roth GmbH (8952.2)
Tween-20	Sigma Life Science (P5927-500ML)
Yeast extract	Carl Roth GmbH (2904.3)

2.1.4 Kits used

Name	Manufacturer (Catalogue no.)
QIAquick PCR purification kit	Qiagen (28104)
QIAquick Gel Extraction kit	Qiagen (28706)
GenElute five-minute plasmid miniprep kit	Sigma life science (PFM250-1KT)
JetStar 2.0 plasmid purification maxikit	Genomed GmbH (220020)
miRVana miRNA isolation kit	Ambion (AM 1560)
RNeasy Plus mini kit	Qiagen (74134)
Qubit Protein Assay kit	Life Technologies (Q33212)

2.1.5 Buffer recipes

SDS PAGE sample buffer (2x)	
EDTA	25mM
Tris	100 mM
Glycerol	20%
SDS	4%
2 Mercaptoethanol	2%
Bromophenol blue	0.004%
SDS PAGE buffer (1x)	
Tris	25 mM
Glycine	190 mM
SDS	0.1%

Blotting buffer (1x)	
Tris	48 mM
Glycine	44 mM
SDS	0.04%
Methanol	20%

Tris Buffered Saline (TBS) (1x)	
Tris	20 mM
NaCl	150 mM
pH 7.6	

Tris Buffered Saline Tween-20 (1x)	
Tris	20 mM
NaCl	150 mM
pH 7.6	
Tween-20	0.1%

Developing solution A	
Luminol (500 mM in DMSO)	1 mL
0.1M Tris pH 8.0	400 mL
Developing solution B	
Coumaric acid (7 mM in DMSO)	
Developing solution: 10 mL Solution A + 1 mL Solution B + 5 µL 30% (w/w) H_2O_2	

TAE buffer (1x)	
Tris	40 mM
Acetic acid	20 mM
EDTA	1 mM

Balanced Salt Solution (BSS) (1x)	
Tris	25 mM
NaCl	120 mM
Glucose	15 mM
KCl	5.4 mM
$CaCl_2$	1.8 mM
$MgCl_2$	0.8 mM
pH 7.4	

D-Luciferin buffer (Firefly luciferase substrate)	
Solution A (4x)	
Tricine pH 7.8	120 mM
$MgSO_4$	15 mM
ATP	3 mM
DTT	5 mM
Coenzyme A	0.27 mM
Solution B	
D-Luciferin, sodium salt	100 mM
Working solution of D-Luciferin buffer	
Solution A (4x) 10 mL + Solution B 0.2 mL + 29.8 mL H_2O	

Coelenterazine buffer (Renilla luciferase substrate)
50x Stock solution: Coelenterazine 2 mM in CH_3OH
Working solution: Coelenterazine 0.04 mM in H_2O

2.1.6 Primers

ATXN3 3‘ UTR amplification primers	
Atxn3_utr1_xho1_for Atxn3_utr1_not1_rev	CTATGACTCGAGAAGGCCAGCCACCAGTTC TCACGCGGCCGCCAATGGAAAAAGGTAATG
DNAJB1 3‘ UTR amplification primers	
Dnajb1-utr-for-xho1 Dnajb1-utr-rev-not1	CCGCGGCTCGAGATAGCTATCTGAGCTCC TATCATGCGGCCGCGAGGTTTAGCATCAGTC
MID1 3‘ UTR amplification primers	
MID1UTR1_xho_for MID1UTR1_not1_Rev	GATACTCGAGGCGTCTGGCCACATGGAGCT CAATGCGGCCGCCTTAATTCATGGACCATTCCAACG
ATXN3 3’ UTR mutagenesis primers	
ATXN3_mir25_For ATXN3_mir25_Rev	TTTTCTTTTTTGAGTGTGCTTTATGTAACATGTCTAAAG CTTTAGACATGTTACATAAAGCACACTCAAAAAAGAAAA
ATXN3_miR181#1_For ATXN3_miR181#1_Rev	TTCCCAGATGCTTTATGAAACTCTTTTCACTTATATC GATATAAGTGAAAAGAGTTTCATAAAGCATCTGGGAA
ATXN3_miR181#2_For ATXN3_miR181#2_Rev	CATACGTACCCACCATGAAACTATGATACATGAAATT AATTTCATGTATCATAGTTTCATGGTGGGTACGTATG
ATXN3_mir125_For ATXN3_mir125_Rev	GCTGCACACATTTTATCACCGAAAGTTTTTTGATCTA TAGATCAAAAAACTTTCGGTGATAAAATGTGTGCAGC
ATXN3_miR9_For ATXN3_miR9_Rev	TCTTCCAAATATTAGCCATTGAGGCATTCAGCAATT AATTGCTGAATGCCTCAATGGCTAATATTTGGAAGA
ATXN3_miR383_For ATXN3_miR383_Rev	TCTTGTGTTGTTTTCTCTGTACACAACTTTTCTGCTAC GTAGCAGAAAAGTTGTGTACAGAGAAAACAACACAAGA
DNAJB1 3’UTR mutagenesis primers	
DNAJB1_370_1mutFor DNAJB1_370_1mutRev	CATCAGGTGGTGGGAACAGCGTGAAAAGGCATTCCAGTC GACTGGAATGCCTTTTCACGCTGTTCCCACCACCTGATG
DNAJB1_370_2mutFor DNAJB1_370_2mutRev	CAATACCTCTCGTTCCAGCGTGACCAAGGGAGCCAGC GCTGGCTCCCTTGGTCACGCTGGAACGAGAGGTATTG
DNAJB1 mir-543 For DNAJB1 mir-543 Rev	GGCTTTCGTACTGCTGAATCATTTCCAGAGCATATAT ATATATGCTCTGGAAATGATTCAGCAGTACGAAAGCC
DNAJB1 miR-449b For DNAJB1 miR-449b Rev	CTCATTGTAAGTTGCCACTGTTAACATGAGACCAAAGT ACTTTGGTCTCATGTTAACAGTGGCAACTTACAATGAG
DNAJB1 mir-143 For DNAJB1 mir-143 Rev	TGTCTTCTCTTTGGCCATCAGAAATTGAGAACCTAAA TTTAGGTTCTCAATTTCTGATGGCCAAAGAGAAGACA

MID1 3'UTR mutagenesis primers	
miR-216_sitemut_for miR-216_sitemut_rev	CTGGAAGAACATTAAGAATGAGTATGCAATTGAAAATAGT GACTATTTTCAATTGCATACTCATTCTTAATGTTCTTCCAG
miR-374_sitemut_for miR-374_sitemut_rev	GCTAGATTCATGCCTCAAAAGTTATTTAAAACAGACCTTTATTAA TTAATAAAGGTCTGTTTTAAATAACTTTTGAGGCATGAATCTAGC
miR-542_sitemut_for miR-542_sitemut_rev	GAGTAAATAAACATGTTCTGTGTCAAATAGCAGCACCACT AGTGGTGCTGCTATTTGACACAGAACATGTTTATTTACTC
premiR-32 amplification primers	
premiR-32_for premiR-32_rev	TGCATCTAGAATGATCATTGCTGAC CTGCTGAATTCATTGAAGTTTTGAACC
Sequencing primer	
Rluc3end	GTGCTGAAGAACGAGCAG
Real-time PCR primers	
Real-time PCR primers (Human)	
ACTB_for_qpcr	AAAAGCCACCCCACTTCTCT
ACTB_rev_qpcr	CTCAAGTTGGGGGACAAAAA
DNAJB1_for_qpcr	GCAGTCTTGATTCCCAGACC
DNAJB1_rev_qpcr	GCTGGAACGAGAGGTATTGC
ATXN3_for_qpcr	CCGCAGGGCTATTCAGCTAA
ATXN3_rev_qpcr	CTCGTCTCTTCCGAAGCTCTTC
GAPDH_for_qpcr	CCACCCATGGCAAATTCC
GAPDH_rev_qpcr	TGGGATTTCCATTGATGACAAG
MID1_for_qpcr	CTGCCAGGTCTGGTGTCATG
MID1_rev_qpcr	AATCAGGCTTAGGGCCCTTCT
Real-time PCR primers (Mouse)	
GAPDH_MM_For	GCACAGTCAAGGCCGAGAAT
GAPDH_MM_Rev	GCCTTCTCCATGGTGGTGAA
Dnajb1_MM_For2	AGGCTCTCTGTGGTTGCACT
Dnajb1_MM_Rev2	TTCTGGATGAGACGGGAATC

2.1.7 miRNA mimics/siRNAs

miRNA mimics	Sequence
hsa-miR-32	UAUUGCACAUUACUAAGUUGCA
hsa-miR-181c	AACAUUCAACCUGUCGGUGAGU
hsa-miR-216a-5p	UAAUCUCAGCUGGCAACUGUGA
hsa-miR-374a-5p	UUAUAAUACAACCUGAUAAGUG
hsa-miR-542a-3p	UGUGACAGAUUGAUAACUGAAA
hsa-miR-370	GCCUGCUGGGGUGGAACCUGGU
hsa-miR-543	AAACAUUCGCGGUGCACUUCUU
control siRNA1	AATTCTCCGAACGTGTCACGT

2.1.8 Antibodies

Primary antibodies

The abbreviations IB and IF stand for immunoblotting and immunofluorescence respectively and denote the application for which a specific antibody dilution was used.

Name	Source	Dilution	Company/Provider
GAPDH	Rabbit monoclonal	IB: 1: 5000	Cell Signalling (2118L/2118S)
DNAJB1 (Hsp40)	Rabbit polyclonal	IB: 1:5000 IF: 1:300	Enzo (ADI-SPA-400)
α-Tubulin	Rat monoclonal	IB: 1:5000	Serotec (MCA77G)
c-Myc	Mouse monoclonal	IF: 1:300	Clontech (631206)
ATXN3, clone 1H9	Mouse monoclonal	IB: 1: 1000	Millipore (MAB5360)
MID1	Rabbit polyclonal	IB: 1:200	AG Krauss (DZNE, Bonn)
ATXN3 (no.986)	Rabbit polyclonal	IB: 1:5000	Dr. Peter Breuer (Uniklinik Bonn)

Secondary antibodies

Name	Dilution	Company
goat α rat igG-HRP conjugated	IB: 1:3000	SantaCruz biotech (SC-2303)
goat α mouse igG-HRP conjugated	IB: 1:3000	Dianova (115-035-003)
donkey α rabbit igG-HRP conjugated	IB: 1:3000	Amersham (NA-9340)
goat α mouse igG-Cy3 conjugated	IF: 1: 1000	Dianova (715-166-151)
goat α rabbit igG-Alexa Fluor 647 conjugated	IF: 1: 1000	Invitrogen (A 21244)

2.1.9 Cell lines

Cell line	Source
Hela	Human cervical cancer
HEK-T 293	Human embryonic kidney
iPSC-derived neurons	Neurons differentiated from iPSCs derived from control and SCA3 patient fibroblasts

2.1.10 Cell and bacterial culture media

Hela/HEK-T 293 culture medium	
DMEM+GlutaMAX	89%
FBS	10%
Penicillin (10,000 U/mL) + Streptomycin (10,000 µg/mL)	1%

Cell freezing medium	
DMEM+GlutaMAX	50%
FBS	40%
DMSO	10%

Luria Broth and Luria Broth agar	
LB powder	20.6 g (per 1 litre of H_2O)
Agar (optional; used for plates)	15 g
Autoclave 15 min at 121°C	

Section 2.2 Methods

2.2.1 Prediction of miRNA target sites

Predictions for miRNA binding sites on 3'UTRs of ATXN3, MID1, DNAJB1 were done using the following two target prediction tools:

1. TargetScan Human prediction database Release 6.2, June 2012 (www.targetscan.org) (Lewis et al, 2005)

TargetScan considers several parameters contributing to mRNA targeting by stable mRNA-miRNA binding at specific sites such as:

- Type of Watson-Crick (WC) match at the seed region of the miRNA (8mer, 7mer-m8, 7mer-A1) (Grimson et al, 2007)
- WC match at the 3' end of the miRNA (Friedman et al, 2009; Grimson et al, 2007)
- Number of A and U nucleotides flanking the miRNA sequence (Grimson et al, 2007)
- Position of the target site within the entire mRNA (Grimson et al, 2007)
- Free energy of the mRNA-miRNA duplex (Garcia et al, 2011)
- Abundance of mRNAs with target sites for a particular miRNA (Garcia et al, 2011)
- Preferential evolutionary conservation of the specific target site to maintain miRNA targeting (Lewis et al, 2005)

For the TargetScan predictions, the longest 3'UTR of the respective mRNAs was considered. miRNAs belonging to miRNA families either conserved only in mammals or conserved broadly in vertebrates were considered for the predictions.

2. miRanda-miRSVR database, August 2010 Release (www.mirna.org) (Betel et al, 2010; Betel et al, 2008)

For the miRanda-miRSVR predictions, the species was defined (*Homo sapiens*) and the predictions for the suggested transcript were considered along with miRNA binding alignment details.

2.2.2 Molecular cloning

Cloning of 3'UTR sequence into the luciferase reporter vector

Sequence of the 3' UTRs of ATXN3, MID1, DNAJB1 containing the miRNA binding sites of interest were cloned downstream of the Renilla luciferase gene in the psiCHECK-2 vector. Figure 2.1 shows as an example the 3'UTR of ATXN3 cloned into the pSICHECK-2 vector.

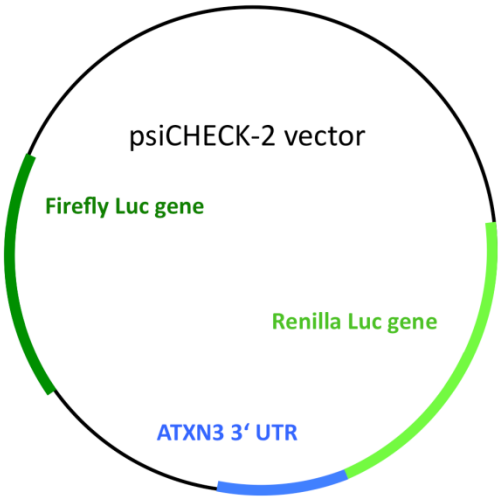

Figure 2.1: Map of the psiCHECK-2 reporter vector with partial sequence of ATXN3 3'UTR cloned downstream of the Renilla luciferase gene. The Firefly luciferase also present on the vector is used for signal normalization.

ATXN3, MID1 and DNAJB1 3'UTR fragments were PCR amplified prior to being cloned into the psiCHECK-2 luciferase reporter vector according to the procedure as follows.

Forward and reverse primers to PCR amplify the 3'UTR fragments were designed containing digestion sites for the restriction enzymes *xho1* and *not1* respectively (**table 2.1.6**). The amplification reaction mix and the reaction conditions are shown in the table below. Genomic DNA extracted from Hela cells was used as template for the PCR reaction. All reagent additions were done on ice.

Reagent	Volume (µL)	Final conc.
Gotaq Green master mix (2x)	12.5 µL	1x
Forward primer (10 µM)	1 µL	400 nM
Reverse primer (10 µM)	1 µL	400 nM
DNA template (100ng/µL)	1 µL	4 ng/µL
DMSO	0.5 µL	2%
ddH_2O	9 µL	
Cycling conditions		
3 min 95°C; 34x(30 sec 95°C, 30 sec 58°C, 2 min 72°C); 10 min 72°C		

Following the PCR reaction, the molecular weight of the PCR product was analysed by agarose gel electrophoresis of 3 µL aliquot of the PCR product using a gel containing 1% agarose in 1x TAE. The PCR product was purified using the QIAquick PCR purification kit according to the manufacturer's instructions. The concentration of the purified PCR product was measured using the Nanodrop spectrometer. Digestion reactions to digest the PCR product and psiCHECK-2 vector by *xho1* and *not1* restriction enzymes were prepared as shown in the table below. All reagent additions for the restriction digestion reaction were done on ice.

Reagent	Volume (µL)	Final conc.
10x NEB buffer 3	5	1x
xho1 (20 U/µL)	1	0.4U/µL
not1(10 U/µL)	1	0.4U/µL
100x BSA	0.5	1x
Purified DNA (PCR product/psiCHECK-2 vector) (50 ng/µL)	20	1µg/50µL
ddH_2O	22.5	
Double digestion mix incubated at 37°C for 4 hours		

The digested psiCHECK-2 vector was separated from the undigested vector by agarose gel electrophoresis of the digestion mix (1% agar in 1x TAE). The gel piece carrying the digested vector was cut out with a scalpel and the vector DNA extracted using the

QIAquick Gel extraction kit using the manufacturer's instructions. Meanwhile the double digested PCR product was purified using the QIAquick PCR purification kit according to the manufacturer's instructions. The DNA concentration of the digested, purified PCR product and psiCHECK-2 vector was measured using the Nanodrop spectrometer.

A ligation reaction to ligate the double digested insert (PCR product) into the double digested psiCHECK-2 vector was setup with insert:vector molar ratio of 3:1 as shown in the table below.

Reagent	Volume (µL)	Final conc.
10x T4 DNA ligase buffer	2	1x
Insert (20ng/µL)	3.5	75ng/20µL
Vector (25ng/µL)	3	70ng/20µL
ddH_2O	10.5	
T4 DNA ligase (400U/µL)	1	20U/µL
Ligation mixture incubated at 16°C for 16 hours		

Bacterial transformation of *E.coli* Top10 with ligation mixture

A 50µL aliquot of the competent cells was transformed with 2µL of the ligation mixture following which cells were placed on ice for 20 minutes, given a heat shock at 42°C for 1 minute, further kept on ice for 30 minutes, 250 µL of LB medium was added and the cells were incubated at 37°C for 45 minutes on bench top shaker. 50 µL and 250 µL aliquots of the cell suspension were plated onto two LB agar plates with 100 µg/mL Ampicillin. Plates were incubated for 16 hours at 37°C.

Following incubation, 5-10 colonies appearing on the plates were picked and used to inoculate 500 µL aliquots of LB medium with 100 µg/mL Ampicillin in microcentrifuge tubes. Following incubation at 37°C for 16 hours on the shaker, the aliquots which showed visible signs of bacterial growth (medium getting turbid) were further utilized to extract plasmid DNA using the GenElute Five minute plasmid miniprep kit (Sigma Life Science).

Plasmid DNA extracted was double digested with *xho1* and *not1* in order to verify the insertion of the required fragment in the vector. The digestion reaction was set up similar to the one in the table above but with smaller total reaction volume (total reaction volume being 15µL) with the volumes of the reagents reduced proportionally. The digested

plasmid DNA was run on 1% agarose gel to separate the cleaved insert from the vector. Up to three clones carrying the insert as suggested by agarose gel electrophoresis were sequenced using the reverse primer used for PCR amplification and the Rluc3'end primer. The sequencing was done by GATC Biotech and the sequences were analysed using the 4Peaks software.

Based on the sequencing results a bacterial clone carrying the plasmid with the desired insert sequence was chosen for generation of large amounts of the plasmid to be used for transfection experiments of mammalian cells. For this, 100 mL of LB with 100µg/mL of Ampicillin was inoculated with an aliquot of the bacterial clone. The inoculum was incubated in a shaker incubator at 37°C for 16 hours at 150 rpm. Plasmid DNA was extracted from the bacterial suspension using the Jetstar 2.0 plasmid maxiprep kit. The purified plasmid DNA was eluted in 1 mL of Nuclease free H_2O and the DNA concentration measured using the Nanodrop spectrometer.

The presence of the insert and its sequence were verified once more by repeating the *xho1, not1* double digest and sequencing as described above.

Site directed mutagenesis of miRNA binding sites in 3'UTR sequences

Complementary forward and reverse primers were designed to include the intended base pair substitution mutations in the middle of the primer sequence with flanking regions of unmodified sequence on both sides (**table 2.1.6**). Using the psiCHECK-2 vector with the wild type 3'UTR of ATXN3, MID1 or DNAJB1 as the DNA template, the vector carrying the mutations in the insert was PCR amplified using the high fidelity *Pfu ultra II* DNA polymerase as per the reaction mix in the table below.

Reagent	Volume (µL)	Final conc.
10x *Pfu ultra II* HF reaction buffer	5	1x
Forward primer (10 µM)	1	200 nM
Reverse primer (10 µM)	1	200 nM
DNA template (50 ng/µL)	1	1ng/µL
dNTP mix (40 mM)	1	800 µM
DMSO	3	6%
ddH_2O	37	
Pfu ultra II HF polymerase (2.5U/µL)	1	0.05U/µL
Cycling conditions		
1 min 95°C; 18x (50 sec 95°C, 50 sec 60°C, 8 min 68°C); 7 min 68°C		

1 µL of *Dpn I* restriction enzyme (10U/µL) was added to the PCR product and the product was incubated at 37°C for 2 hours to digest the non-mutated vector. 5 µL of the digested product was separated on 1% agarose gel. Presence of a band at the expected molecular weight confirmed the PCR amplification of the vector with the mutant insert. The subsequent procedure including bacterial transformation, plasmid DNA extraction, sequencing was the same as described before.

Cloning of premiR-32 into the pMIRNA1 vector

pMIRNA1 vector containing premiR-181c was purchased. The miR-32 stem loop sequence alongwith 200 nt on either flanks was cloned into the pMIRNA1 vector after cleaving out the premiR-181c sequence. A representation of this is shown in **Figure 2.2**. In order to clone premiR-32 into the vector, the premiR-181c sequence was cleaved out using sequential digestion with *Xba1* and *EcoRI*. Cloning primers to amplify premiR-32 were designed containing digestion sites for *Xba1* and *EcoRI*. PCR amplification reaction was set up according to the table below.

Reagent	Volume (µL)	Final conc.
Gotaq Green master mix (2x)	12.5 µL	1x
Forward primer (10 µM)	1 µL	400 nM
Reverse primer (10 µM)	1 µL	400 nM
DNA template (100ng/µL)	1 µL	4 ng/µL
DMSO	0.5 µL	2%
ddH_2O	9 µL	
Cycling conditions		
3 min 95°C; 34x(30 sec 95°C, 30 sec 60°C, 2 min 72°C); 10 min 72°C		

The molecular weight of the amplified PCR product was verified using 1% agarose gel electrophoresis. The product was purified using QIAquick PCR purification kit. The PCR product as well as pMIRNA1 vector were digested by *xba1*, purified and then digested by *EcoRI* as per the table below

Reagent	Volume (µL)	Final conc.
10x NEB buffer 4/EcoRI buffer	5	1x
xba1 (20 U/µL)/*EcoRI* (20 U/ µL)	1	0.4U/µL
100x BSA	0.5	1x
Purified DNA (PCR product/pMIRNA1 vector) (50 ng/µL)	20	1µg/50µL
ddH_2O	22.5	
Digestion mix incubated at 37°C for 2 hours for each digestion step		

The digested vector as well as the PCR product were gel extracted using the QIAquick gel extraction kit. The ligation of the vector and the insert, bacterial transformation and the Maxiprep extraction were as described for the cloning procedure for inserts in the psiCHECK-2 vectors.

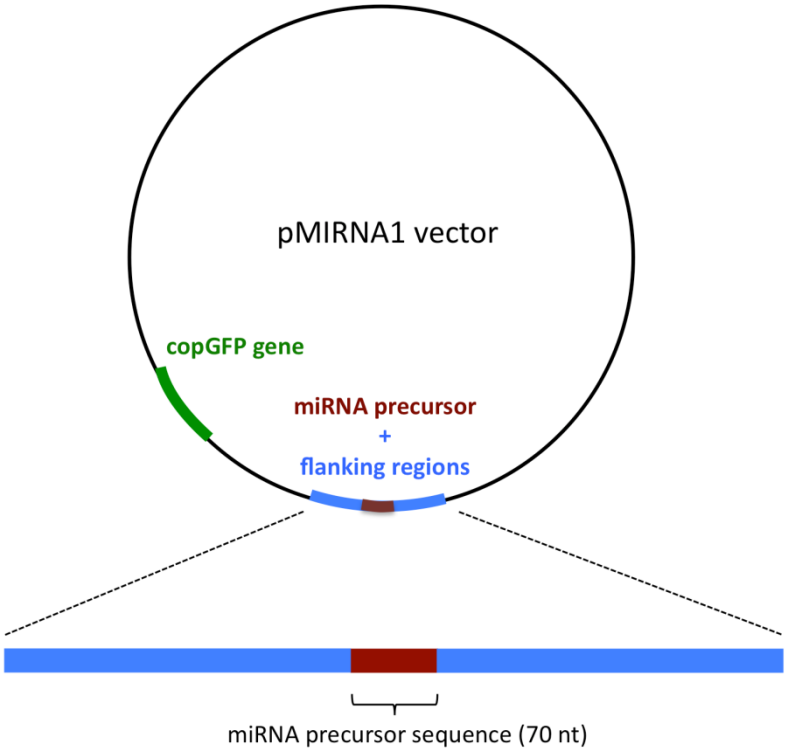

Figure 2.2: The pMIRNA1 vector was used to over express miR-32 and miR-181c. Precursor sequence of miR-32 (70 nt, shown in red) along with flanking sequences on both sides (200 nt, shown in blue) was cloned in the pMIRNA1 vector.

2.2.3 Cell culture methods

Maintenance of human cancer cell lines

Details regarding the origin of Hela and HEK T-293 cells used are given in **table 2.1.9**. The cells were cultured in DMEM supplemented with 10% FBS, 100 U/mL of Penicillin, 100 µg/mL of Streptomycin. Cells were grown in 75/150 cm^2 tissue culture flasks at 37°C and 5% CO_2. For subculturing the cells were washed 1x in PBS and dislodged from the flask surface by incubation with Trypsin-EDTA for 5 minutes. The trypsinized cells were resuspended in complete medium. The cells were subcultured at a dilution of 1:10-1:20 depending on the cell line three times a week. The subculturing was done in sterile conditions under the Laminar airflow hood.

Counting of cells

Cells were trypsinized and resuspended in complete medium. 25 µL of the cell suspension was diluted in 10 mL of CASY ton solution in a CASY tube. The capillary of the CASY cell analysis system was washed 1x in CASY ton. The CASY tube carrying the cell suspension was placed under the capillary and the cells counted choosing the appropriate program (default programs for Hela and HEK T-293 cells were used). Cell count per mL was calculated by considering the dilution factor (by multiplying the displayed cell count by 4).

Freezing of cells

Cells grown to about 80% confluency in tissue culture flasks were trypsinized, suspended in complete medium and transferred to 50 mL centrifuge tube. Cells were counted to determine the cell count per mL and centrifuged at 1500 rpm for 5 minutes in order to pellet them. The supernatant was removed and the cells were resuspended in ice cool freezing medium (50% DMEM, 40% FBS, 10% DMSO). The volume of freezing medium for resuspension was such that the cell count would be 2 million cells per mL of freezing medium. 1 mL aliquots of the resuspended cells were prepared in cryo tubes. The cryo tubes were immediately transferred to a pre cooled cell freezing container containing isopropyl alcohol and transferred to -80°C freezer. After storage -80°C for 24 hours the cells were transferred to the liquid nitrogen tank for long term storage.

Thawing of cells

Cells frozen in liquid nitrogen were thawed by immersing the cryo tube in water bath at 37°C till the ice crystals inside the cryo tube had melted. Cells from each cryo tube were transferred to 150 cm^2 tissue culture flask containing complete medium. Cells were incubated under appropriate culture conditions (37°C, 5% CO_2) for 24 hours after which the medium was replaced with fresh complete medium.

Transfection of miRNA mimics and control siRNAs

Cells were transfected with miRNA mimics and control siRNAs using the method of reverse transfection, in which the transfection mix was added to the cell culture plate first and cells were then seeded into the mix. Two separate solutions, solution A containing the miRNA mimics or control siRNAs and solution B containing the transfection reagent Lipofectamine 2000 were prepared separately in microcentrifuge tubes. For the miRNA mimics, each mimic was transfected at a final amount of 30 picomoles per well of the 12-well plate. The control siRNA amounts were adjusted according to the number of miRNA mimics transfected together such that the total RNA amount was equal in the control/test wells. Therefore, 60 picomoles of control siRNA were used in the experiment where two miRNAs transfected, 90 picomoles of control siRNA for experiment where three miRNAs were transfected. The table below shows the transfection mix preparation for experiment with two miRNA mimics.

		Volume per one well of 12-well plate (µL)
Solution A	Opti-MEM	47
	miRNA1 stock (20 µM)	1.5
	miRNA2 stock (20 µM)	1.5
Solution B	Opti-MEM	49
	Lipofectamine 2000	1

Solution A was added dropwise to solution B to make up the transfection mix. The transfection mix was incubated on the benchtop for 20 minutes. The transfection mix was then added to each well of a 12-well plate. While the transfection mix was incubating, the cells were trypsinized, counted and a cell suspension with a cell count of 100,000 cells/mL was prepared in complete medium. 1 mL of the cell suspension was added dropwise to each well of the 12-well plate already containing the transfection mix. The cells were grown for 48 hours under appropriate culture conditions (37°C, 5% CO_2).

Transfection of Luciferase reporter vectors

Cells were transfected with Luciferase reporter constructs using the method of forward transfection, in which the cells were seeded in plates prior to transfection. In this experiment, the cells were seeded in 12-well tissue culture plates at a density of 100,000

cells/well 24 hours prior to transfection. On the day of transfection, two separate solutions, solution A containing the luciferase reporter constructs and solution B containing the transfection reagent Lipofectamine 2000 were prepared separately in microcentrifuge tubes as per the calculations in the table below.

		Volume per one well of 12-well plate (µL)
Solution A	Opti-MEM	96
	Luciferase reporter vector (100 ng/µL)	4
Solution B	Opti-MEM	98
	Lipofectamine 2000	2

Solution A was added dropwise to solution B to make up the transfection mix. The transfection mix was incubated on the benchtop for 20 minutes and added to each well of the 12-well plate containing the seeded cells. The cells were grown for 48 hours under appropriate culture conditions (37°C, 5% CO_2).

Transfection of pMIRNA1 vector containing precursor miRNA sequence inserts

Transfection of Hela cells with pMIRNA1 vectors containing precursor miRNA sequence inserts was carried out similar to the transfection of luciferase constructs in terms of the cell density, transfection time, incubation conditions. The transfection mix was prepared as shown in the table below.

		Volume per one well of 12-well plate (µL)
Solution A	Opti-MEM	96
	pMIRNA vector (500 ng/µL)	4
Solution B	Opti-MEM	98
	Lipofectamine 2000	2

Co-transfection of miRNA mimics and c-terminal ATXN3 contruct

Cells were co-transfected with miRNA mimics/control siRNAs and c-terminal ATXN3 constructs using the method of forward transfection. In this experiment, the cells were seeded in lab-Tek II chamber slides at a density of 40,000 cells/chamber, 24 hours prior to transfection. On the day of transfection, two separate solutions, solution A containing the miRNA mimics/control siRNAs and the c-terminal ATXN3 construct and solution B containing the transfection reagent Lipofectamine 2000 were prepared separately in microcentrifuge tubes. 7.5 picomoles of two miRNAs were transfected together. Therefore, the control siRNA amount transfected in the control wells was 15 picomoles. The transfection mix was prepared as shown in the table below.

		Volume per one chamber of a slide (µL)
Solution A	Opti-MEM	10.5
	miRNA stock (20 µM)	0.375
		0.375
	c-terminal ATXN3 contruct (200 ng/µL)	1.25
Solution B	Opti-MEM	11.75
	Lipofectamine 2000	0.75

Solution A was added dropwise to solution B to make up the transfection mix. The transfection mix was incubated on the benchtop for 20 minutes and added to each well of the 12-well plate containing the seeded cells. The cells were grown for 48 hours under appropriate culture conditions (37°C, 5% CO_2).

Harvesting and pelleting of cells

Cell pellets were prepared for RNA or protein extraction. Cells were trypsinized, resuspended in complete medium and transferred to microcentrifuge tubes. The cells were centrifuged at 1500 rpm for 10 minutes at 4°C. The cell pellet was washed 1x with ice cold PBS and the centrifugation step above was repeated. The PBS was aspirated and the cell pellets were either lysed in appropriate buffers for RNA/protein extraction or stored at -20°C.

Cells transfected with luciferase reporter vectors and used for luciferase assays were washed 1x in PBS in the tissue culture plate followed by addition of 100 µL of passive lysis buffer to each well of 12-well plate. The plates were incubated on shaker at room temperature for 20 minutes followed by transfer of the cell lysate into microcentrifuge tubes. The cell lysates were either used directly for luciferase assays or stored at -20°C.

Harvesting of iPSC derived neurons

Control and SCA3 iPSC derived neurons grown in 6 cm dishes were washed three times in balanced salt solution (BSS), gently dislodged from the dish surface with a cell scrapper and transferred to a 50 mL centrifuge tube. The cells were pelleted by centrifugation at 1500 rpm for 10 minutes. The BSS was aspirated, the pellets were flash frozen in liquid nitrogen and stored at -80°C.

2.2.4 Molecular biology methods

Total RNA quantification

Total RNA extraction including small RNAs from iPSC derived neurons was conducted using the miRVana miRNA isolation kit according to the manufacturer's instructions. Total RNA extraction from human cell lines, mouse brain samples was conducted using the RNeasy plus mini kit according to the manufacturer's instructions. In both cases, the total RNA was eluted in nuclease-free H_2O preheated to 70°C.

Reverse transcription

Reverse transcription was carried out using the Taqman reverse transcription kit according the manufacturer's instructions. The reverse transcription reaction was set up with a final volume of 50 µL. 1 µg of total RNA was used as template, with random hexamers used as primers. The reaction mixture and the cycling conditions are shown in the table below.

Reagent	Volume (µL)	Final conc.
10x Reverse transcriptase buffer	5	1x
$MgCl_2$ (25 mM)	11	5.5 mM
dNTPs (10 mM)	10	2 mM
Random hexamers (50 µM)	2.5	2.5 µM
RNase Inhibitor (20 U/µL)	1	0.4 U/µL
Multiscribe reverse transcriptase (50 U/µL)	2.5	1 U/µL
RNA template (500 ng/µL)	2	20 ng/µL
Nuclease free H_2O	16	
Cycling conditions		
10 min 25°C; 30 min 37°C; 5 min 95°C; hold 4°C		

SYBR Green Real-time PCR

SYBR Green dye based real-time PCR amplification was done in the 7900HT Fast Real-time PCR cycler in 384 well plates. SYBR Green PCR master mix (Life technologies) containing SYBR Green1 dye, Amplitaq DNA polymerase and dNTPs with dUTP was used for amplification. cDNA produced by reverse transcription of RNA samples was diluted 1:10 to be used as template for the real-time PCR. Primers used in the real-time PCR have been listed in table 2.1.6. In each experiment, serial dilutions of one of the samples (usually one of the controls) were prepared to serve as reference for plotting of a standard curve plot for cDNA quantification. The PCR mix in each well and the cycling conditions were as described in the table below. All samples were loaded in triplicates. A dissociation stage was added at the end of each amplification cycle to check for amplification of multiple products. Following the amplification, wells flagged for errors in the signal were omitted from the calculations. Data was exported to MS Excel for analysis.

Reagent	Volume (µL)
SYBR Green PCR master mix (2x)	10
Forward primer (10 µM)	1.5
Reverse primer (10 µM)	1.5
cDNA (1:10 diluted)	7
Cycling Conditions	
2 min 94°C; 40x (15 sec 94°C, 1 min 60°C)	

Protein quantification

Total protein in samples was quantified using the Qubit fluorometer and Qubit Protein assay kit according to manufacturer's instructions. Prior to quantification, the samples were homogenized by pipetting gently.

SDS PAGE

Protein separation on the basis of molecular weight was carried out according to the method described by Shapiro and Laemmli (Laemmli, 1970; Shapiro et al, 1967). The SDS polyacrylamide gel was prepared using two glass plates separated by spacers with a thickness of 1.5 mm placed inside a casting chamber. For separation of the proteins, a 'running gel' containing 10% acrylamide/bisacrylamide was prepared (formula given in table below) and poured to cover around 70% of the space between the glass plates. Isopropyl alcohol was poured to cover up the rest of the space between the glass plates till the running gel polymerized. Upon gel polymerization, the isopropyl alcohol was poured off by inverting the glass plates and the space was filled by pouring in the 'stacking gel' containing 5% acrylamide/bisacrylamide. A plastic comb containing 10/15 teeth was placed on top of the stacking gel to prepare sample wells. Upon polymerization of the stacking gel, the comb was removed and the sample wells formed were washed with electrophoresis buffer to remove any gel residue. The gel within the glass plates was transferred to the gel electrophoresis chamber and the chamber was filled with

electrophoresis buffer to an appropriate level as denoted on the chamber. The samples were loaded onto the sample wells, with one well reserved for the protein molecular weight ladder. Protein separation by electrophoresis was carried out by keeping the voltage constant at 100V. The electrophoresis was terminated once the visible migration border of the sample loading dye had passed out of the gel.

Reagent	Volume (mL) for a total of 10 mL	
	Running gel (10% acrylamide/bisacrylamide)	Stacking gel (5% acrylamide/bisacrylamide)
H_2O	4	6.8
30% Acrylamide mix	3.3	1.7
1.5 M Tris (pH 8.8)	2.5	1.25
10% SDS	0.1	0.1
10% Ammonium persulfate	0.1	0.1
TEMED	0.004	0.01

Immunoblotting

The transfer of proteins from SDS gels to membranes is based on the technique described by Renart and Towbin (Renart et al, 1979; Towbin et al, 1979). Following electrophoretic separation of the proteins, the gel was removed from the glass plates and incubated in 1x blotting buffer for 10 minutes. Meanwhile, PVDF membrane of appropriate size was immersed in 100% methanol, washed in distilled H_2O and immersed in 1x blotting buffer. In the semi dry blotting apparatus used, a Whatman paper of appropriate size soaked in 1x blotting buffer was placed followed by the PVDF membrane, the gel and finally another Whatman paper soaked in 1x blotting buffer. The lid containing other electrode of the apparatus was placed on top and the immunoblotting was carried out for 40 minutes at 20V. The molecular weight ladder bands were marked using a pen to serve as reference marks during immunostaining.

Immunostaining

The PVDF membrane with the transferred proteins was blocked in the blocking solution (3% BSA in TBST) for 1 hour at room temperature. The membrane was incubated with a solution containing the primary antibody at appropriate dilution (see table 2.1.8 for antibody dilutions) in blocking buffer for 12-15 hours at 4°C. The membrane was washed 3x in TBST, followed by incubation with secondary antibody diluted in TBST for 1 hour at room temperature. Following incubation with the secondary antibody the membrane was again washed 3x in TBST. The developing solution was prepared as described in section 2.1.5. The washed membrane was briefly incubated in the developing solution containing substrate for the horse radish peroxidase enzyme. The membrane was then placed between plastic sheets and placed inside the Stella immunoblot imaging system. Images were taken at intervals ranging from 5 seconds to 10 minutes. Signals from the blots were quantified using AIDA imaging software.

Immunocytochemistry

Cells grown in Lab-Tek II chamber slides were washed once in PBS and fixated by incubation with 200 µL of 4% PFA in PBS for 15 minutes at room temperature. Following the fixation, the cells were washed thrice in PBS. The cells were then permeabilized by incubation with 200 µL of 0.5% Triton-X in PBS for 10 minutes at room temperature. The cells were again washed thrice in PBS and incubated with blocking solution, i.e. 200 µL of 0.5% BSA in PBS for 20 minutes at room temperature. Following blocking, the cells were incubated in 150 µL of blocking solution containing appropriate dilutions (table 2.1.8) of one or two primary antibodies for 16 hours at 4°C. The cells were again washed thrice in PBS and incubated with 150 µL of PBS containing the secondary antibodies for 30 minutes at room temperature in dark. Following incubation with the secondary antibody solution, the cells were washed thrice in PBS, the chamber walls were removed and Fluoroshield mounting medium containing DAPI was applied drop wise to the samples. Coverslips were gently placed over the mounted samples and the sides were sealed using a suitable sealant. Slides were directly used for sample visualization using the Laser scanning microscope, or were stored in the dark at 4°C.

Luciferase assay

Lysates to be used for luciferase assay were diluted in H_2O to attain a concentration of 1 µg/µL. 10 µg of the protein lysate was pipetted into each well of a 96-well white plate. Each sample was pipetted in triplicate, for both the renilla and firefly luciferase measurements. Substrates for firefly and renilla luciferase were prepared as per the recipe given in section 2.1.5. The luciferase assay was conducted in Envision plate reader (Perkin Elmer). The reader was programmed to inject 40 µL renilla and firefly substrates in each well and measure luminescence signal following a lag of 2 seconds. Signal values were exported to and analysed in MS Excel.

2.2.5 Microscopy and image analysis

Confocal optical images of immunostained cells were taken using the Zeiss LSM 700 microscope with a 20x air objective. Images were acquired using the Zen 2009 software through tilescans of multiple replicate chambers on the slide with identical transfection conditions. Image analysis to count the number of cells with aggregates was done using an algorithm setup by Dr. Möhl (Data and Image Analysis facility, DZNE Bonn).

2.2.6 Mouse hindbrain isolation

The maintenance and work with the B6.SCA3-YAC-84Q mice was conducted according to relevant national authority guidelines. 26 week old control and transgenic mice were sacrificed and the brain dissected to separate the hindbrain including the cerebellum, pons and the brain stem. The hindbrain was flash frozen in liquid nitrogen and broken up using a mortar and a pestle.

Total RNA was extracted from the pulverized hindbrain using the RNEasy plus mini kit. RNA was quantified using the Nanodrop spectrometer. cDNA extraction and SYBR Green real-time PCR was done according to the procedure described before. Protein was extracted by homogenizing the pulverized hindbrain samples in SDS PAGE sample buffer, sonication and boiling at 95°C for 10 minutes.

2.2.7 Gene and miRNA expression profiling and analysis

Gene and miRNA expression profiling by RNA-seq

The gene expression and miRNA expression profiling was done using the technique of RNA-seq by the group of Dr. Stefan Bonn (Work group for computational analysis of biological networks, DZNE Göttingen) on an Illumina HiSeq2000TM with libraries prepared according to the Illumina TruSeq mRNA and small RNA protocols respectively. The FASTQ files generated for the gene expression profiling were used for analysis by the CLC Workbench (details below) in house. The analysis of the miRNA expression profile including steps such as trimming, sequence quality check, alignment of the sequences to small RNA transcript databases and differential small RNA analysis was conducted by the aforementioned group.

Differential gene expression analysis by CLC genomics workbench

The gene expression profile data was analysed using the CLC genomics workbench. RNA-seq files for the gene expression profile were imported to the CLC server. The sequences were trimmed using default parameters to remove low quality sequences, ambiguous nucleotides and sequences below specific, defined length. The sequences were then assembled, i.e. they were aligned by comparing to reference sequences from GenBank, in order to make contiguous sequences. Default parameters were used for sequence assembly. The control and SCA3 patient samples were grouped into ‘control’ and ‘patient’ groups respectively. An experiment was then set up to analyse the differential expression of genes between the control and patient groups. Results were displayed including parameters such as mean expression values in the groups, fold changes in gene expression between the two groups with the p-values corrected for False Discovery Rate (FDR). The data was exported to MS Excel where it was sorted, filtered and arranged in lists which served as starting points for Gene Ontology analysis, pathway analysis.

Gene ontology and pathway analysis of dysregulated genes

Gene Ontology analysis and Pathway analysis was conducted using the Toppfun tool from the Toppgene Suite (https://toppgene.cchmc.org/enrichment.jsp) (Chen et al, 2009). Default parameters for the correction, p-value cutoff were used. Lists were exported to MS Excel to be sorted.

Protein interaction analysis

Protein interaction analysis was conducted using the STRING database, ver 9.1 (http://string-db.org) (Franceschini et al, 2013). The multiple names input option was used for gene list and the actions view was used for the graphic representation of the protein interaction analysis.

Pathway analysis of dysregulated miRNAs

miRNA pathway analysis was done using the MIRSYSTEM, May 2014 release (Lu et al, 2012). The 'miRNAs to targets' tool was used to calculate the enrichment of the predicted miRNA targets into pathways via the 'pathway ranking summary' option in the tool. Results were exported to MS Excel for sorting, filtering.

2.2.8 Software used

4Peaks

DNA sequences obtained from Sanger sequencing were analyzed using the 4Peaks software. The quality of the sequence was verified by analyzing the peaks representing the four nucleotides in the DNA sequence.

AIDA image analyzer

Immunoblot images were quantified using the AIDA image analysis software from Raytest. The areas containing signal bands from individual samples were selected and the

signal intensity measured. After subtraction of the background signal, the signal values were exported to MS Excel.

GraphPad Prism version 6

Statistical analysis and bar graph images were prepared using the Prism version 6 software.

Chapter 3 Results

3.1 miRNA targeting of ATXN3

One of the main goals of this project was the identification of miRNAs able to target the ATXN3 mRNA by binding at specific sites on the 3'UTR leading to modulation of the ATXN3 protein expression. Therefore, the following steps were taken:

- *In silico* prediction of miRNAs targeting the 3'UTR of ATXN3 mRNA .
- Validation of the ability of the selected miRNAs to bind at specific sites on the 3'UTR of ATXN3 mRNA.
- Analysis of the miRNAs' effect on endogenous ATXN3 mRNA and protein levels in human cell lines.

3.1.1 *In silico* prediction of miRNAs targeting the 3'UTR of ATXN3 mRNA

The 3'UTR of ATXN3 mRNA is 5904 nt long. Several tools that enable miRNA target prediction are available, each with a different algorithm for predicting the strength of the miRNA-target mRNA binding. The TargetScan tool was primarily used for predictions. TargetScan considers several parameters contributing to mRNA targeting by stable mRNA-miRNA binding at specific sites as elaborated in the section of materials and methods (see 2.2.1). Based on these parameters, there are more than 40 miRNAs predicted to target ATXN3 3'UTR according to TargetScan. From amongst these, five miRNAs were chosen for validation experiments as given in **table 3.1**. Apart from TargetScan, the chosen miRNAs are also predicted to target ATXN3 3'UTR by miRanda-mirSVR, which is another widely used algorithm to predict miRNA target predictions.

miRNA	TargetScan	miRanda-miRSVR
hsa-miR-9	✗	✗
hsa-miR-32	✗	✗
hsa-miR-125a-5p	✗	✗
hsa-miR-181c	✗	✗
hsa-miR-383	✗	✗

Table 3.1: miRNAs that are chosen for ATXN3 targeting experiments. These miRNAs are predicted to target the ATXN3 3'UTR by the tools TargetScan and miRanda-miRSVR.

The details of the location of binding sites of the chosen miRNAs on the ATXN3 3'UTR as well as their seed match type are given in **table 3.2**. The locations of the binding sites of the selected miRNAs on the ATXN3 3'UTR are shown in **figure 3.1**.

miRNA family	Number of conserved target sites	Location on the 3'UTR sequence (from the 5' end)	Type of site
hsa-miR-9	1	190-196	7mer
hsa-miR-32/25/92a/92b/363/367	1	259-266	8mer
hsa-miR-125a-5p/125b	1	1488-1494	7mer
hsa-miR-181a/181b/**181c**/181d	3	a. 770-776 b. 929-936 c. 1381-1387	a. 7mer b. 8mer c. 7mer
hsa-miR-383	1	551-558	8mer

Table 3.2: Binding site characteristics of the chosen miRNAs. Shown above is the number of binding sites of the miRNAs, their location on the ATXN3 3'UTR and the number of complementary nucleotides in each site.

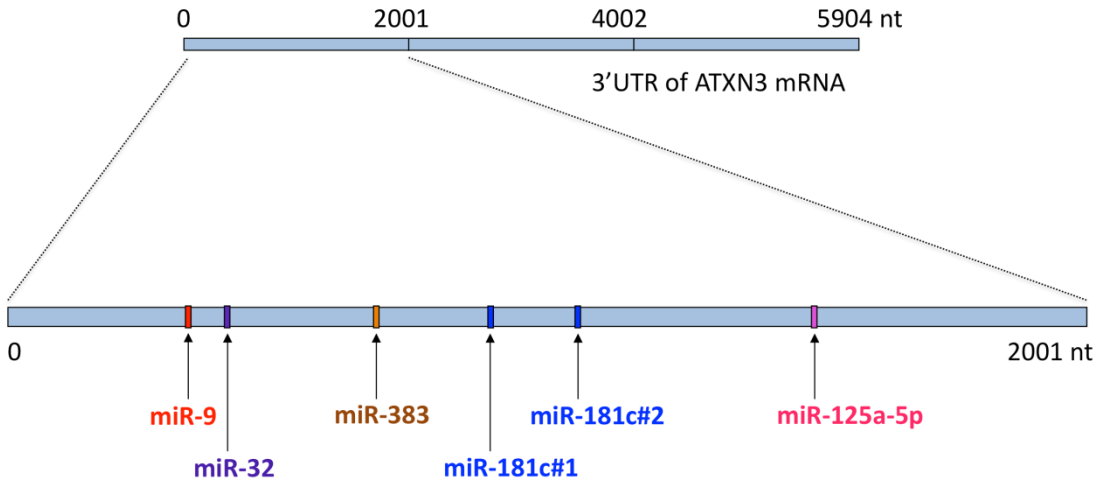

Figure 3.1: A pictorial representation of the ATXN3 3'UTR with the locations of the binding sites of the selected miRNAs. The binding sites of the miRNAs selected lie within the initial 2000 nt of the ATXN3 3'UTR.

3.1.2 Validation of the ability of the selected miRNAs to bind at specific sites on the 3'UTR of ATXN3 mRNA

In order to analyse the ability of miRNAs from the above families to target the ATXN3 3'UTR at the specific binding sites, the initial 2000 nt sequence of the ATXN3 3'UTR was cloned into the luciferase reporter vector psiCHECK-2 downstream of the Renilla luciferase. The binding sites for the selected miRNAs were individually mutated by substitution of two nucleotides at the location corresponding to nucleotide 2 and 3 on the miRNA seed region. An example for the miR-32 binding site mutant is shown in **figure 3.2** (figures for the other miRNA mutants are shown in the appendix). In each miRNA binding site, the two bases at these locations were replaced by bases that would be unable to form a Watson-Crick base pairing with corresponding bases in the miRNA. The resulting mismatch prevents miRNA mediated targeting of the mutant ATXN3 3'UTR, which in turn prevents the degradation of the mRNA molecules which contain the Renilla luciferase sequence preceding the mutant ATXN3 3'UTR.

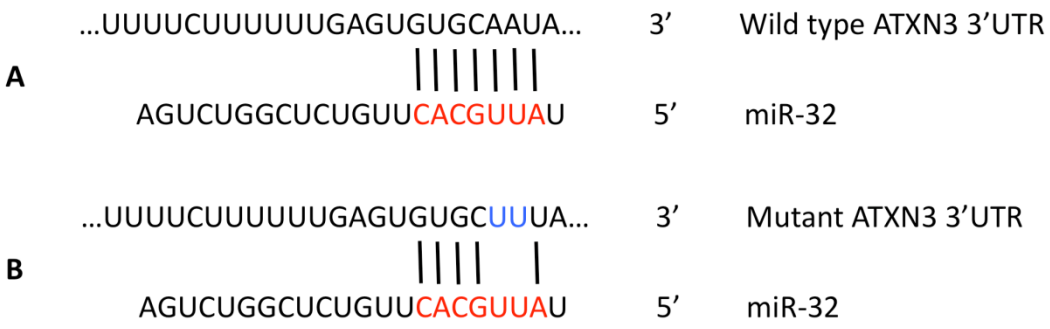

Figure 3.2: Representation of miR-32 binding to ATXN3 3'UTR at its predicted binding site. The binding of miR-32 to the wild type ATXN3 3'UTR is shown in (A), while the disruption to binding caused by mutations at two nucleotides in the miR-32 binding site in ATXN3 3'UTR is shown in (B).

Hela cells were transfected with either wild type or mutant ATXN3 3'UTR cloned downstream of the Renilla luciferase. The psiCHECK-2 vector also contains the sequence for Firefly luciferase. The cells were lysed 48 hours after transfections and Renilla and Firefly luciferase activity in the cell lysates was measured in a luciferase assay. The Firefly luciferase signal was used for normalization of the Renilla luciferase signal. As shown in **figure 3.3**, mutations of the miRNA binding sites on the ATXN3 3'UTR led to a significant increase in the ratio of the Renilla/Firefly luciferase for all the mutant constructs. The percentage increase in the signal ratio differed for each mutant from 20.5% for the miR-9 binding site mutant, to 117% for the mutant with binding site number 2 for miR-181c. This suggests that the endogenously expressed miRNAs from the Hela cells were able to target their predicted binding sites on ATXN3 3'UTR. Worth noting was the difference for the mutants of the two miR-181c binding sites with a 27.8% increase for binding site-1 and as mentioned above a 117% increase for binding site-2. This was expected, since the binding site-1 is a 7mer whereas the binding site-2 is an 8mer and therefore the binding of miR-181c to the ATXN3 3'UTR at binding site-2 is stronger, leading to enhanced targeting.

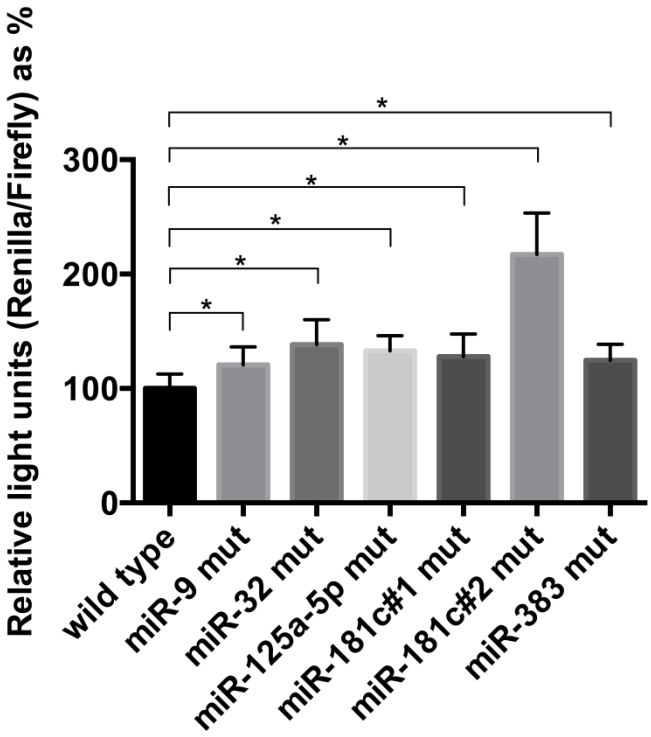

Figure 3.3: Mutations of miRNA binding sites of miR-9, 32, 125a-5p, miR-181c and miR-383 on ATXN3 3'UTR lead to increased Renilla/Firefly signal ratio. Binding sites of miRNAs on partial ATXN3 3'UTR sequence were mutated. Wild type and mutant constructs were transfected in Hela cells and Renilla, Firefly luciferase signals measured 48 hours after transfection. Columns represent values +/- standard deviation. n = 27, P-value = <0.0001

3.1.3 Analysis of the miRNAs' effect on endogenous ATXN3 mRNA and protein levels in human cell lines

On the basis of the predicted thermodynamics of miRNA targeting of the ATXN3 mRNA, miR-32 and miR-181c have the strongest binding ability as compared to the other miRNAs considered. Hence these two miRNAs were chosen for further experiments involving analysis of effects of over-expression of these miRNAs on ATXN3 protein and mRNA levels. The overexpression of these two miRNAs was carried out in Hela cells using two strategies:

- miRNA mimic oligonucleotides
- miRNA precursor sequence containing expression vector

miRNA overexpression using miRNA mimic oligonucleotides

One of the strategies to overexpress miR-32 and miR-181c was to transfect cells with mimic oligonucleotides of these two miRNAs. miRNA mimics are synthetically produced oligonucleotides that mimic the action of endogenously generated miRNAs. Hela cells were transfected with miR-32 and miR-181c mimics or control siRNA with a scrambled sequence and lysed 48 hours after transfections. The effect of miR-32 and miR-181c on the amount of ATXN3 protein was analysed using immunoblotting whereas the effect on ATXN3 mRNA was analysed using SYBR Green real time PCR. As compared to cells transfected with a control siRNA, a significant decrease of up to 55% was observed in the amount of ATXN3 mRNA in Hela cells transfected with miR-32 and miR-181c mimics for 48 hours, as seen in **figure 3.4**. Corresponding to the downregulation in ATXN3 mRNA levels, the levels of ATXN3 protein were also found to be decreased substantially upon miR-32 and miR-181c mimic transfection as seen in **figure 3.5**.

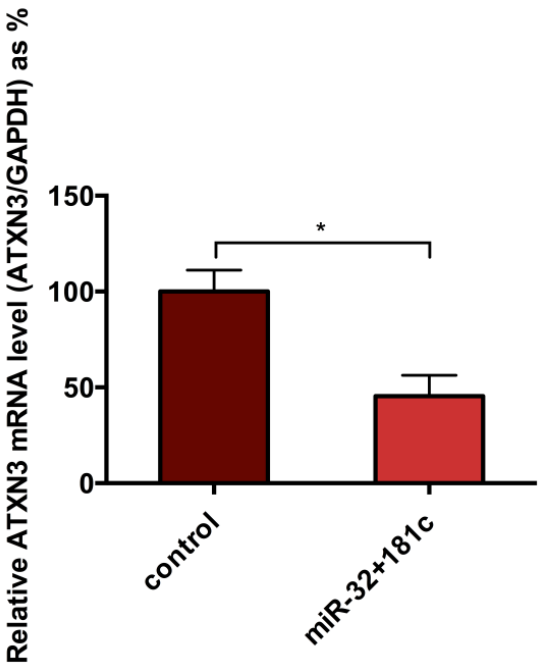

Figure 3.4: Overexpression of miR-32 and miR-181c decreases ATXN3 mRNA level in Hela cells. miR-32 and miR-181c mimics were co-transfected in Hela cells. ATXN3 and GAPDH mRNA levels (as loading control) were checked by SYBR Green real-time PCR 48 hours after transfection. Columns represent values +/- standard deviation. n = 4, P-value = 0.0004

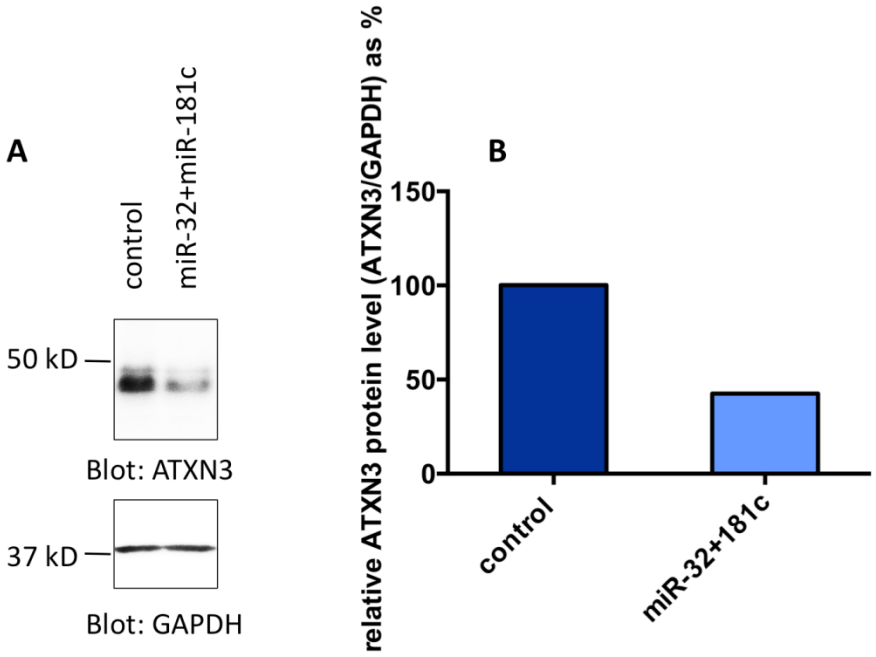

Figure 3.5: Overexpression of miR-32 and miR-181c decreases ATXN3 protein levels in Hela cells. miR-32 and miR-181c mimics were cotransfected in Hela cells. The ATXN3 (A; upper panel) and GAPDH (A; lower panel) protein levels 48 hours post transfection were determined by immunoblotting using specific antibodies. As shown in (B) the ATXN3 protein levels were quantified based on the ratio of ATXN3 to the loading control GAPDH. Columns represent percentage value of ATXN3/GAPDH ratio.

miRNA overexpression using and expression vector containing the miRNA precursor sequence

The overexpression of miR-32 and miR-181c in Hela cells was also conducted using the strategy of cloning the sequence of miRNA precursor and flanking regions into the miRNA expression vector pMIRNA1. The precursor sequence of around 70 nt along with 200 nt flanking regions on both sides is necessary for overexpression of the miRNAs. Upon transfection of this construct into Hela cells and expression of the precursor sequence, the protein Dicer involved in the RNAi machinery cleaves the precursor miRNAs to form the mature miRNAs, which associate with the miRISC complex to actively take part in post-transcriptional regulation of gene expression.

Hela cells were transfected with pMIRNA1 constructs expressing the precursor sequences of miR-32 and miR-181c. As control, empty vector was transfected. The pMIRNA1 vector includes the sequence for copGFP gene and hence GFP fluorescence was used as a visual marker to estimate the efficiency of cell transfection. A transfection efficiency of around 70-80% was achieved 48 hours after transfection.

The cells were lysed 48 hours after transfection and ATXN3 protein levels from the cell lysates were analysed by immunoblotting. Transfected cells were also used for RNA extraction and SYBR Green real time PCR to analyse the ATXN3 mRNA levels.

Upon overexpression of miR-32 and miR-181c in Hela cells, the ATXN3 mRNA levels were significantly downregulated as seen in **Figure 3.6**. In unison with this result, the immunoblotting of cell lysates with an antibody specific for ATXN3 showed a downregulation in the ATXN3 protein levels upon miR-32 and miR-181c overexpression as seen in **figure 3.7**.

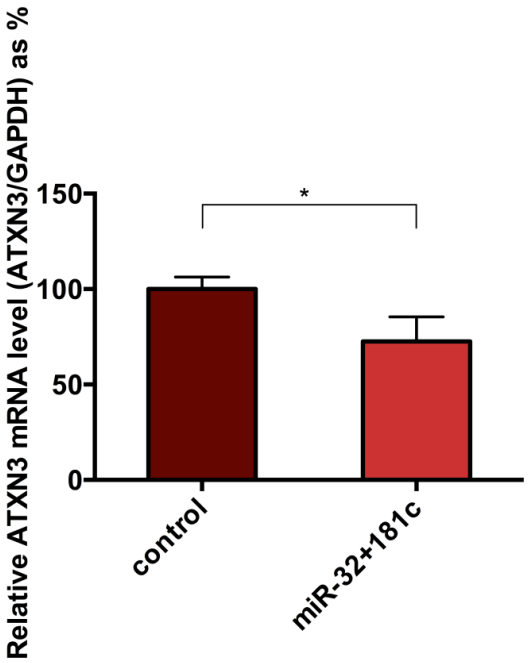

Figure 3.6: Precursor based overexpression of miR-32 and miR-181c leads to significant decrease in ATXN3 mRNA levels. Hela cells were transfected with pMIRNA1 vectors with precursors of both miRNAs. ATXN3 and GAPDH mRNA levels (as loading control) were checked by SYBR Green real-time PCR 48 hours after transfection. Columns represent values +/- standard deviation. n = 3, P-value = 0.002

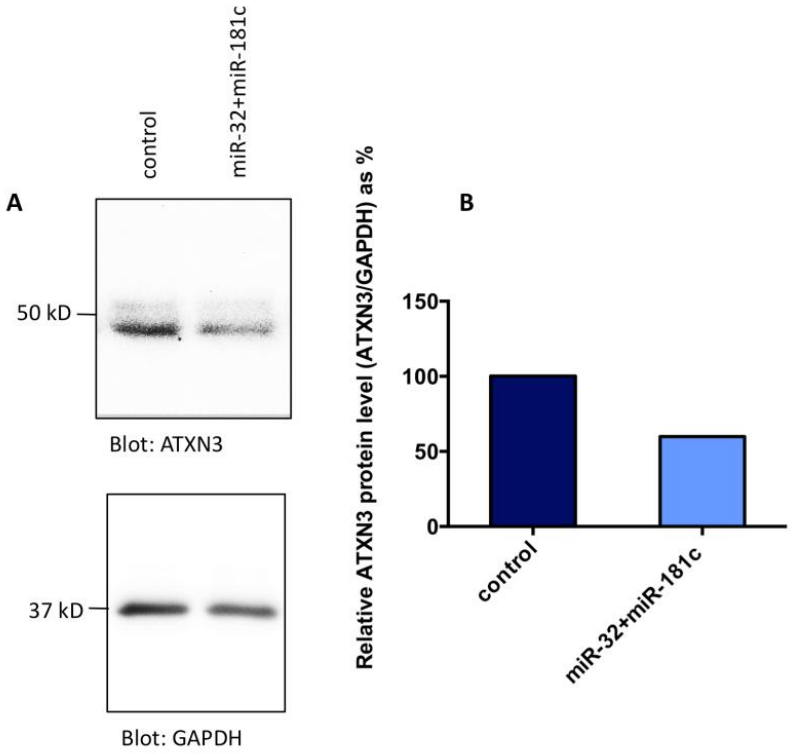

Figure 3.7: Precursor based overexpression of miR-32 and miR-181c causes a decrease in ATXN3 protein levels. Hela cells were transfected with pMIRNA1 vectors with precursors of both miRNAs. ATXN3 (A; upper panel) and GAPDH (A; lower panel) protein levels 48 hours post transfection were determined by immunoblotting using specific antibodies. As shown in (B) the ATXN3 protein levels were quantified based on the ratio of ATXN3 to the loading control GAPDH.

3.2 miRNAs targeting Midline 1 (MID1)

As described in the introduction, the MID1 protein has been shown to play an important role in the expression of polyQ expanded proteins through its action on the translation of mRNAs containing expanded CAG repeats. Hence, modulation of MID1 expression might affect the expression of polyQ protein and disease progress. Deciphering which miRNAs might be able to target MID1 and modulate its expression was therefore one of the aims of this project.

The strategy employed to discover the miRNAs targeting MID1 was similar to the one used for finding miRNAs targeting ATXN3.

Hence the experiments were again divided into the following parts:

- *In silico* prediction of miRNAs targeting the 3'UTR of MID1 mRNA
- Validation of the ability of selected miRNAs to bind at specific sites on the 3'UTR of MID1 mRNA
- Analysis of the miRNAs' effect on endogenous MID1 mRNA and protein levels in human cell lines

3.2.1 *In silico* prediction of miRNAs targeting the 3'UTR of MID1 mRNA

The TargetScan miRNA target prediction tool was used to predict miRNAs, which potentially target the 3'UTR of MID1 mRNA. The MID1 mRNA is 4058 nt long. TargetScan predicted more than 60 miRNAs, which can potentially target the MID1 3'UTR. Of these, three miRNAs were chosen for validation experiments (**table 3.3**). Apart from TargetScan, these miRNAs were also predicted to target MID1 3'UTR by another miRNA target prediction tool miRanda-miRSVR.

miRNA	TargetScan	miRanda-miRSVR
hsa-miR-216a-5p	✗	✗
hsa-miR-374a-5p	✗	✗
hsa-miR-542a-3p	✗	✗

Table 3.3: miRNAs that are chosen for MID1 targeting experiments. These 3 miRNAs are predicted to target MID1 3'UTR by both TargetScan and miRanda-miRSVR.

The details regarding the predicted binding of these miRNAs on MID1 3'UTR, such as the number of conserved target sites, location of these target sites on 3'UTR, the type of site in terms of WC match to the miRNA seed sequence are given in **table 3.4** below. hsa-miR-374a belongs to the family of miRNAs, which also includes hsa-miR-374b. Hence, both miR-374a and miR-374b are predicted to bind at the same target site. The relative locations of the miRNA binding sites on the MID1 3'UTR is shown in **figure 3.8**.

miRNA family	Number of conserved target sites	Location on the 3'UTR sequence (from the 5' end)	Type of site
hsa-miR-216a-5p	1	738-744	7mer
hsa-miR-374a, 374b	1	1154-1161	8mer
hsa-miR-542-3p	1	975-982	8mer

Table 3.4: Binding site characteristics of miRNAs predicted to bind MID1 3'UTR. Shown above is the number of binding sites of the miRNAs, their location and the number of complementary nucleotides in each site.

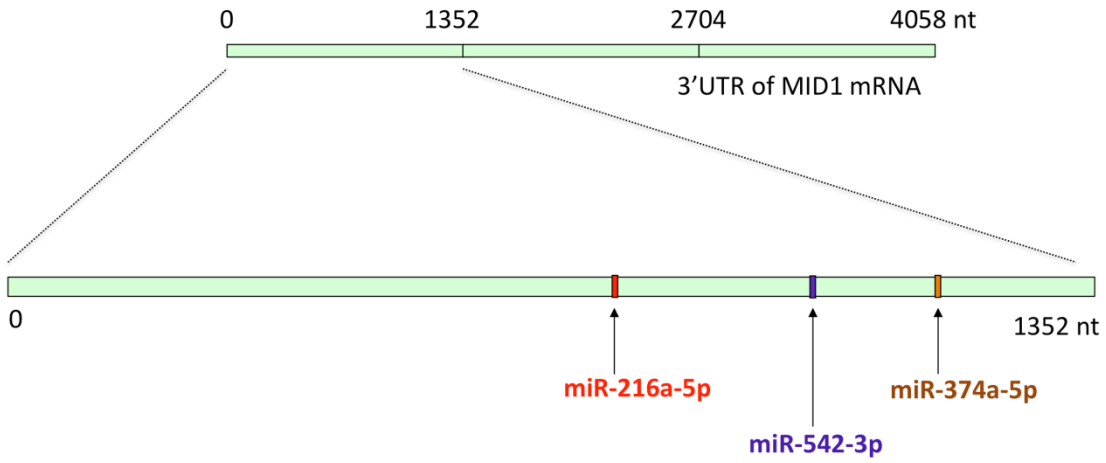

Figure 3.8: A graphical representation of the MID1 3'UTR with the locations of the binding sites of the three chosen miRNAs. All the chosen miRNA binding sites lie in the initial 1352 nucleotides of the MID1 3'UTR.

3.2.2 Validation of the ability of selected miRNAs to bind at specific sites on the 3'UTR of MID1 mRNA

To verify the ability of miR-216a-5p, miR-374a-5p and miR-542-3p to bind the MID1 3'UTR at specific binding sites, the 1352 nucleotides of the MID1 3'UTR containing the predicted miRNA binding sites were cloned downstream of the Renilla luciferase in the luciferase reporter vector psiCHECK-2. The binding sites of the three miRNAs were mutated by two nucleotide base substitutions on the 3'UTR corresponding to position 2, 3 of the miRNA seed region (example for miR-216a-5p in **figure 3.9**; figs for other two mutants in appendix). Wild type and mutant MID1 3'UTRs in psiCHECK-2 were transfected in Hela cells. Luciferase assays were conducted 48 hours after transfection. Signals from the Renilla luciferase were normalized by the Firefly luciferase signals.

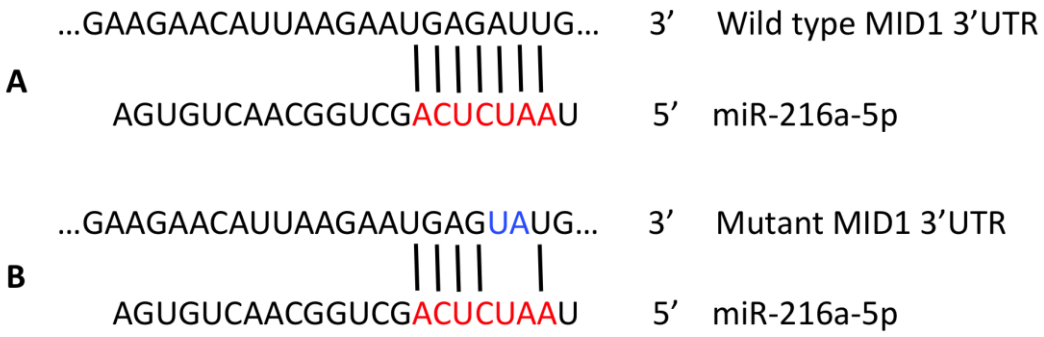

Figure 3.9: Representation of miR-216a-5p binding to MID1 3'UTR at its specific binding site. The binding of miR-216a-5p to the wild type MID1 3'UTR is shown in (A), while the disruption to the binding caused by mutations at two nucleotides in the miR-216a-5p binding site on MID1 3'UTR is shown in **(B)**.

As seen in **figure 3.10**, compared to the wild type 3'UTR of MID1, a significant increase in the signal ratio of Renilla/Firefly was observed for the 3'UTR variants with mutations in the binding sites of miR-216a-5p, miR-374a-5p and miR-542-3p. This suggests that the

endogenously expressed miRNAs from the Hela cells were able to target their predicted binding sites on MID1 3'UTR.

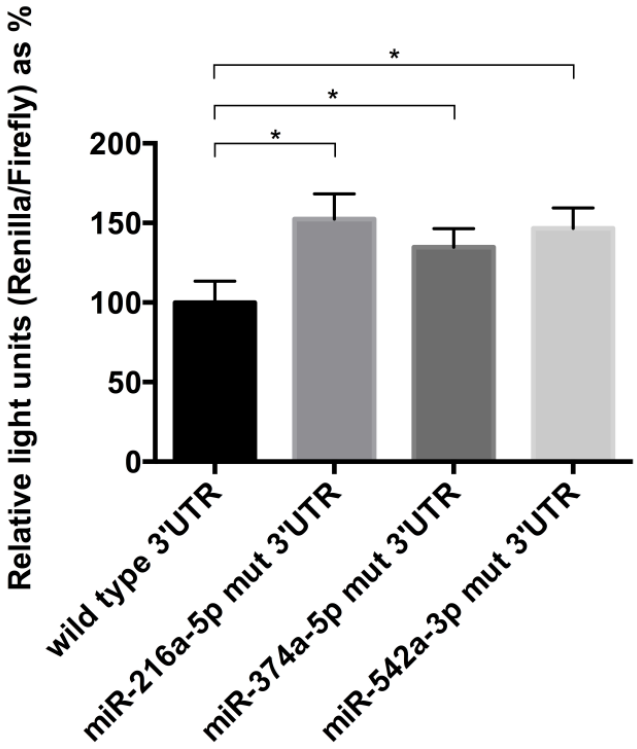

Figure 3.10: Mutations of miRNA binding sites on MID1 3'UTR lead to increased Renilla/Firefly signal ratio. Binding sites of miRNAs in partial MID1 3'UTR sequence were mutated. Wild type and mutant constructs were transfected in Hela cells and Renilla, Firefly luciferase signals measured 48 hours after transfection. Columns represent values +/- standard deviation. n = 6, P-value = < 0.0001

3.2.3 Analysis of the miRNAs' effect on endogenous MID1 mRNA and protein levels in human cell lines

To analyse the effect of miR-216a-5p, miR-374a-5p and miR-542-3p on MID1 protein and mRNA levels, these miRNAs were over expressed in HEK-T 293 cells using their respective mimic oligonucleotides. The transfected HEK-T 293 cells were lysed 72 hours after transfections and MID1 protein levels were analysed by immunoblotting and mRNA levels were analysed by SYBR Green real time PCR.

As shown in **figure 3.11**, MID1 mRNA levels were downregulated in the cells transfected with the three miRNA mimics compared to controls. Correspondingly, MID1 protein levels were also reduced after transfection with the miRNA mimics as shown in **figure 3.12**.

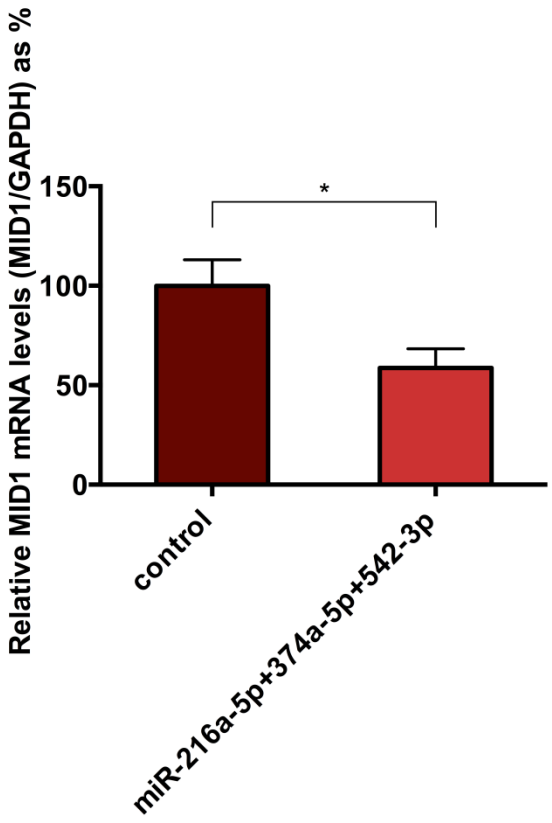

Figure 3.11: Overexpression of miR-216a-5p, miR-374a-5p, miR-542-3p decreases MID1 mRNA levels in HEK-T 293 cells. miR-216a-5p, miR-374a-5p, miR-542-3p mimics were cotransfected in HEK-T 293 cells. MID1 and GAPDH mRNA levels (as loading control) were checked by SYBR Green real-time PCR 72 hours after the transfection. Columns represent values +/- standard deviation. n = 4, P-value = 0.0029

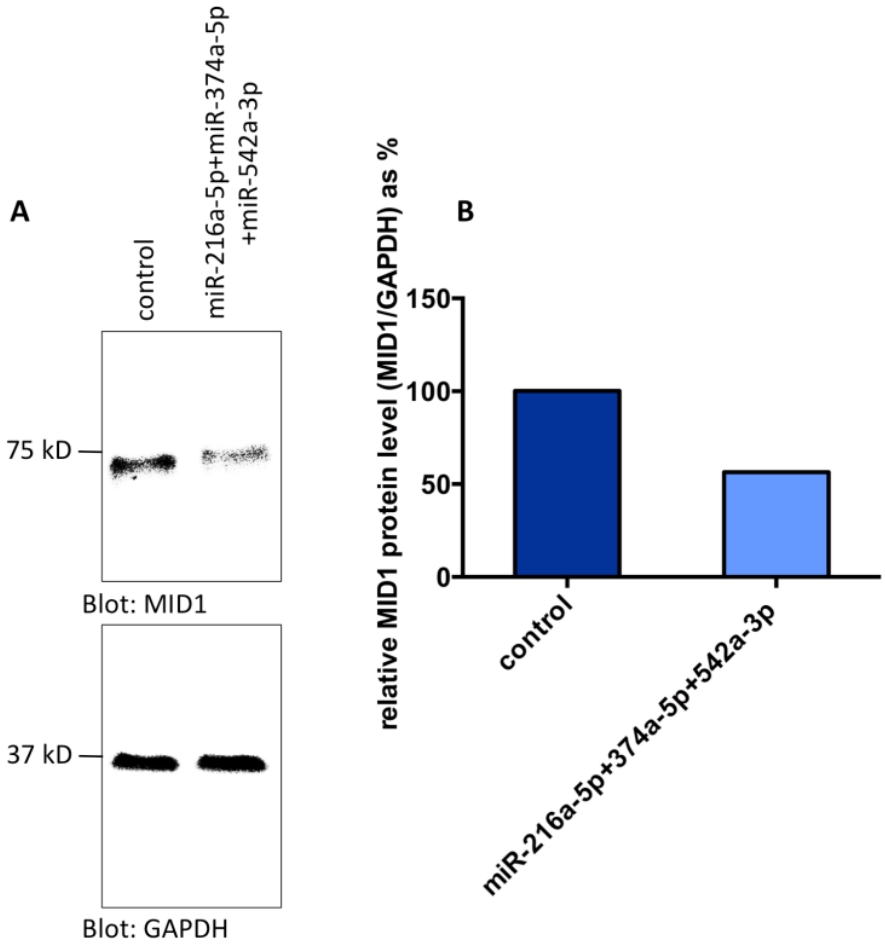

Figure 3.12: Overexpression of miR-216a-5p, miR-374a-5p, miR-542-3p decreases MID1 protein levels in HEK-T 293 cells. miR-216a-5p, miR-374a-5p, miR-542-3p mimics were cotransfected in HEK-T 293 cells. The MID1 (A; upper panel) and GAPDH (A; lower panel) protein levels 72 hours post transfection were determined by immunoblotting using specific antibodies. As shown in (B) the MID1 protein levels were quantified based on the ratio of MID1 to the loading control GAPDH. Columns represent percentage value of MID1/GAPDH ratio.

3.3 Analysis of differentially expressed miRNAs in iPSC-derived SCA3 neurons

3.3.1 Neurons derived from SCA3 iPSCs express wild type as well as the mutant ATXN3 allele

To find miRNAs involved in SCA3 pathogenesis, neurons differentiated from Induced Pluripotent Stem Cells (iPSCs) from SCA3 patients and healthy controls were used. The iPSC generation, neuronal differentiation, characterization, and culture was conducted by collaborators in the Institute of Reconstructive Neurobiology, University of Bonn. In iPSC-derived SCA3 neurons, proteolytic cleavage of expanded ATXN3 by calpains induced by glutamate treatment of the neurons leads to formation of ATXN3 aggregates, which is a hallmark of SCA3 pathology (Koch et al, 2011). iPSC-derived neurons from three SCA3 patients and two healthy controls that had been differentiated for 8 weeks were used in this study. The details regarding the age, sex, repeat length, age of onset of the individuals are given in **table 3.5**. Although the formation of ATXN3 aggregates requires treatment of the neurons with glutamate, untreated neurons were used for experiments to decipher dysregulations in mRNAs and miRNAs which might be involved in the pathogenic mechanisms apart from the obvious, i.e. the toxicity mediated by the formation of ATXN3 aggregates. The 8 week old neurons were used for extraction of total RNA including small RNAs as well as the extraction of total protein. The total RNA was used to generate gene expression and miRNA expression profiles using the technique of RNA sequencing (RNA-seq). Proteins extracted from these neurons were utilized for quantification of proteins by immunoblotting. The expression of wild type and mutant alleles of ATXN3 in the SCA3 neurons was validated by immunoblotting using total proteins extracts as shown in **figure 3.13**.

	Age (yrs) at time of biopsy	Sex	Repeat length	Age of onset
Patient 1	40	male	74/21	30
Patient 2	38	male	74/22	31
Patient 3	42	female	73/27	28
	Age (yrs) at time of biopsy	**Sex**	**comments**	
Control 1	24	female		
Control 2	68	male	non-affected father of patient 1	

Table 3.5: Background details for the individual sources for the iPSC-derived neurons. The age of the individuals at the time of biopsy, sex, as well as the CAG repeat length and age of onset of the SCA3 symptoms for the SCA3 patients are included.

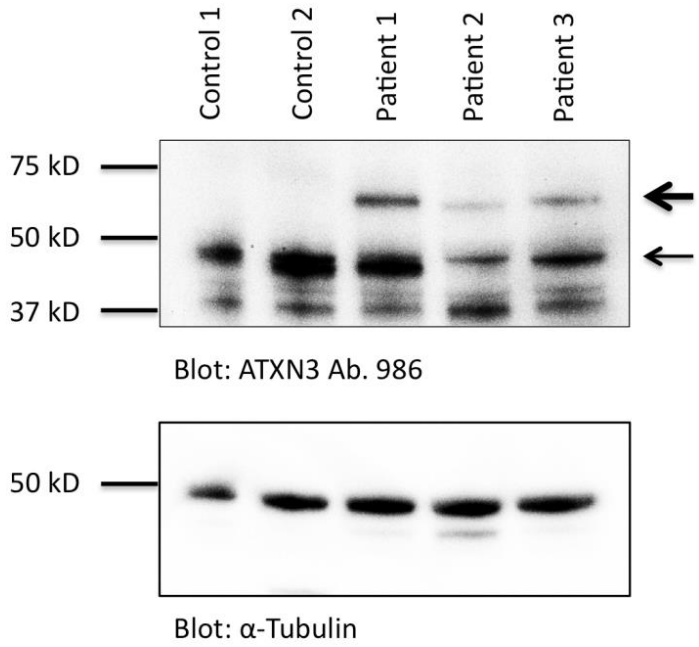

Figure 3.13: **ATXN3 expressed in iPSC-derived neurons from controls and SCA3 patients.** While **t**he wild type ATXN3 allele (approx.50 kDa, thin arrow) is expressed in the controls and the SCA3 neurons, the expanded, mutant allele (approx.70 kDa, thick arrow) is expressed only in the SCA3 neurons.

3.3.2 Gene expression profiling of SCA3 neurons

Gene expression profiles were analysed by RNA-seq using the RNA extracted from the iPSC-derived neurons. The RNA-seq experiment was conducted by the group of Dr.

Stefan Bonn (Computational analysis of biological networks, DZNE Göttingen). Gene expression profiles of two controls were compared to the three SCA3 patients with the aim of finding dysregulated mRNAs in the SCA3 patient neurons. The gene expression profiles revealed that in SCA3 patient neurons, 71 mRNAs were dysregulated: 41 were upregulated and 30 were downregulated compared to healthy controls. The top five upregulated and downregulated genes in the SCA3 neurons are shown in **table 3.6.** (The complete list of dysregulated mRNAs is given in the appendix).

Gene symbol	Gene name	Fold change in SCA3 neurons	FDR P-value
Genes upregulated in SCA3 neurons			
ELAVL2	ELAV like neuron specific RNA-binding protein 2	4.94	8.37E-03
KIAA1549L	KIAA1549-like	4.3	4.00E-02
ANK3	ankyrin 3, node of Ranvier (ankyrin g)	3.96	2.26E-03
DCC	DCC netrin 1 receptor	3.81	2.00E-02
MEX3A	mex3 RNA-binding family member A	3.37	1.96E-04
Genes downregulated in SCA3 neurons			
COLEC12	collectin sub-family member 12	-24.41	4.80E-15
SERPINF1	serpin peptidase inhibitor, clade F	-14.26	4.10E-07
LUM	lumican	-10.29	6.29E-38
EFEMP2	EGF containing fibulin like extracellular matrix protein 2	-6.81	7.01E-04
EVA1C	eva-1 homolog C (*C.elegans*)	-5.82	5.00E-02

Table 3.6: The five most upregulated and downregulated genes in SCA3 neurons. Genes have been displayed with fold change in expression in the SCA3 neurons as compared to healthy controls along with the P-values of differential expression.

To understand the relevance of the dysregulation of specific gene expression, the set of dysregulated mRNAs was analysed using techniques of Gene Ontology (GO) term enrichment, Pathway enrichment analysis and Protein interaction analysis.

3.3.3 Gene Ontology (GO) term enrichment analysis

The GO term enrichment analysis elucidated the enrichment of the dysregulated genes with respect to three categories, namely: molecular function, biological process and cellular component. As seen in **table 3.7**, the top ranked enriched GO terms pertaining to molecular function were associated with structural molecule activity, cytoskeletal regulation and poly(A) RNA binding. The dysregulation status (up or downregulation) of mRNAs in each of these terms is shown in **figure 3.14**. The top ranked enriched GO terms with respect to biological process revealed that the dysregulated genes were associated with neuron projection, neuron development, axon development, neuron differentiation and neurogenesis (**table 3.8**). The up and downregulated genes related to each of these terms is shown in **figure 3.15**. The top ranked GO terms associated with cellular component revealed an enrichment of genes associated with cell projection, neuron projection and axon (**table 3.9**). The split-up of the dysregulated genes related to each term is shown in **figure 3.16.** It is worth noting that the enrichment of the genes as ascertained by the False Discovery Rate (FDR) corrected p-values, is highest for the terms in the category biological process, followed by cellular component and molecular function in that order.

Gene ontology ID	Name	FDR P-value	Genes dys-regulated in SCA3 neurons	Total genes in the GO term
GO:0005198	structural molecule activity	9.24E-03	11	641
GO:0005519	cytoskeletal regulatory protein binding	1.36E-02	2	4
GO:0008092	cytoskeletal protein binding	2.04E-02	11	792
GO:0044822	poly(A) RNA binding	3.14E-02	13	1160
GO:0043495	protein anchor	3.23E-02	2	9

Table 3.7: The top ranked GO terms relating to molecular function enriched for the dysregulated mRNAs in the iPSC-derived SCA3 neurons.

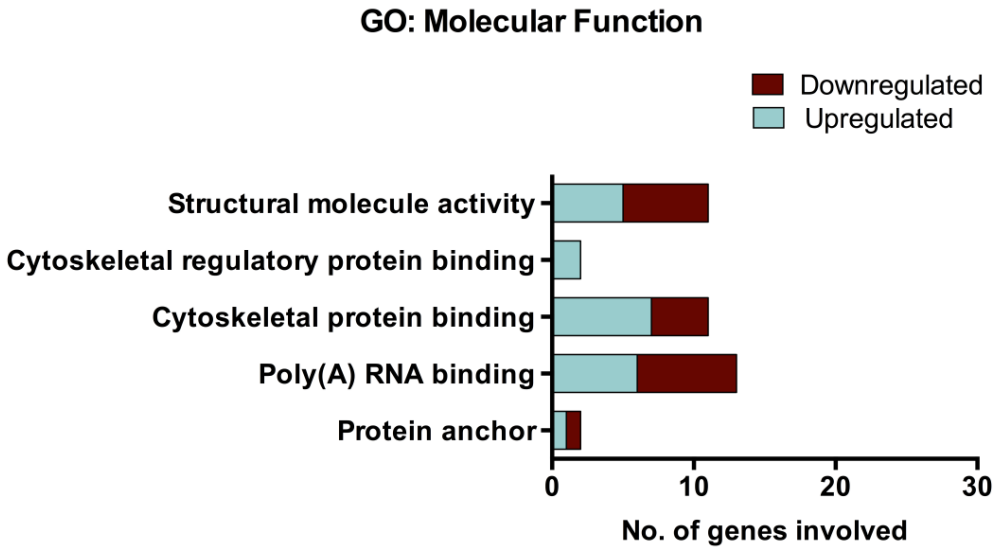

Figure 3.14: The downregulated and upregulated mRNAs included in each enriched GO term relating to the category 'molecular function'.

Gene ontology ID	Name	FDR P-value	Genes dys-regulated in SCA3 neurons	Total genes in the GO term
GO:0031175	neuron projection development	6.41E-08	20	878
GO:0048666	neuron development	6.41E-08	21	1009
GO:0061564	axon development	2.76E-07	16	590
GO:0030182	neuron differentiation	2.76E-07	22	1257
GO:0022008	neurogenesis	4.81E-07	23	1441

Table 3.8: The top ranked GO terms relating to biological process enriched for the dysregulated mRNAs in SCA3 neurons.

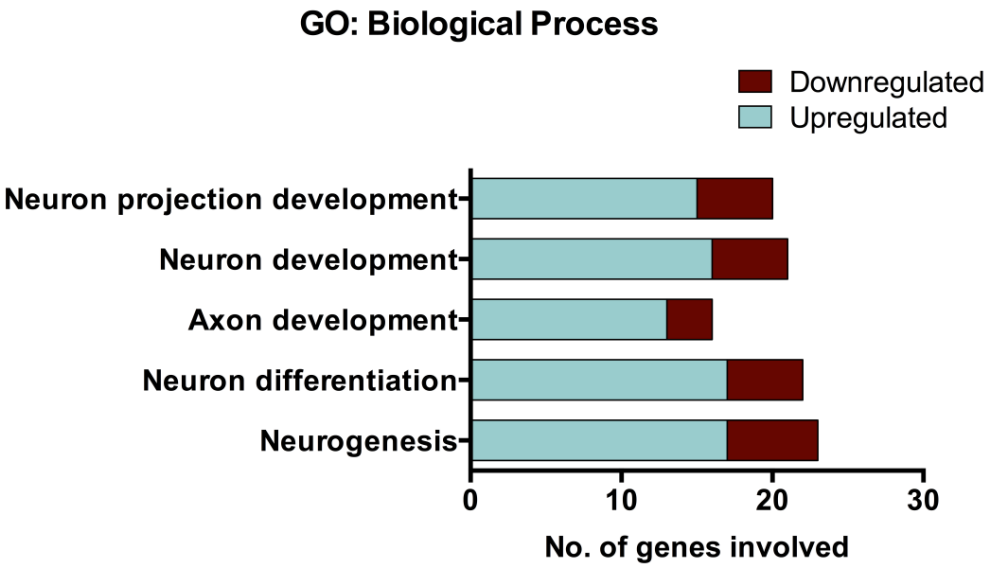

Figure 3.15: The upregulated and downregulated mRNAs included in the enriched GO terms corresponding to the category 'biological process'.

Gene ontology ID	Name	FDR P-value	Genes dys-regulated in SCA3 neurons	Total genes in the GO term
GO:0042995	cell projection	1.19E-06	24	1711
GO:0043005	neuron projection	5.52E-06	17	945
GO:0097458	neuron part	8.61E-06	18	1130
GO:0030424	axon	1.24E-03	9	409
GO:0044463	cell projection part	2.34E-03	12	839

Table 3.9: The top ranked GO terms enriched for the dysregulated mRNAs in SCA3 neurons corresponding to the category 'cellular component'.

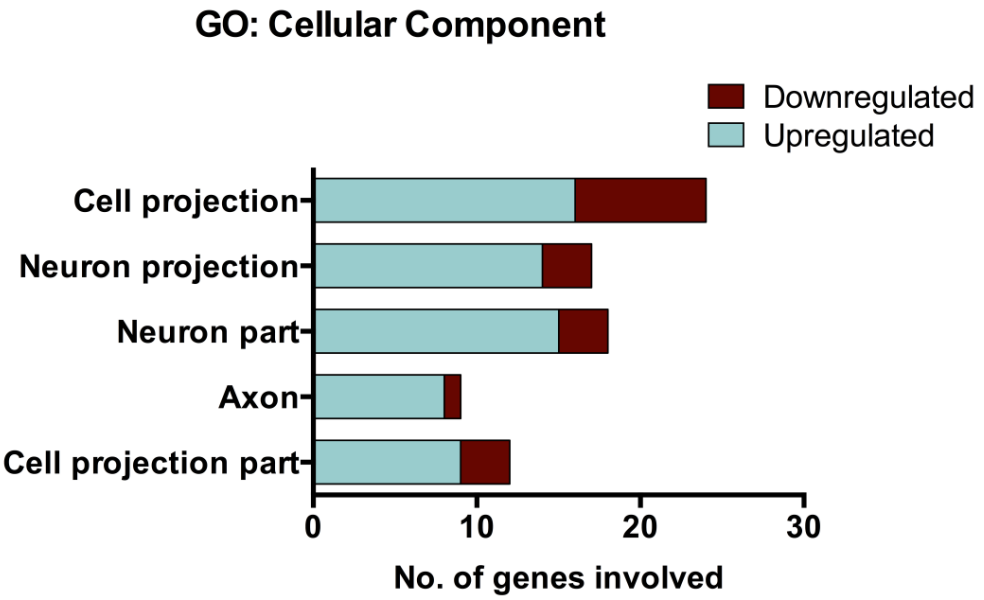

Figure 3.16: The upregulated and downregulated mRNAs in SCA3 neurons corresponding to the top ranked GO terms in the category 'cellular component'.

3.3.4 Pathway enrichment analysis

The genes whose expression was dysregulated in SCA3 patient neurons were also analysed for enrichment or over-representation of genes associated with particular pathways. This analysis was conducted using the Reactome pathway database. **Table 3.10** displays the results of the top ranked pathways with the respective P-values for enrichment. The axon guidance pathway was the top ranked pathway with 8 of the dysregulated genes coding for proteins that are members of this pathway. The 'developmental biology' pathway that includes 9 of the dysregulated genes is a group of pathways, which includes the axon guidance pathway. The other three pathways in the list, namely: Role of second messengers in netrin-1 signaling, Semaphorin interactions, interaction between L1, and Ankyrins are all 'daughter pathways', which are among the subsets of the axon guidance pathway. The list of dysregulated genes associated with each pathway is given in the appendix.

Reactome Pathway ID	Name	FDR P-value	Genes dys-regulated in SCA3 neurons	Total genes in the pathway
REACT-18266	Axon guidance	1.76E-02	8	345
REACT-111045	Developmental Biology	4.20E-02	9	531
REACT-22228	Role of second messengers in netrin-1 signaling	1.22E-01	2	10
REACT-19271	Semaphorin interactions	2.71E-01	3	67
REACT-22266	Interaction between L1 and Ankyrins	2.71E-01	2	31

Table 3.10: Pathways enriched for the genes dysregulated in SCA3 neurons. The axon guidance pathway is the most enriched with 8 of the 71 dysregulated genes expressing proteins associated with this pathway.

3.3.5 Protein interaction analysis

The genes dysregulated in SCA3 patient neurons were also analysed using the protein interaction database STRING-DB. The input list fed into the algorithm included the 71 dysregulated mRNAs and the addition of ATXN3, with the aim of elucidating if proteins expressed from the dysregulated genes interact with ATXN3. The results are displayed in **Figure 3.17** as a graphic, where each dysregulated gene product i.e. the resultant protein is denoted by a sphere. Proteins with known interactions (interactions validated from published experiments) are connected by lines. The ATXN3 protein is highlighted in the figure. The only protein known to interact with ATXN3 from amongst all the candidates is the DNAJB1 protein, coded by the DNAJB1 gene which is found to be downregulated in SCA3 patient neurons. The DNAJB1 protein is a well-studied chaperone (also known as one of the Hsp40 chaperones) and has been documented to co-localize with intra-nuclear inclusions, which are mediated by the expanded ATXN3 in SCA3 neurons (Seidel et al, 2012a).

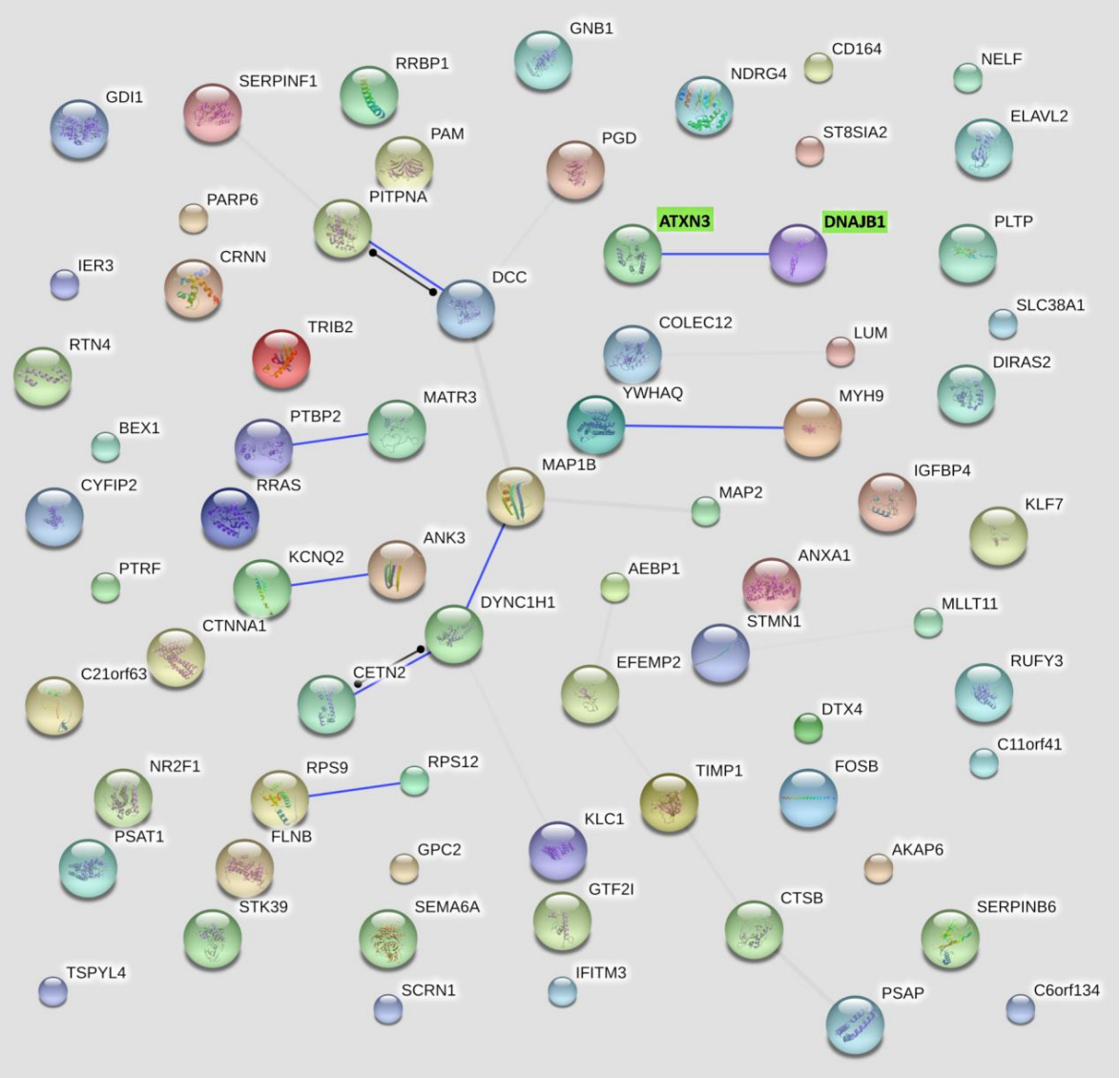

Figure 3.17: Protein interaction analysis reveals the DNAJB1 protein as an interaction partner of ATXN3. Using the STRING database, network analysis was done for all the proteins expressed by the genes dysregulated in SCA3 neurons. The ATXN3 protein was added to the analysis to check which of the proteins are validated interaction partners. The DNAJB1 protein is the only protein that has been validated to interact with it.

3.3.6 MicroRNA expression profiling of the SCA3 neurons

From the miRNA expression profile, it was found that in the SCA3 patient neurons, a total of 90 miRNAs were dysregulated. 71 miRNAs were upregulated and 19 miRNAs were downregulated compared to healthy controls. The top five miRNAs up and downregulated (in terms of fold-change) are as shown in **table 3.11**.

miRNA name	Fold change in iPSC-derived SCA3 neurons	FDR P-value
miRNAs upregulated in SCA3 neurons		
hsa-miR-431-5p	586.6214	1.27E-07
hsa-miR-337-5p	352.2233	3.55E-06
hsa-miR-770-5p	191.9895	7.60E-07
hsa-miR-376a-3p	182.4585	1.78E-06
hsa-miR-539-5p	134.6055	7.88E-05
miRNAs downregulated in SCA3 neurons		
hsa-miR-449a	-108.2534889	1.78E-03
hsa-miR-449c-5p	-93.32553078	9.54E-03
hsa-miR-449b-5p	-80.34681096	1.78E-03
hsa-miR-199a-5p	-66.25275354	3.01E-02
hsa-miR-4490	-65.61140287	3.85E-03

Table 3.11: The five most upregulated and downregulated miRNAs in SCA3 neurons. miRNAs have been displayed along with fold change in expression in the iPSC-derived SCA3 neurons as compared to healthy controls along with the P-values of differential expression.

The miRNAs that were dysregulated in patients were analysed to check if their predicted targets were enriched in a particular pathway(s). This analysis was conducted using the web-based tool miRSystem, which considers predicted as well as validated miRNA targets (Lu et al, 2012). The miRSystem tool uses the Reactome pathway database to identify the association of a specific gene with a pathway. As seen in **Table 3.12**, pathways were ranked according to their score, where the score was calculated using an algorithm that considers the absolute value of fold change of the miRNAs and the enrichment of its target genes in a particular pathway. The Axon guidance pathway had the highest score with 61 of the dysregulated miRNAs predicted to target 165 out of a total 266 genes in this pathway. The second ranked pathway was the developmental biology, where 237 out of 494 genes were predicted to be targeted by 61 of the dysregulated miRNAs. As mentioned in the gene expression pathway analysis, the developmental biology pathway in fact

constitutes a group of pathways, of which axon guidance pathway is a part. Other pathways that were amongst the top ranked were the L1CAM interactions pathway (a sub-pathway of the axon guidance pathway), the neuronal system pathway, and the homeostasis pathway (both independent from the first three pathways).

Reactome pathway ID	Reactome pathway name	Total genes of the term	Genes as predicted targets of dys-regulated miRNAs	Dys-regulated miRNAs with predicted targets	Score
REACT-18266	Axon guidance	345	165	61	1.955
REACT-111045	Developmental biology	531	237	61	1.931
REACT-22205	L1CAM interactions	111	63	57	1.25
REACT-13685	Neuronal system	280	131	60	1.14
REACT-604	Hemostasis	512	215	62	1.124

Table 3.12: Prediction for specific pathways enriched with putative targets of miRNAs dysregulated in SCA3 neurons. Table shows total genes associated with each pathway, along with the number of genes which are putative targets and the number of dysregulated miRNAs predicted to target the mRNAs of these genes.

A combined analysis for the axon guidance pathway was done considering the pathway analysis of the mRNAs dysregulated in the gene expression profile (**table 3.10**) and the pathway analysis of the dysregulated miRNAs in the miRNA profile (**table 3.12**). According to the Reactome pathway database, 345 proteins are involved in the axon guidance pathway. In the iPSC-derived SCA3 neurons, the mRNAs for 8 of these were

dysregulated. On the other hand, 61 miRNAs predicted to target 165 mRNAs of the axon guidance pathway were also dysregulated in SCA3 neurons. 7 out of the 8 dysregulated mRNAs were among the predicted targets as shown in **figure 3.18.** (Names of the dysregulated genes have been provided in the appendix)**.** As seen in the figure, the mRNAs of each of these proteins was targeted by multiple miRNAs with a mixed pattern of up and downregulation.

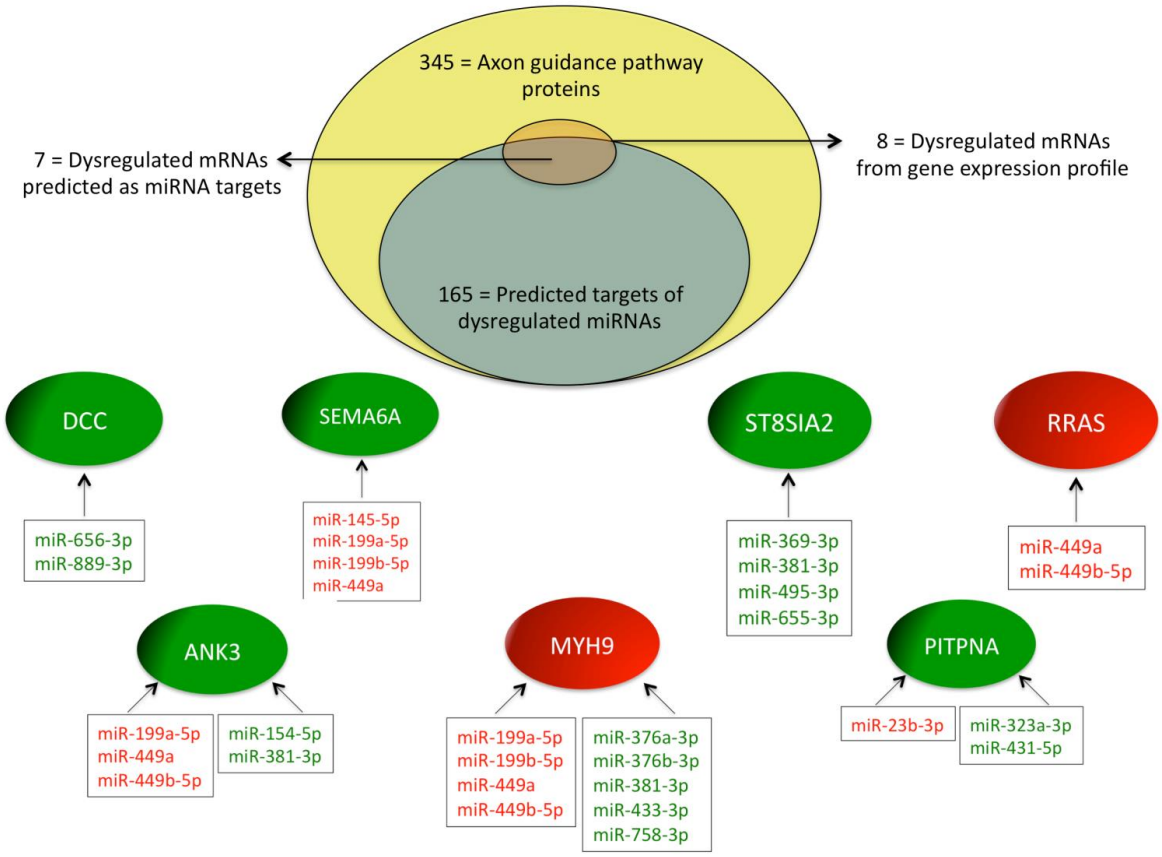

Figure 3.18: Analysis of the mRNAs and miRNAs involved in the axon guidance pathway that are dysregulated in iPSC-derived SCA3 neurons. Of a total of 345 proteins in the axon guidance pathway, the mRNAs of 165 are predicted to be targeted by the dysregulated miRNAs. The mRNAs of 7 of these exhibit significant dysregulation. These seven proteins are coloured either in green (mRNA upregulated) or red (mRNA downregulated). The targeting miRNAs are also displayed as green (upregulated) or red (downregulated) in SCA3 neurons as compared to control neurons.

3.3.7 Target selection from gene expression and miRNA expression profiling for further validation

The next step after the high throughput RNA-seq experiment was to choose targets, which might be relevant to SCA3 pathogenesis and whose dysregulation in the iPSC-derived SCA3 neurons might be due to miRNA targeting.

In the SCA3 neurons, the dysregulated mRNAs that are involved in the axon guidance pathway and are predicted targets of dysregulated miRNAs are obvious choices (**table 3.10**). However, none of the proteins coded by these mRNAs are known and experimentally validated interaction partners of ATXN3. Also, choosing the right candidate(s) for validation, when several proteins involved in the axon guidance pathway might be modulated by the dysregulated miRNAs, is complicated. Hence, priority for validation was given to another gene, whose mRNA is dysregulated in the SCA3 neurons, namely: the DNAJB1 gene that codes for the DNAJB1 chaperone protein.

The DNAJB1 chaperone is known to interact with intranuclear inclusions formed in SCA3 as well as other polyQ diseases (Seidel et al, 2012a). In the gene expression profile from the iPSC-derived neurons, the DNAJB1 mRNA was one of the 71 dysregulated mRNAs with a 2.56 fold downregulation (or -2.56) in the profiles from 3 SCA3 neuronal cell lines compared to 2 control cell lines. As is evident from the protein interaction analysis of the gene expression profile (**figure 3.17**), DNAJB1 is the only protein of the 71 proteins coded by the dysregulated mRNAs that is known to directly interact with ATXN3. Also, 11 of the 90 dysregulated miRNAs in SCA3 neurons are predicted to target the DNAJB1 mRNA via binding at specific target sites on the 3'UTR of DNAJB1 mRNA according to the target prediction tool TargetScan (**table 3.13**).

miRNA name	Fold change in iPSC-derived SCA3 neurons	Conservation of DNAJB1 3'UTR binding site across species
DNAJB1 targeting miRNAs upregulated in SCA3 neurons		
hsa-miR-370	45.14309	Conserved
hsa-miR-543	25.32928	Conserved
hsa-miR-299-3p	33.5104	Poorly conserved
hsa-miR-377-3p	35.65163	Poorly conserved
hsa-miR-379-5p	48.05916	Poorly conserved
hsa-miR-485-5p	38.617	Poorly conserved
hsa-miR-494	45.15569	Poorly conserved
DNAJB1 targeting miRNAs down regulated in SCA3 neurons		
hsa-miR-449a	-108.2534889	Conserved
hsa-miR-449b-5p	-80.34681096	Conserved
hsa-miR-143-3p	-17.50185064	Poorly conserved
hsa-miR-193a-3p	-13.50312411	Poorly conserved

Table 3.13: miRNAs dysregulated in SCA3 neurons with predicted binding sites on the 3'UTR of DNAJB1 mRNA. Profiling data from 3 SCA3 neuronal cell lines and 2 control neuronal cell lines. The target predictions were done using the TargetScan tool. Seven of the dysregulated miRNAs are upregulated while four are downregulated in SCA3 neurons. The conservation of the each miRNA binding site across species is also denoted.

Once DNAJB1 was chosen as a candidate to be validated as a miRNA target of relevance in SCA3, the succeeding experiments dealt with the following points:

- Quantification of DNAJB1 mRNA and protein levels in iPSC-derived neurons.
- Validation of the ability of specific miRNAs to bind at specific binding sites on the 3'UTR of DNAJB1 mRNA.
- Analysis of the miRNAs' effect on endogenous DNAJB1 mRNA and protein levels in human cell lines.
- Analysis of the miRNAs' effect on aggregation of expanded ATXN3.
- Quantification of DNAJB1 mRNA and protein levels in a transgenic mouse model of SCA3.

3.3.8 Quantification of DNAJB1 mRNA and protein levels in iPSC-derived neurons

The quantification of DNAJB1 mRNA and protein levels in the iPSC-derived neurons was the first step in the validation of DNAJB1 as a miRNA target in SCA3. DNAJB1 mRNA levels were analysed by real-time PCR with the aim of verifying the results of the gene expression profile in which the SCA3 neurons had a -2.56 fold downregulation in the DNAJB1 mRNA compared to controls. As shown in **figure 3.19**, the DNAJB1 mRNA levels are significantly lower in the SCA3 patients as compared to the controls.

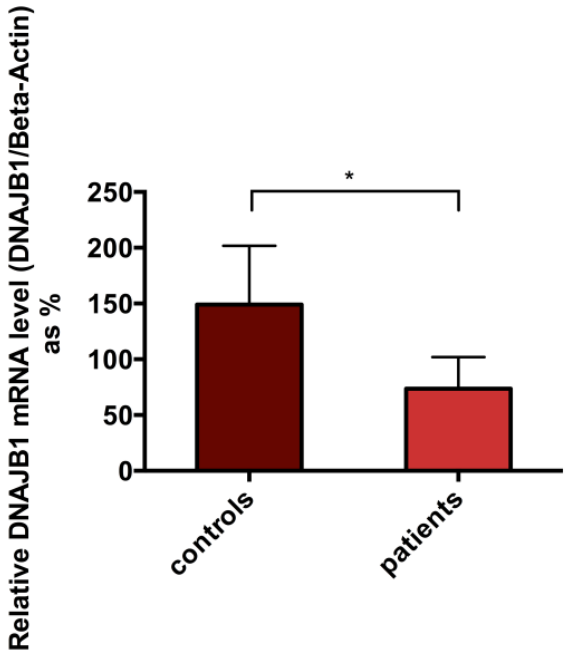

Figure 3.19: DNAJB1 mRNA levels are reduced in the SCA3 neurons as compared to the controls. DNAJB1 and beta-actin mRNA levels (as loading control) were checked by SYBR Green real-time PCR. Columns represent values +/- standard deviation from 2 control neuronal cell lines (controls) and 3 SCA3 neuronal cell lines (patients).

The DNAJB1 protein level in the iPSC-derived neurons was quantified by immunoblotting using an antibody against DNAJB1 as shown in **figure 3.20a**. On quantification and normalization of the signal intensities to the housekeeping protein alpha tubulin, it is evident that the SCA3 neurons have a reduced level of DNAJB1 protein as compared to the control neurons (**figure 3.20b**).

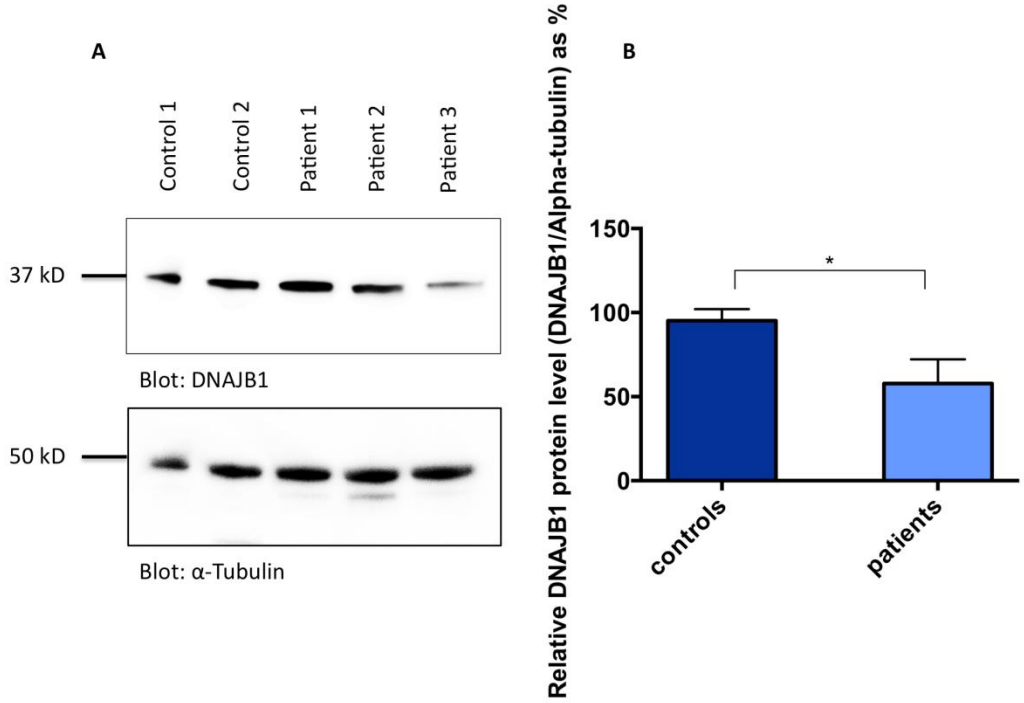

Figure 3.20: DNAJB1 protein levels are reduced in SCA3 neurons as compared to the controls. DNAJB1 (A; upper panel) and alpha-tubulin (A; lower panel) protein levels were determined by immunoblotting against specific antibodies. As shown in (B) the DNAJB1 protein levels were quantified based on the ratio of DNAJB1 to the loading control alpha-tubulin. Columns represent values +/- standard deviation from 2 control neuronal cell lines (controls) and 3 SCA3 neuronal cell lines (patients).

3.3.9 Validation of the ability of specific miRNAs to bind at specific binding sites on the 3'UTR of DNAJB1 mRNA

From the dysregulated miRNAs predicted to target the 3'UTR of DNAJB1 mRNA, four miRNAs were chosen for validation experiments: miR-543, miR-370, miR-449a and miR-143. These miRNAs were chosen because they are highly dysregulated in the SCA3 neurons (**table 3.13**) and because the binding sites of three of them (miR-543, miR-370 and miR-449a) are conserved across species. miR-370 has two conserved binding sites on DNAJB1 3'UTR. The 3'UTR of DNAJB1 mRNA is 1170 nt long. The locations of the binding sites for the chosen miRNAs are shown in **figure 3.21**.

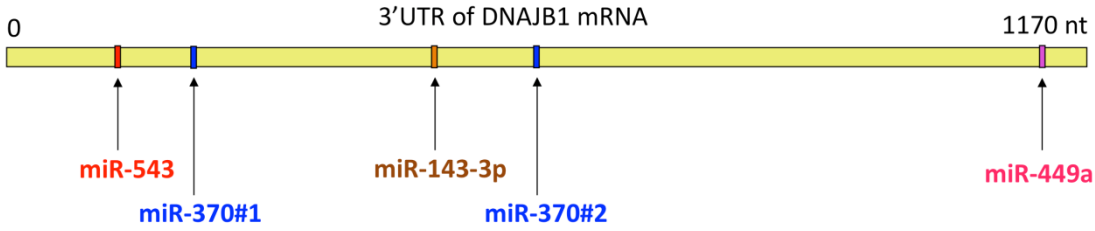

Figure 3.21: A pictorial representation of the DNAJB1 3'UTR with the locations of the binding sites of the selected miRNAs.

To validate the ability of these miRNAs to target specific sites on the DNAJB1 3'UTR, the 3'UTR was cloned into the luciferase reporter vector psiCHECK-2. As in previous sections, the 3'UTR was fused to Renilla luciferase. The binding sites for the four chosen miRNAs were mutated by substitutions of two nucleotides complementary to positions 2, 3 on the miRNA seed region. An example of this is shown in **figure 3.22**, where the miR-543 binding site mutant is depicted (figures for the other miRNA binding site mutants are included in the appendix).

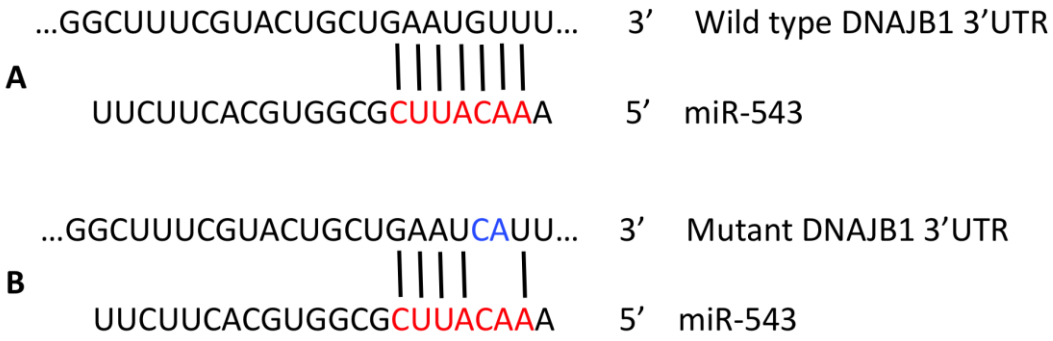

Figure 3.22: Representation of miR-543 binding to DNAJB1 3'UTR at its predicted binding site. The binding of miR-543 to the wild type DNAJB1 3'UTR is shown in (A), and the disruption of binding caused by mutations at two nucleotides in the miR-543 binding site in DNAJB1 3'UTR is shown in (B).

To analyse if the specific miRNAs target at their predicted binding sites, Hela cells were transfected with constructs containing either the wild type 3'UTR of DNAJB1 or the

3’UTR with miRNA binding site mutants. Cells were lysed 48 hours after transfections and the Renilla and Firefly signals from the cell lysates were measured in the luciferase assay. Mutations at the binding sites for miR-143, miR-449a and miR-543 in the DNAJB1 3’ UTR led to an increased signal ratio of Renilla/Firefly luciferase (**figure 3.23**) suggesting that the mutations led to a decrease in miRNA targeting of the Renilla-DNAJB1 3’UTR mRNA. Therefore the endogenously expressed miRNAs from the Hela cells were able to target their predicted binding sites on DNAJB1 3’UTR. Mutating either one or both the binding sites of miR-370 on DNAJB1 3’UTR also led to an increased signal ratio of Renilla/Firefly luciferase (**figure 3.24**). The double mutant with both binding sites mutated gave a significantly increased signal ratio compared to the mutants with either the first or the second miR-370 binding site mutated. This suggests that although miR-370 can target the DNAJB1 3’UTR by binding at either of its two binding sites, the targeting is enhanced by binding at both the sites.

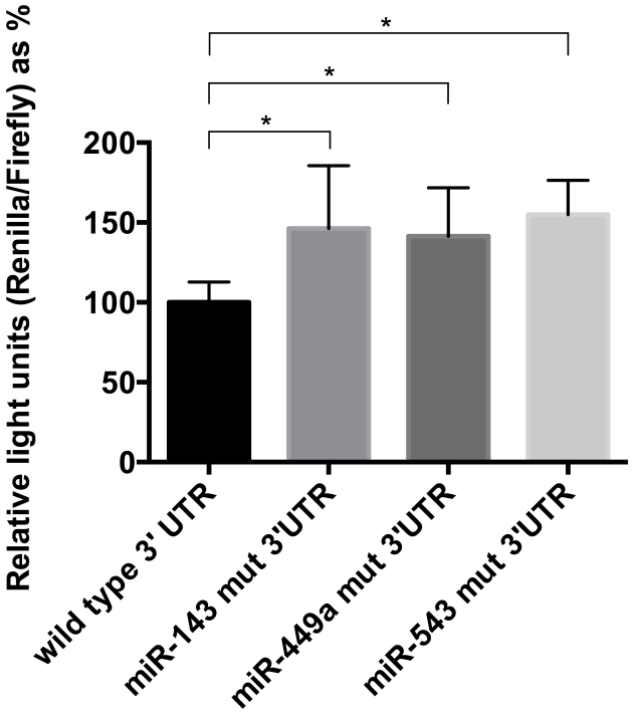

Figure 3.23: Mutations of miRNA binding sites in DNAJB1 3’UTR lead to increased Renilla/Firefly signal ratio. Binding sites of miR-143, miR-449 or miR-543 in DNAJB1 3’UTR sequence in psiCHECK-2 vector were mutated. Wild type and mutant constructs were transfected in Hela cells and Renilla, Firefly luciferase signals measured 48 hours after transfection. Columns represent values +/- standard deviation. n = 27, P-value = 0.0001

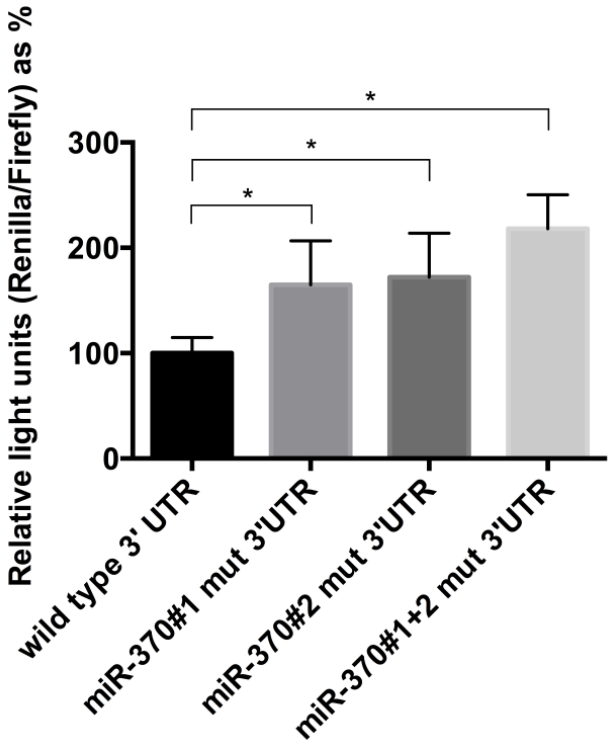

Figure 3.24: Mutations of miR-370 binding sites in DNAJB1 3'UTR lead to increased Renilla/Firefly signal ratio. Both the binding sites of miR-370 in DNAJB1 3'UTR sequence in psiCHECK-2 vector were mutated. Wild type and mutant constructs were transfected in Hela cells and Renilla, Firefly luciferase signals measured 48 hours after transfection. Columns represent values +/- standard deviation. n = 27, P-value = 0.0002

3.3.10 Analysis of the miRNAs' effect on endogenous DNAJB1 mRNA and protein levels in human cell lines

DNAJB1 mRNA and protein were downregulated in iPSC-derived SCA3 neurons (**figure 3.19 and figure 3.20 resp**.), whereas the miRNA expression profile suggested that miR-370 and miR-543 were upregulated in iPSC-derived SCA3 neurons as compared to control neurons (**table 3.13**). Hence the relationship between DNAJB1 mRNA, protein and these miRNAs fits exactly to what would be expected from a miRNA-target pair. The results from the luciferase assays support this assumption. Therefore, miRNAs miR-370 and miR-543 were analysed for their ability to modulate DNAJB1 mRNA and protein expression.

To analyse their ability to modulate DNAJB1 mRNA and protein expression, miR-370 and miR-543 were overexpressed in Hela cells using their mimic oligonucleotides. Hela cells were transfected with miR-370 and miR-543 mimics for 48 hours. Cell lysates were immunoblotted to analyse the DNAJB1 protein levels whereas RNA extracted from the transfected cells and further reverse transcribed into cDNA was used for analysing the DNAJB1 mRNA in the cells by SYBR green real time PCR.

The overexpression of miR-370 and miR-543 led to a significant decrease in DNAJB1 mRNA levels 48 hours after transfections (**figure 3.25)**. Consequently an accompanying substantial decrease in DNAJB1 protein expression was also seen in immunoblots (**figure 3.26)**.

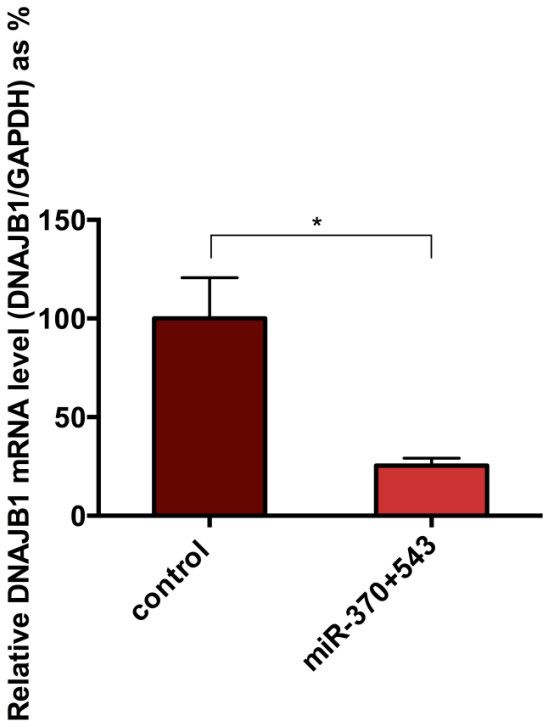

Figure 3.25: Overexpression of miR-370 and miR-543 decreases DNAJB1 mRNA levels in Hela cells. miR-370 and miR-543 mimics were co-transfected in Hela cells. DNAJB1 and GAPDH mRNA levels (as loading control) were checked by SYBR Green real-time PCR 48 hours after the transfection. Columns represent values +/- standard deviation. n = 3, P-value = 0.0047

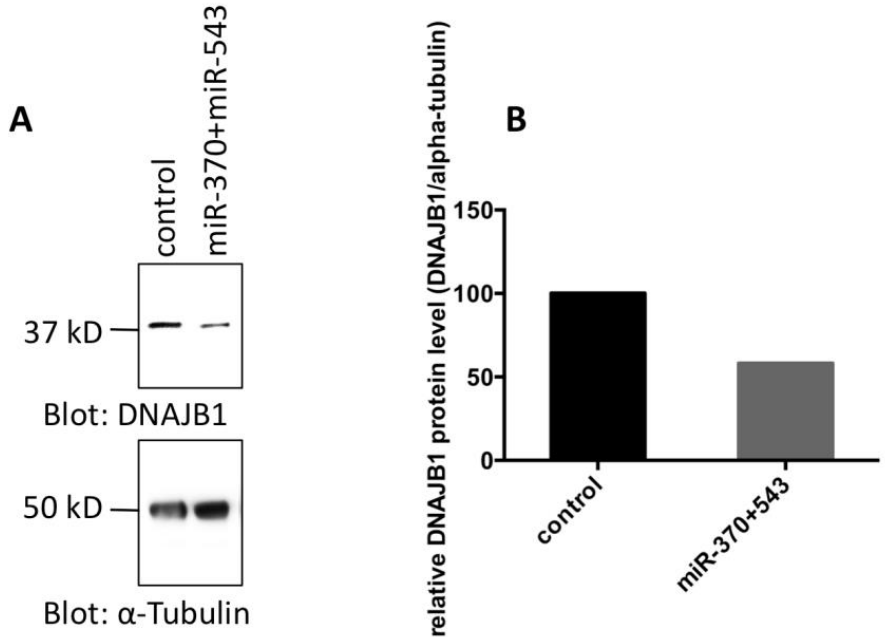

Figure 3.26: Overexpression of miR-370 and miR-543 decreases DNAJB1 protein levels in Hela cells. miR-370 and miR-543 mimics were co-transfected in Hela cells. The DNAJB1 (A; upper panel) and alpha-tubulin (A; lower panel) protein levels 48 hours post transfection were determined by immunoblotting using specific antibodies. As shown in (B) the DNAJB1 protein levels were quantified based on the ratio of DNAJB1 to the loading control alpha-tubulin. Columns represent percentage value of MID1/alpha-tubulin ratio.

3.3.11 Analysis of the miRNAs' effect on aggregation of expanded ATXN3

Since DNAJB1 has been shown to colocalize with aggregates formed by expanded ATXN3, an experiment was set up to check the effect of miR-370 and miR-543 overexpression on DNAJB1 expression and ATXN3 aggregate formation in Hela cells. Hela cells were co-transfected with miR-370, miR-543 mimics and myc-tagged c-terminal Q71 ATXN3 cloned into the pcDNA 3.1 construct (kind gift from Dr. P Breuer, Uniklinik Bonn) for 48 hours. Cells were immunostained with antibodies against myc or DNAJB1, followed by secondary antibodies tagged with Cy3 and Alexa 647 respectively. As shown in **figure 3.27**, c-terminal Q71 ATXN3 formed aggregates in a certain percentage of cells (green signal). No visible co-localization of DNAJB1 (red signal) with the aggregates was

seen in cells co-transfected with either control siRNA (**figure 3.27A**) or miR-370 and miR-543 mimics (**figure 3.27B**). Upon counting cells with aggregates, around 12.6% cells co-transfected with control siRNA and c-terminal Q71 ATXN3 had aggregates, while around 7.4% of the cells co-transfected with miR-370, miR-543 and c-terminal Q71 ATXN3 had aggregates, thus exhibiting no significant difference in the number of cells bearing aggregates upon co-transfection with either the control siRNA or miR-370, miR-543 mimics.

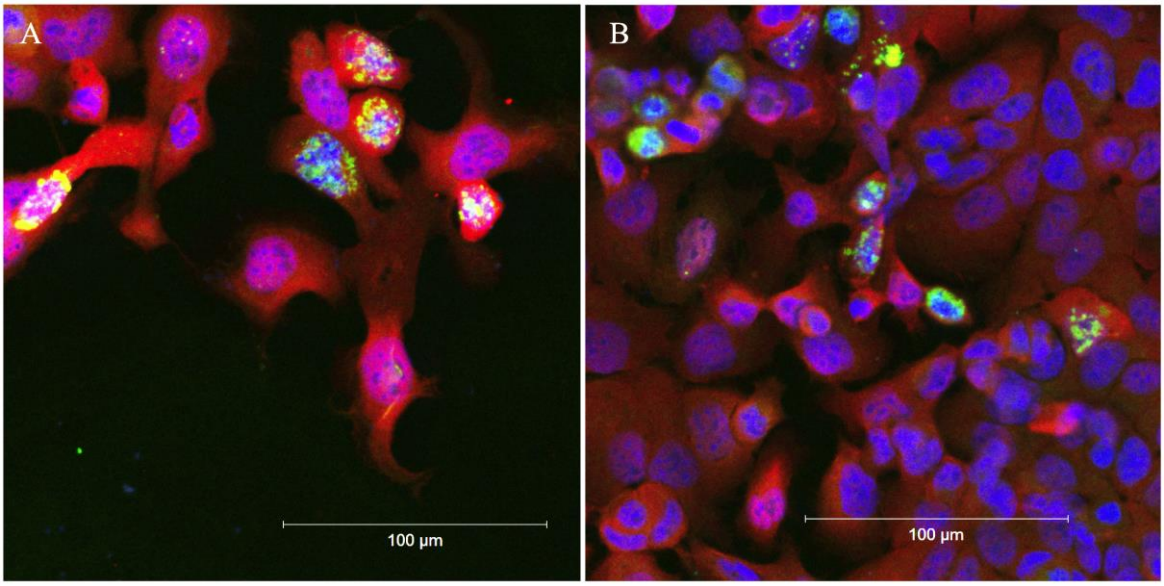

Figure 3.27: Transfection of miR-370, miR-543 does not alter aggregation of expanded ATXN3. Upon co-transfection of Hela cells with the aggregate prone c-terminal Q71 ATXN3 with either control siRNA (A) or miR-370, miR-543 (B) no significant differences in the number of cells bearing aggregates were seen.

3.3.12 Quantification of DNAJB1 mRNA and protein levels in a transgenic mouse model of SCA3

B6.SCA3-YAC-84Q mice expressing the human ATXN3 gene with 84 CAG repeats have been shown to exhibit SCA3 related symptoms such as motor dysfunction, progressive ataxia, presence of ATXN3 aggregates in neurons (Cemal et al, 2002). DNAJB1 mRNA and protein levels were checked in hindbrains of 6 month old male control and SCA3 mice. As shown in **figure 3.28**, DNAJB1 mRNA levels in the SCA3 mice were reduced as

compared to the controls. However no significant difference was seen in DNAJB1 protein levels in the SCA3 mice as compared to the controls as seen in **figure 3.29**.

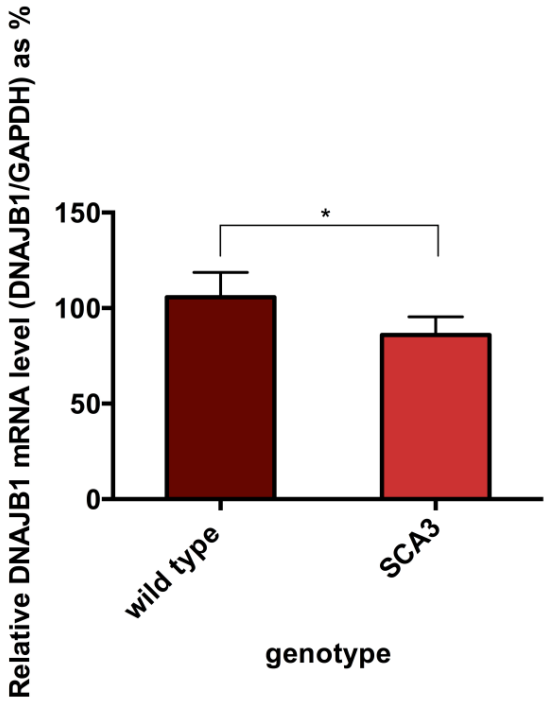

Figure 3.28: DNAJB1 mRNA levels are reduced in the hindbrains of transgenic SCA3 mice as compared to wild type mice. DNAJB1 and GAPDH mRNA levels (as loading control) were checked by SYBR Green real-time PCR. Columns represent values +/- standard deviation. n = 4, P-value = 0.0004

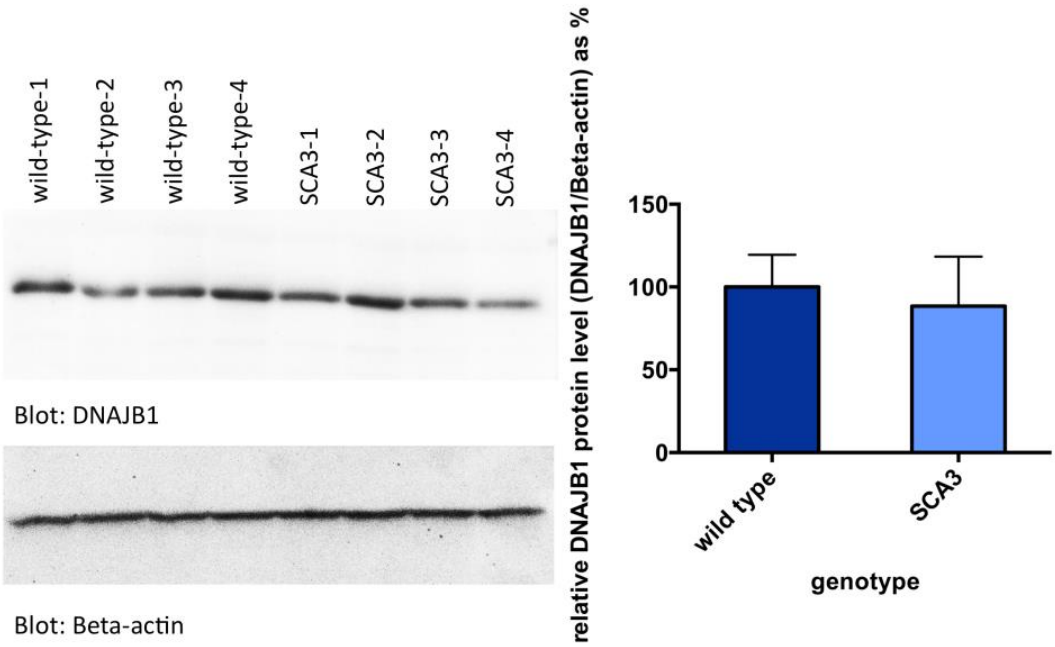

Figure 3.29: DNAJB1 protein levels are unchanged in the hindbrains of transgenic SCA3 mice as compared to wild type mice. DNAJB1 (A; upper panel) and beta.actin (A; lower panel) protein levels were determined by immunoblotting using specific antibodies. As shown in (B) the DNAJB1 protein levels were quantified based on the ratio of DNAJB1 to the loading control beta-actin. Columns represent values +/- standard deviation. n = 4, P-value = 0.5431

Chapter 4 Discussion

MicroRNAs are important regulators of gene expression and have been linked to several diseases including neurodegenerative diseases. In this study, miRNAs that modulate the expression of specific proteins relevant in the pathogenesis of SCA3 were investigated. Two miRNAs, hsa-miR-32 and hsa-miR-181c were found to target ATXN3, the protein mutated in SCA3. Moreover, the study revealed the ability of three miRNAs, hsa-miR-216a-5p, hsa-miR-374a and hsa-miR-542-3p to target MID1, a protein that stimulates the translation of expanded CAG repeat mRNAs. Finally, two miRNAs, namely hsa-miR-370 and hsa-miR-543 were ascertained to target DNAJB1, a chaperone that has been shown to play a role in prevention of SCA3 toxicity. This study suggests that these miRNAs might act as disease modifiers in SCA3 due to their ability to target the expression of proteins playing a role in the cell toxicity observed in SCA3.

4.1 miRNAs target ATXN3 3'UTR and downregulate ATXN3 mRNA and protein expression

Polyglutamine diseases are characterized by the expression of mutant proteins with expanded glutamine repeats. The mutant proteins form aggregates into which several other proteins are sequestered contributing to the neurotoxicity observed in polyQ diseases (McCampbell et al, 2000; Perez et al, 1998). Several cellular mechanisms such as regulation of protein folding or proteasomal degradation of the aggregate prone proteins suppress aggregate formation and toxicity (Chai et al, 1999b). The neuronal cell death seen in the brains of polyQ disease patients over several years can be considered as a result of a lost battle by the neurons trying to restrict the expression of the mutant protein as well as other neurotoxic proteins, while at the same time maintaining the expression of neuroprotective proteins. miRNAs are important for the regulation of gene expression with up to 30% of human genes estimated to be regulated by miRNAs (Lewis et al, 2005). Studies are gradually casting a light on the crucial role miRNAs play in the pathogenic mechanisms in polyQ diseases. Previous studies have shown that the mutant proteins whose expression is the basis of toxicity in polyQ diseases are directly targeted by miRNAs and disease progression is modulated by the expression of miRNAs. This has

been shown to be the case for DRPLA (Karres et al, 2007) and SCA1 (Lee et al, 2008; Persengiev et al, 2011). In this study, miRNAs predicted to target the 3'UTR of ATXN3 were analysed and the ability of five candidate miRNAs: miR-9, miR-32, miR-125a-5p, miR-181c and miR-383 to target ATXN3 3'UTR at specific binding sites was validated. These studies suggest that all the five miRNAs are able to target the ATXN3 3'UTR at their specific binding sites. The targeting by two of the five miRNAs could be verified, namely miR-32 and miR-181c led to a downregulation of expression of ATXN3 mRNA and protein. miR-32 and miR-181c have been previously shown to be associated with the spread of tumours in colorectal carcinoma and breast cancer respectively (Tominaga et al, 2015; Wu et al, 2013), however this is the first study implicating these miRNAs in the regulation of ATXN3 expression. Individual overexpression of either miR-32 or miR-181c did not yield a substantial decrease in ATXN3 levels (data not shown), while a combination of both miRNAs did. This is not surprising, since there is evidence that miRNAs function in combination to effectively repress the expression of a common target mRNA (Vo et al, 2010; Wu et al, 2010). The 3'UTR sequence of wild type and mutant ATXN3 is identical, therefore miR-32 and miR-181c can be expected to downregulate both the wild type and the mutant allele of ATXN3. Huang *et al* have recently shown the ability of miR-25 to downregulate wild type as well as mutant ATXN3, leading to a decrease in cell toxicity in a SCA3 model (Huang et al, 2014). miR-25 binds to ATXN3 3'UTR at the same binding site as miR-32 with similar predicted efficiency. These results taken together suggest that several miRNAs target the ATXN3 3'UTR and regulate ATXN3 protein expression. Unravelling multiple miRNAs, which target ATXN3, will help to identify a pool of miRNAs which can be used to build a therapeutic strategy. Using such a pool will help to overcome the problems of high concentrations of individual miRNAs and the resultant off target effects.

Further experiments regarding miRNA targeting of ATXN3 would include the use of lentiviral mediated delivery of miRNAs to iPSC-derived SCA3 neurons. This would verify the ability of these miRNAs to modulate the expression of the mutant ATXN3 allele as well as the formation of microaggregates that are formed in these neurons upon glutamate excitation (Koch et al, 2011). Alternately, such a lentiviral delivery approach could be used to assess miRNA mediated control of expanded ATXN3 expression in YAC transgenic mice carrying the expanded ATXN3 locus, or primary neuronal cells prepared from these mice (Cemal et al, 2002). Although miRNA mediated targeting of ATXN3 is

not exclusive for the mutant allele (since the mutant and the wild type allele share the same 3'UTR sequence), a decrease in the wild type ATXN3 as a side-effect might not be deleterious to the cells. Studies in ATXN3 knock-out mice have shown that these mice, despite the absence of ATXN3 are viable and fertile (Schmitt et al, 2007; Switonski et al, 2011). Hence, miRNA targeting of ATXN3 might be a viable strategy to counter SCA3 toxicity.

4.2 miRNAs target MID1 3'UTR and downregulate MID1 mRNA and protein expression

Apart from targeting the mutant proteins in polyQ diseases, there is growing evidence that miRNAs also modulate the expression of other proteins that contribute to neurotoxicity in polyQ diseases. In several cases, the disease progression is associated with reduced expression of these miRNAs leading to an elevated expression of their neurotoxic targets. In HD, it has been shown that reduced levels of miRNAs as a result of transcriptional repression by the REST repressor results in elevated levels of miRNA targets, which might be associated with the pathogenicity of HD (Johnson et al, 2008). A study in animal and cell models of SCA3 has shown that reduced expression of miRNAs as a result of mutation in miRNA processing proteins causes enhanced toxicity of the mutant ATXN3 protein suggesting that miRNAs play a protective role by controlling the expression of pathogenic proteins (Bilen et al, 2006). The protein MID1 was chosen as a neurotoxic protein candidate for analysing miRNA targeting relevant to SCA3. MID1 is part of a protein complex that binds CAG repeat mRNAs in a length dependent manner and stimulates their translation to expanded polyQ repeat proteins. Although studies relevant to this observation were conducted in a HD model (Krauss et al, 2013), preliminary studies suggest that MID1 also binds to expanded ATXN3 mRNA in a length dependent manner (unpublished data according to personal communication with Dr. Sybille Krauss, DZNE Bonn). MID1 was therefore a valid candidate to study putative miRNA mediated regulation. This study revealed that three miRNAs: miR-216a-5p, miR-374a, miR-542-3p target the 3'UTR of MID1 at specific binding sites. Overexpression of these three miRNAs in HEK T-293 cells led to a decrease in endogenous levels of MID1 mRNA and protein in these cells. Previous studies have shown MID1 to be a target of miR-135b in breast cancer (Arigoni et al, 2013), however the ability of miR-216a-5p, miR-374a and

miR-542-3p to target MID1 has not been previously documented. Since MID1 binds and aids translation of ATXN3 mRNA in a length dependent manner, the miRNA mediated downregulation in MID1 might lead to reduction in the translation of the mutant ATXN3 mRNA leaving the wild type allele unaffected. Furthermore, this miRNA mediated repression of MID1 expression might be beneficial for controlling polyQ toxicity beyond the repression of mutant ATXN3. It has been shown that the aggregates formed in polyQ neurons sequester other proteins containing glutamine stretches such as as TATA-binding protein (TBP), Eyes Absent (EYA) protein (Perez et al, 1998). Although it is not yet proven, MID1 might be able to bind and stimulate the expression of the CAG repeat mRNAs of these proteins as well. Therefore, a reduction in MID1 levels might function to reduce the expression of several proteins that partake in the formation of aggregates in polyQ diseases. Targeting of MID1 expression using miRNAs could also be a strategy employed in other CAG repeat disorders.

Further experiments concerning the effects of miRNA targeting of MID1 expression on CAG repeat mRNAs are required to ascertain if miRNA targeting of MID1 might play a role in SCA3 and in general polyQ pathogenesis. Reporter constructs carrying different lengths of CAG repeats, which are available in the laboratory, will be used for further experiments (Krauss et al, 2013).

4.3 The use of iPSC-derived SCA3 neurons to analyse SCA3 associated gene and miRNA expression

In parallel to the studies to find miRNAs targeting the neurotoxic proteins ATXN3 and MID1, access was gained to a recent model system to study SCA3 pathogenesis, *viz* neurons derived from Induced Pluripotent Stem Cells (iPSCs) from SCA3 patients (Koch et al, 2011). The use of iPSCs as model systems to understand pathogenic mechanisms of diseases, as well as to device therapeutic strategies has been increasing in the recent years (Okano & Yamanaka, 2014; Park et al, 2008). As compared to other cell lines or animal models, an important advantage of the use of iPSCs is that they represent patient derived material that can be further differentiated into cells that are relevant to that particular disease. In the case of neurodegenerative diseases, the ability to differentiate iPSCs into neurons provides a very appropriate tool to study disease pathogenesis as well as device therapeutic strategies. iPSCs derived from primary cells such as fibroblasts or peripheral

blood lymphocytes from patients of several neurodegenerative diseases such as Alzheimer's disease (AD), Parkinson's disease (PD), Huntington's disease (HD) have been studied and in many cases these iPSCs have been further differentiated into neurons that exhibit pathogenic mechanisms associated with these disorders (Camnasio et al, 2012; Nguyen et al, 2011; Soldner et al, 2009; Yagi et al, 2011).

Neurons used were differentiated from iPSCs derived from SCA3 patients and healthy controls to study changes in gene expression and miRNA expression profiles associated with the expression of the expanded CAG repeat containing ATXN3 allele. Microaggregates containing ATXN3 have been observed in these neurons upon excitation with glutamate or NMDA (Koch et al, 2011). However the neurons used in this study, were not subjected to glutamate excitation. The reason for this was the assumption that glutamate excitation and resulting flow of Ca^{2+} ions into the neurons probably leads to massive and short term changes in gene expression and miRNA expression as the cells respond to the excitation. The focus in this study was understanding the differences in gene and miRNA expression in SCA3 and control neurons, which are associated with the expression of the mutant allele over a longer period of time, and hence, might be associated with the relatively slower acting mechanisms of cell toxicity.

The RNA isolated from two control lines and three SCA3 lines of iPSC-derived neurons was used for mRNA and miRNA expression profiling. Although a higher number of samples would have been preferable in terms of the statistical strength of the results, additional cell lines were not available at that time.

Comparison of the gene expression profiles of the SCA3 neurons with the control neurons revealed dysregulation in the expression of several genes. To understand the relevance of this dysregulation in terms of mechanisms that might be altered due to the presence of mutant ATXN3, the gene expression data was analysed using gene ontology analysis, pathway analysis and analysis of the interaction of proteins coded by the dysregulated genes with the ATXN3 protein.

Gene and miRNA expression profile suggests alterations in the axon guidance pathway and the DNAJB1 chaperone in the SCA3 neurons

The gene and miRNA expression profiles from iPSC-derived control and SCA3 neurons were analysed using various tools which enabled analyses such as gene ontology analysis, pathway analysis and protein interaction analysis. The gene ontology analysis of the dysregulated genes is categorized into three categories: molecular function, biological process and cellular compartment. Considering the enriched terms in all three categories gives an idea of the significance of the dysregulated gene expression. The enriched terms for molecular function of the dysregulated genes suggests that the SCA3 neurons might have altered structural molecule activity, cytoskeletal regulatory protein binding, cytoskeletal protein binding, poly(A) RNA binding and protein anchor activity. The enriched terms for the biological processes associated with the dysregulated genes suggest that the SCA3 neurons have altered neuron development, especially axonal development. In terms of the cellular location of the proteins coded by the dysregulated genes, the enriched terms associated with cellular compartment suggest that the proteins are predominantly located in cellular projections, especially in axonal projections. In summary, the GO analysis of the dysregulated genes suggests that in comparison with the controls, the SCA3 neurons have alterations in the binding of cytoskeletal and RNA binding proteins which might be associated with changes in neurite outgrowth and axonal development, with localization of a significant number of dysregulated proteins in the cellular projections such as the axonal projections.

The mechanisms suggested by the GO analysis are reinforced by the pathway analysis of the dysregulated genes as well as the dysregulated miRNAs in the SCA3 neurons. The pathway analysis of the dysregulated genes suggests that the SCA3 neurons might have alterations in the axon guidance pathway. Axon guidance is the process in which neuronal axons respond to guidance cues to grow and form synapses with specific target neurons eventually leading to the formation of a neuronal network (Tessier-Lavigne & Goodman, 1996). The guidance cues for axons in this process are molecules expressed by other neurons and are either secreted or expressed on the cell surface. There are several classes of proteins such as netrins, semaphorins, Cell Adhesion Molecules (CAMs) that act as guidance cues enabling attraction or repulsion of axons (Varela-Echavarria & Guthrie, 1997). The recognition of these guidance cues triggers downstream signalling cascades in the neurons that lead to appropriate response to the cues. The pathway analysis of the

dysregulated genes in the gene expression profile of SCA3 and control neurons suggests that the SCA3 neurons might have alterations in mechanisms included in axonal guidance pathway such as netrin-1 signalling, semaphorin signalling and interactions of the cell adhesion molecule L1. Several genes that are upregulated in SCA3 neurons code for proteins that aid in neurite outgrowth via interaction with netrins (such as the genes DCC, PITPNA), semaphorins (SEMA6A), neural cell adhesion molecules (ANK3, KCNQ2, ST8SIA2) or the cytoskeleton (MAP1B, MAP2). A higher level of neurite growth in the SCA3 neurons can be explained by observations from previous studies connecting the expression of polyQ proteins to altered axonal development and transport. Although polyQ inclusions, a hallmark of polyQ diseases, have been traditionally observed in neuronal soma, there are several studies showing the presence of such inclusions in axons. Axonal inclusions have been in seen in axonal fiber tracts that are degenerated in the brains of SCA3 patients and HD patient brains (Rub et al, 2014; Seidel et al, 2010). Besides, axonal inclusions have been observed in cell culture and animal models of HD (Krench & Littleton, 2013; Li et al, 2001), SBMA (Piccioni et al, 2002) and SCA3 (Cemal et al, 2002). These axonal inclusions interfere with axonal transport, leading to defects and even degeneration of neurites (Gunawardena & Goldstein, 2005; Li et al, 2001; Piccioni et al, 2002). There is also a suggestion that the mere presence of polyQ proteins disturbs retrograde and anterograde transport along the axons, even when the polyQ protein is not recruited into inclusions (Szebenyi et al, 2003). Therefore, the elevated neurite growth in SCA3 neurons as suggested by the profiling experiments might be a protective mechanism employed by the neurons in response to hindrances in axonal transport leading to disruption in the supply of molecules that are required in neurite growth. It is also possible that the elevated neurite growth is simply the result of the individual iPSC-derived cell lines being in varying stages of neuronal differentiation in culture. Conversely, the elevated neurite growth could also be associated with MID1 activity. The loss of MID1 function is associated with enhanced axonal growth and elongation in mouse cortex due to the enhanced activity of PP2A which is targeted for degradation by MID1 (Lu et al, 2013). Although the study exhibiting this observation was not associated with a polyQ disorder, it is possible that in the SCA3 neurons the association of MID1 with expanded CAG repeat ATXN3 mRNA prevents it from carrying out its degradative function towards PP2A, leading to enhanced axonal growth. Further studies are necessary to establish any relationship between MID1 and axonal growth in SCA3 neurons.

The pathway analysis of the putative targets of the miRNAs that are dysregulated in SCA3 neurons also suggests an enrichment of the targeted genes involved in the axon guidance pathway. Many of the dysregulated miRNAs have putative targets in the axon guidance pathway and these miRNAs are upregulated as well as downregulated in the SCA3 neurons. While most of the putative targets do not show altered mRNA levels in the SCA3 neurons, a few targets are dysregulated as seen in the gene expression profile. Although validation studies would be necessary prior to drawing conclusions, enrichment of the axon guidance pathway in both the gene as well as the miRNA expression profile suggests that miRNA targeting of gene expression plays a role amongst the mechanisms the SCA3 neurons use to deal with the effects of the presence of pathogenic ATXN3. A short mention must be made here regarding the expression of miRNAs directly targeting the expression of ATXN3 and MID1 in the miRNA profile of the SCA3 neurons. As seen in the profiles, none of the miRNAs analysed to target ATXN3 or MID1 mRNA are dysregulated in the SCA3 neurons, neither are the ATXN3 or MID1 mRNAs. This suggests that in these particular neurons, miRNA mediated targeting of ATXN3 and MID1 was either not active, or was carried out with other miRNAs which are not amongst those predicted to target ATXN3 or MID1 mRNAs.

Protein interaction analysis was done to check if genes coding for known interaction partners of ATXN3 are dysregulated in SCA3 neurons. This analysis revealed that the chaperone DNAJB1, which is a known interaction partner of ATXN3, was downregulated in SCA3 neurons. DNAJB1 is one of the HSP40 chaperones and being a co-chaperone of HSP70, is essential for the ability of HSP70 to refold proteins that are misfolded (Michels et al, 1999). DNAJB1 plays a key role in the cellular response to polyQ aggregates including mutant ATXN3 aggregates in SCA3. It is known that DNAJB1 co-localizes with SCA3 aggregates and along with HSP70 is involved in the process of converting the toxic fibril like aggregates into amorphous aggregates which can be degraded (Muchowski et al, 2000). Therefore, the maintenance of DNAJB1 expression levels in the cell would be important in counteracting the aggregate mediated toxicity seen in SCA3. However the gene expression profile suggested a downregulation in DNAJB1 mRNA in the SCA3 neurons. Moreover, miRNA expression profile suggested that several miRNAs predicted to target the DNAJB1 mRNA by binding at 3'UTR are also dysregulated in SCA3 neurons. Considering the importance of DNAJB1 in SCA3, miRNA targeting of DNAJB1 occurring in SCA3 neurons as seen in the profiling experiments was validated.

4.4 miRNAs target DNAJB1 3'UTR and downregulate DNAJB1 mRNA and protein expression

To validate the observed DNAJB1 modulation in the iPSC-derived SCA3 neurons as suggested by the profiling experiment, DNAJB1 mRNA and protein levels in SCA3 and control neurons were checked and it was found that there was indeed a downregulation in the levels of DNAJB1 mRNA as well as protein in SCA3 neurons. From amongst the dysregulated miRNAs predicted to target DNAJB1 3'UTR, four miRNAs: miR-143, miR-370, miR-449c and miR-543 were able to target DNAJB1 3'UTR at specific binding sites. Furthermore the overexpression of two of these miRNAs, miR-370 and miR-543 led to a decrease in DNAJB1 mRNA and protein levels. So far, this is the first study exhibiting miRNA targeting of DNAJB1 in human cells. miR-370 and miR-543 have previously been associated with the spread of prostate cancer and hepatocellular carcinoma respectively but have not been previously shown to target any chaperone or be associated with any neurodegenerative disease (Wu et al, 2012; Yu et al, 2014).

Since DNAJB1 is involved in modulation of toxic aggregate formation, miR-370 and miR-543 were overexpressed to check if it led to any change in the formation of inclusions mediated by co-expression of the aggregate prone C-terminal fragment of expanded ATXN3. No significant changes in aggregate formation were detected. However, drawing conclusions from these experiments is difficult since the validation of whether the transfected individual cells receive both miRNAs and plasmids could not be performed.

YAC transgenic mice carrying the expanded ATXN3 locus exhibit the formation of intranuclear inclusions along with progressive motor defects (Cemal et al, 2002). Levels of DNAJB1 in these YAC transgenic mice expressing the human ATXN3 transgene with 84 CAG repeats were checked. Transgenic mice at the age of 52 weeks had SDS-insoluble ATXN3 aggregates in their brains (data not shown). The DNAJB1 mRNA levels in the hindbrains of these mice were reduced as compared to controls of the same age. However, there was no significant change in the DNAJB1 protein levels. However, since the RNA and protein quantification was conducted from mouse hindbrains, it is possible that any differences in the DNAJB1 protein amounts in the neurons are diluted by the presence of DNAJB1 from other cell types in the brain lysates. Owing to the lack of conservation in miRNA target sites between the 3'UTRs of DNAJB1 in humans and mice it could not

verified if miR-370 and miR-543 might be involved in targeting of DNAJB1 in the transgenic mice. However, the downregulation of DNAJB1 mRNA could be verified both in SCA3 neurons as well as the YAC transgenic mice and hence suggests that this might be a phenomenon associated with SCA3.

This data suggests the existence of a new mechanism of pathogenesis in SCA3, wherein the dysregulation of miRNAs targeting DNAJB1 occurs, causing a decrease in the levels of DNAJB1 mRNA and protein. Owing to the neuroprotective nature of DNAJB1 via breakdown of aggregates, the decrease in its levels might be deleterious to the cells by enhancing aggregation of mutant ATXN3 and its associated toxicity. Although previous studies have shown a decrease in the cytosolic DNAJB1 protein levels in polyQ disease that is attributed to its sequestration into polyQ aggregates (Hay et al, 2004), a decrease on the transcript level has been shown for the first time in this study. An important question pertaining to the decreased DNAJB1 and increased miR-370, miR-543 levels is which is the cause and which is the effect? DNAJB1 is neuroprotective and studies have revealed that it's overexpression might ameliorate the toxicity associated with expanded ATXN3 (Chai et al, 1999a). Therefore, reduction in its expression might be detrimental to the cell. In fact, a study in fibroblasts from SCA3 patients by Zijlstra *et al* showed that SCA3 patients with comparatively lower levels of DNAJB1 in their fibroblasts had an earlier age of onset of the disease symptoms independent of the CAG repeat length (Zijlstra et al, 2010). Several miRNAs predicted to target DNAJB1 also target other mRNAs. Hence, it is possible that the reduction in DNAJB1 mRNA levels is the result of an 'off-target' effect in which miRNAs targeting DNAJB1 were upregulated by the cell to control the expression of some other mRNA. Strategies to prevent miRNA targeting of DNAJB1 mRNA might prove beneficial in SCA3 by preventing the downregulation of DNAJB1 mRNA and protein and thereby decreasing the formation of ATXN3 aggregates and the associated toxicity. There are several methods to inhibit specific miRNAs such as the use of antisense oligonucleotides, miRNA sponges or RNA decoys delivered via lentiviruses (Davis et al, 2006; Ebert et al, 2007; Haraguchi et al, 2009). Some of these strategies, such as the antisense oligonucleotides have also been put to a therapeutic use (Janssen et al, 2013). Therefore, the inhibition of specific miRNAs targeting DNAJB1 might be the basis of a new therapeutic approach to tackle SCA3 pathogenesis.

Concluding remarks

In conclusion, several miRNAs that target the mRNAs of proteins that are disease modifiers in SCA3 were identified. These miRNAs might play a role in SCA3 disease progression. Overexpression of the specific miRNAs targeting neurotoxic proteins, using molecules mimicking their targeting ability or conversely blocking the activity of specific miRNAs that target neuroprotective proteins could be used as therapeutic strategy to alter disease progression at different stages. Overexpression of the miRNAs targeting ATXN3 might prevent the toxic effects of the presence of the mutant protein. Likewise, overexpression of miRNAs targeting MID1 might arrest the translation of the expanded ATXN3 mRNA into the mutant ATXN3 protein. On the other hand, blocking the activity of miRNAs targeting DNAJB1 which protects the cells against the toxic effects of the mutant ATXN3 protein might be beneficial to the counter SCA3 toxicity.

Future studies are needed to understand several aspects of miRNA targeting in SCA3. It would be necessary to verify if the targeting of the above mentioned proteins by the specific miRNAs occurs *in vivo* and its resulting influence on disease pathology. Also helpful would be the identification of further miRNAs that target the expression of each of the proteins included in this study. In case of the neurotoxic proteins ATXN3 and MID1, this would be instrumental in defining a pool of miRNAs that together might be able to exert a stronger inhibitory effect on the expression of these proteins *in vivo*. Consequently, another part of future studies would be to test the *in vivo* side effects of the use of such a pool of miRNAs considering the possibility of off-target effects.

Appendix

List of genes upregulated in iPSC-derived neurons from SCA3 patients in comparison to iPSC-derived neurons from healthy controls. Genes have been arranged in descending order of fold change.

Gene symbol	Gene name	Fold change in iPSC-derived SCA3 neurons	FDR P-value
Genes upregulated in SCA3 neurons			
ELAVL2	ELAV like neuron-specific RNA binding protein 2	4.94	8.37E-03
KIAA1549L	KIAA1549-like	4.3	0.04
ANK3	ankyrin 3, node of Ranvier (ankyrin G)	3.96	2.26E-03
DCC	DCC netrin 1 receptor	3.81	0.02
MEX3A	mex-3 RNA binding family member A	3.37	1.96E-04
KCNQ2	potassium channel, voltage gated KQT-like subfamily Q, member 2	3.35	0.02
DIRAS2	DIRAS family, GTP-binding RAS-like 2	3.3	1.42E-03
KLF7	Kruppel-like factor 7	3.07	0.01
MAP2	microtubule-associated protein 2	2.99	0.05
ST8SIA2	ST8 alpha-N-acetyl-neuraminide alpha-2,8-sialyltransferase 2	2.79	0.02
GPC2	glypican 2	2.67	0.01
SLC38A1	solute carrier family 38, member 1	2.58	0.02
PTBP2	polypyrimidine tract binding protein 2	2.54	0.02
TRIB2	tribbles pseudokinase 2	2.53	3.02E-04
AKAP6	A kinase (PRKA) anchor protein 6	2.43	0.02

MAP1B	microtubule-associated protein 1B	2.35	6.67E-03
STK39	serine threonine kinase 39	2.34	0.04
STMN1	stathmin 1	2.21	0.03
NR2F1	nuclear receptor subfamily 2, group F, member 1	2.17	0.02
NDRG4	NDRG family member 4	2.16	9.14E-03
TSPYL4	TSPY-like 4	2.08	1.51E-03
DTX4	deltex 4, E3 ubiquitin ligase	1.93	1.27E-04
MLLT11	myeloid/lymphoid or mixed-lineage	1.9	0.05
BEX1	brain expressed, X-linked 1	1.86	2.38E-10
SEMA6A	sema domain, transmembrane domain (TM), and cytoplasmic domain, (semaphorin) 6A	1.84	8.44E-03
CYFIP2	cytoplasmic FMR1 interacting protein 2	1.78	0.02
RUFY3	RUN and FYVE domain containing 3	1.73	4.23E-03
KLC1	kinesin light chain 1	1.73	0.01
DYNC1H1	dynein, cytoplasmic 1, heavy chain 1	1.64	0.01
ATAT1	alpha tubulin acetyltransferase 1	1.63	0.03
GTF2I	general transcription factor IIi	1.62	0.01
RTN4	reticulon 4	1.61	8.84E-03
PARP6	poly (ADP-ribose) polymerase family, member 6	1.58	0.04
MATR3	matrin 3	1.53	1.96E-04
PGD	phosphogluconate dehydrogenase	1.52	1.74E-04
PITPNA	phosphatidylinositol transfer protein, alpha	1.52	0.04
SCRN1	secernin 1	1.46	4.39E-03
YWHAQ	tyrosine 3-monooxygenase/tryptophan 5-monooxygenase activation protein, theta	1.44	9.95E-03
PSAT1	phosphoserine aminotransferase 1	1.37	0.03

GNB1	guanine nucleotide binding protein (G protein), beta polypeptide 1	1.28	6.36E-03
GDI1	GDP dissociation inhibitor 1	1.23	3.18E-04

List of genes downregulated in iPSC-derived neurons from SCA3 patients in comparison to iPSC-derived neurons from healthy controls. Genes have been arranged in descending order of fold change.

Gene symbol	**Gene name**	**Fold change in iPSC-derived SCA3 neurons**	**FDR P-value**
Genes downregulated in SCA3 neurons			
COLEC12	collectin sub-family member 12	-24.41	4.80E-15
SERPINF1	serpin peptidase inhibitor, clade F (alpha-2 antiplasmin, pigment epithelium derived factor), member 1	-14.26	4.10E-07
LUM	lumican	-10.29	6.29E-38
EFEMP2	EGF containing fibulin-like extracellular matrix protein 2	-6.81	7.01E-04
FAM176C	eva-1 homolog C	-5.82	0.05
CCDC164	dynein regulatory complex subunit 1	-5.56	0.02
IGFBP4	insulin-like growth factor binding protein 4	-5.13	0.02
AEBP1	AE binding protein 1	-4.89	6.44E-06
ANXA1	annexin A1	-4	0.02
IFITM3	interferon induced transmembrane protein 3	-3.7	3.28E-03
RRBP1	ribosome binding protein 1	-3.55	1.13E-03
RRAS	related RAS viral (r-ras) oncogene homolog	-3.49	0.01
PTRF	polymerase I and transcript release factor	-3.37	9.95E-03

FLNB	filamin B, beta	-3.34	8.03E-03
IER3	immediate early response 3	-3.29	0.03
PLTP	phospholipid transfer protein	-3.06	1.27E-03
TIMP1	TIMP metallopeptidase inhibitor 1	-3.01	2.57E-04
FOSB	FBJ murine osteosarcoma viral oncogene homolog B	-2.99	0.03
MYH9	myosin, heavy chain 9, non-muscle	-2.67	3.36E-03
SERPINB6	serpin peptidase inhibitor, clade B (ovalbumin), member 6	-2.66	0.05
DNAJB1	DnaJ (Hsp40) homolog, subfamily B, member 1	-2.56	5.73E-04
CTSB	cathepsin B	-2.16	1.03E-05
CD164	CD164 molecule, sialomucin	-2.1	1.27E-04
CETN2	centrin, EF-hand protein, 2	-1.94	0.03
NELF	NMDA receptor synaptonuclear signaling and neuronal migration factor	-1.79	7.40E-03
CTNNA1	catenin (cadherin-associated protein), alpha 1, 102kDa	-1.69	2.26E-03
PAM	peptidylglycine alpha-amidating monooxygenase	-1.69	0.04
RPS12	ribosomal protein S12	-1.52	6.65E-07
RPS9	ribosomal protein S9	-1.45	0.03
PSAP	prosaposin	-1.44	1.25E-05

List of miRNAs upregulated in iPSC-derived neurons from SCA3 patients in comparison to iPSC-derived neurons from healthy controls. miRNAs have been arranged in descending order of fold change.

miRNA name	Fold change in iPSC derived SCA3 neurons	FDR P-value
miRNAs upregulated in SCA3 neurons		
hsa-miR-431-5p	586.6214	1.27E-07
hsa-miR-337-5p	352.2233	3.55E-06
hsa-miR-770-5p	191.9895	7.60E-07
hsa-miR-376a-3p	182.4585	1.78E-06
hsa-miR-539-5p	134.6055	7.88E-05
hsa-miR-432-5p	85.25497	6.68E-07
hsa-miR-432-3p	84.53678	2.02E-03
hsa-miR-541-5p	83.10655	3.44E-02
hsa-miR-127-3p	80.14982	6.16E-13
hsa-miR-541-3p	78.95533	4.87E-04
hsa-miR-337-3p	74.32188	3.41E-08
hsa-miR-136-5p	66.85646	2.62E-10
hsa-miR-380-5p	66.44027	2.40E-03
hsa-miR-299-5p	66.33228	3.67E-09
hsa-miR-369-5p	65.50373	1.28E-09
hsa-miR-127-5p	65.33154	1.21E-11
hsa-miR-409-3p	62.79913	2.31E-06
hsa-miR-154-5p	61.49923	1.98E-09
hsa-miR-136-3p	58.97185	6.01E-12
hsa-miR-485-3p	54.48456	7.84E-07
hsa-miR-654-3p	54.26493	1.61E-08
hsa-miR-380-3p	52.58121	1.28E-09
hsa-miR-495-3p	51.78691	1.98E-09
hsa-miR-379-3p	51.31836	8.21E-09
hsa-miR-409-5p	50.65953	7.99E-04
hsa-miR-433	50.51679	9.45E-06

hsa-miR-758-3p	49.5244	8.13E-09
hsa-miR-134	48.39775	2.92E-07
hsa-miR-369-3p	48.19559	4.15E-10
hsa-miR-379-5p	48.05916	2.62E-10
hsa-miR-377-5p	47.36093	6.32E-07
hsa-miR-382-3p	47.25587	3.38E-09
hsa-miR-323b-3p	46.76528	3.01E-02
hsa-miR-382-5p	45.61819	3.20E-07
hsa-miR-494	45.15569	7.63E-07
hsa-miR-370	45.14309	6.47E-06
hsa-miR-323a-3p	43.38047	5.32E-06
hsa-miR-1197	42.06295	6.41E-06
hsa-miR-668	41.84241	1.86E-03
hsa-miR-654-5p	41.30734	7.63E-07
hsa-miR-544a	40.98868	2.50E-02
hsa-miR-431-3p	40.23896	1.45E-08
hsa-miR-376b-5p	39.76311	3.05E-02
hsa-miR-411-5p	39.52897	2.62E-10
hsa-miR-1185-5p	39.2931	1.09E-09
hsa-miR-381-5p	39.1471	3.45E-02
hsa-miR-889	38.68175	2.62E-10
hsa-miR-487b	38.63271	1.28E-09
hsa-miR-485-5p	38.617	6.96E-07
hsa-miR-411-3p	38.05624	3.38E-09
hsa-miR-410	37.85289	1.00E-05
hsa-miR-376c-3p	37.81475	1.05E-09
hsa-miR-1185-1-3p	37.36638	3.41E-08
hsa-miR-656	36.59561	9.33E-09
hsa-miR-376a-5p	36.54073	2.30E-04
hsa-miR-1185-2-3p	36.33916	6.35E-04
hsa-miR-381-3p	35.94446	3.26E-10
hsa-miR-329	35.7301	7.63E-08

hsa-miR-377-3p	35.65163	3.41E-08
hsa-miR-376b-3p	33.61442	1.72E-07
hsa-miR-299-3p	33.5104	2.86E-09
hsa-miR-539-3p	32.90574	2.01E-09
hsa-miR-487a	29.85199	6.70E-09
hsa-miR-543	25.32928	4.73E-04
hsa-miR-496	25.30281	5.99E-05
hsa-miR-758-5p	21.16692	9.54E-03
hsa-miR-493-5p	20.73649	3.19E-07
hsa-miR-493-3p	20.04763	4.52E-07
hsa-miR-655	19.30396	1.86E-05
hsa-miR-2113	6.406751	2.18E-03
hsa-miR-490-3p	4.952	2.08E-03

List of miRNAs downregulated in iPSC-derived neurons from SCA3 patients in comparison to iPSC-derived neurons from healthy controls. miRNAs have been arranged in descending order of fold change.

miRNA name	**Fold change in iPSC derived SCA3 neurons**	**FDR P-value**
miRNAs downregulated in SCA3 neurons		
hsa-miR-449a	-108.2534889	1.78E-03
hsa-miR-449c-5p	-93.32553078	9.54E-03
hsa-miR-449b-5p	-80.34681096	1.78E-03
hsa-miR-199a-5p	-66.25275354	3.01E-02
hsa-miR-4490	-65.61140287	3.85E-03
hsa-miR-199a-3p	-61.29128195	3.47E-02
hsa-miR-199b-3p	-61.29128195	3.47E-02
hsa-miR-199b-5p	-48.63167017	4.46E-02
hsa-miR-2114-5p	-19.71020476	2.19E-03
hsa-miR-143-3p	-17.50185064	5.00E-02
hsa-miR-193a-3p	-13.50312411	2.02E-02
hsa-miR-145-5p	-12.31148516	4.63E-02

hsa-miR-2114-3p	-12.08693102	1.17E-03
hsa-miR-1266	-4.295350381	3.81E-02
hsa-miR-1269a	-4.090803361	8.91E-03
hsa-miR-184	-3.930027022	2.27E-02
hsa-miR-190b	-3.869430519	2.55E-02
hsa-miR-27b-5p	-3.524804277	2.55E-02
hsa-miR-23b-3p	-3.287689506	3.47E-02

Representation of the binding of miR-9, miR-125a-5p, miR-181c (two sites) and miR-383 to ATXN3 3'UTR at their predicted binding sites. In each figure, the binding of the miRNAs to the wild type ATXN3 3'UTR is shown in (A), while the disruption to binding caused by mutations at two nucleotides in the miRNA binding sites in ATXN3 3'UTR is shown in (B).

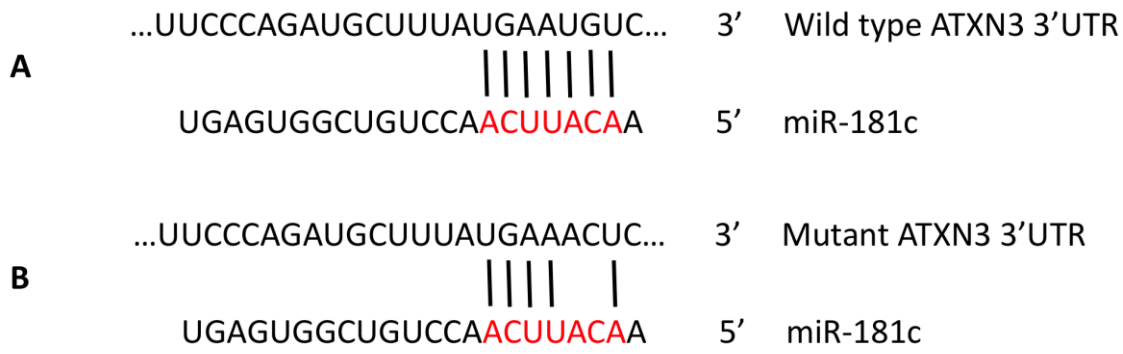
…UUCCCAGAUGCUUUAUGAAUGUC… 3’ Wild type ATXN3 3’UTR
A
UGAGUGGCUGUCCAACUUACAA 5’ miR-181c
…UUCCCAGAUGCUUUAUGAAACUC… 3’ Mutant ATXN3 3’UTR
B
UGAGUGGCUGUCCAACUUACAA 5’ miR-181c

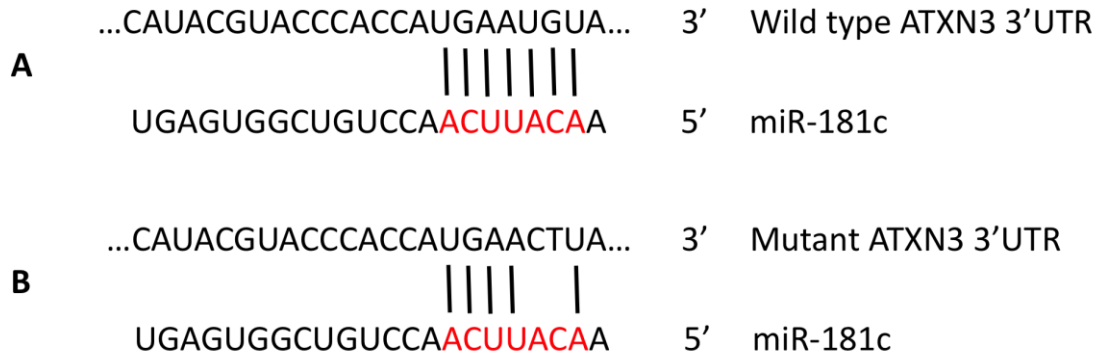
…CAUACGUACCCACCAUGAAUGUA… 3’ Wild type ATXN3 3’UTR
A
UGAGUGGCUGUCCAACUUACAA 5’ miR-181c
…CAUACGUACCCACCAUGAACTUA… 3’ Mutant ATXN3 3’UTR
B
UGAGUGGCUGUCCAACUUACAA 5’ miR-181c

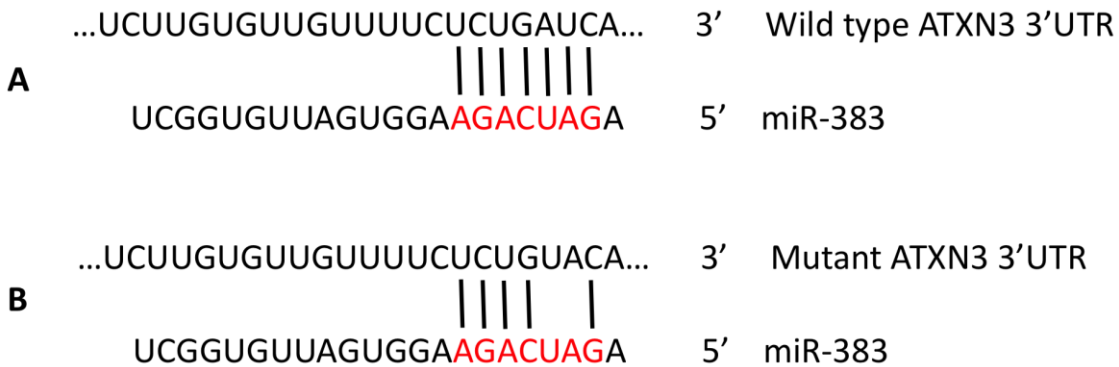
…UCUUGUGUUGUUUUCUCUGAUCA… 3’ Wild type ATXN3 3’UTR
A
UCGGUGUUAGUGGAAGACUAGA 5’ miR-383
…UCUUGUGUUGUUUUCUCUGUACA… 3’ Mutant ATXN3 3’UTR
B
UCGGUGUUAGUGGAAGACUAGA 5’ miR-383

Representation of the binding of miR-374a-5p, miR-542-3p to MID1 3'UTR at their predicted binding sites. In each figure, the binding of the miRNAs to the wild type MID1 3'UTR is shown in (A), while the disruption to binding caused by mutations at two nucleotides in the miRNA binding sites in MID1 3'UTR is shown in (B).

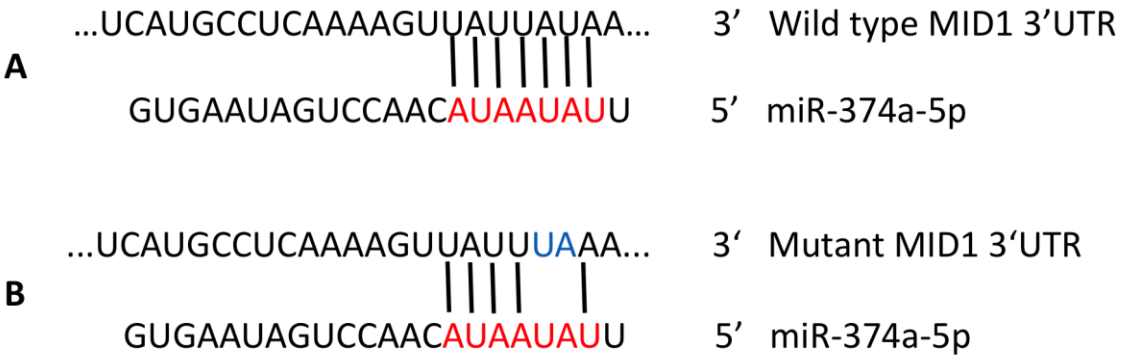

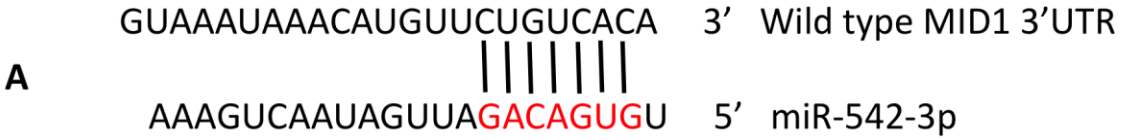

Representation of the binding of miR-143, miR-449a, miR-370 (two sites) to DNAJB1 3'UTR at their predicted binding sites. In each figure, the binding of the miRNAs to the wild type DNAJB1 3'UTR is shown in (A), while the disruption to binding caused by mutations at two nucleotides in the miRNA binding sites in DNAJB1 3'UTR is shown in (B).

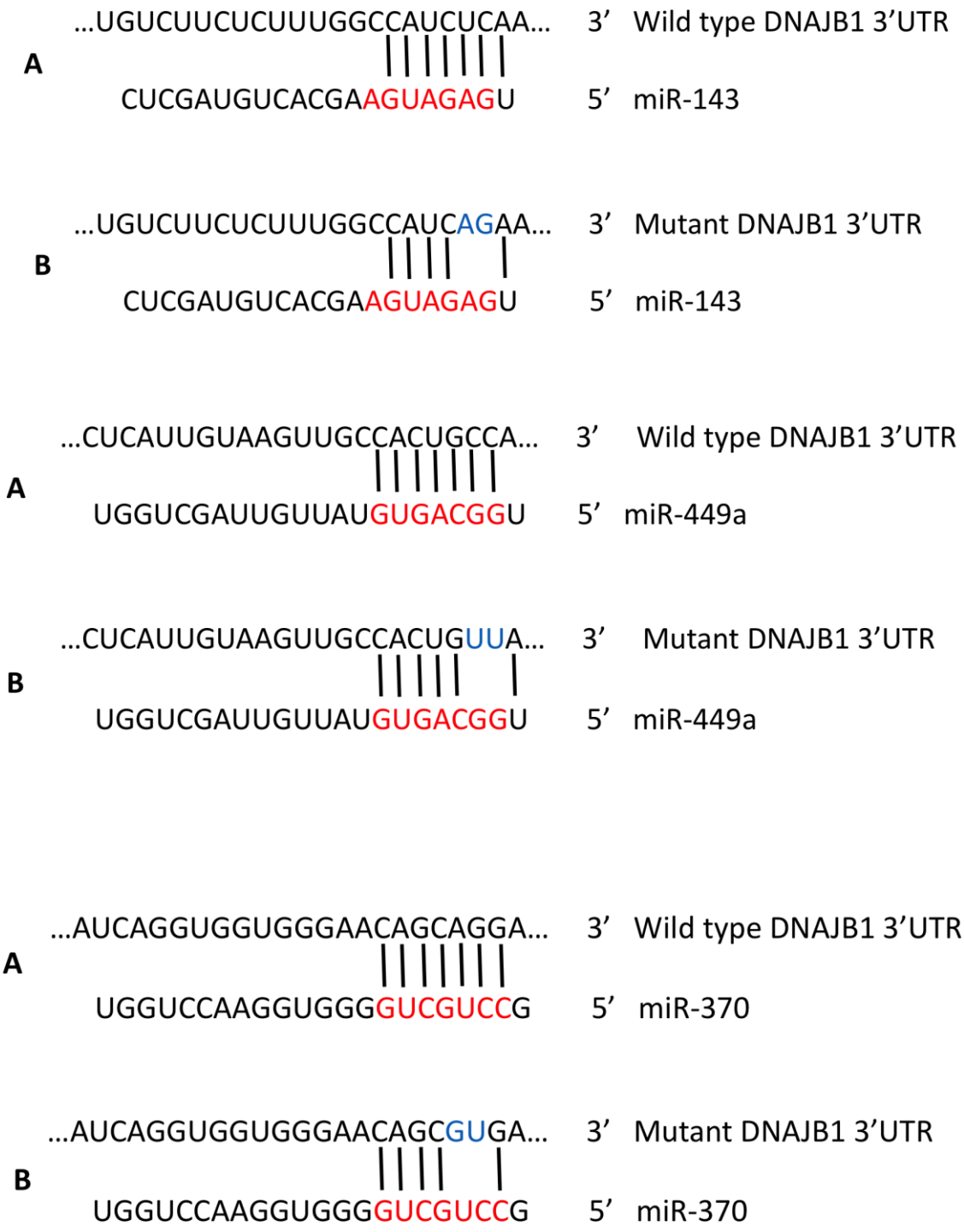


A
…CAAUACCUCUCGUUCCAGCAGGA… 3’ Wild type DNAJB1 3’UTR
UGGUCCAAGGUGGGGUCGUCCG 5’ miR-370
B
…CAAUACCUCUCGUUCCAGCGUGA… 3’ Mutant DNAJB1 3’UTR
UGGUCCAAGGUGGGGUCGUCCG 5’ miR-370

References

Albrecht AN, Kornak U, Boddrich A, Suring K, Robinson PN, Stiege AC, Lurz R, Stricker S, Wanker EE, Mundlos S (2004) A molecular pathogenesis for transcription factor associated poly-alanine tract expansions. *Human molecular genetics* **13:** 2351-2359

Albrecht M, Hoffmann D, Evert BO, Schmitt I, Wullner U, Lengauer T (2003) Structural modeling of ataxin-3 reveals distant homology to adaptins. *Proteins* **50:** 355-370

Alves S, Regulier E, Nascimento-Ferreira I, Hassig R, Dufour N, Koeppen A, Carvalho AL, Simoes S, de Lima MC, Brouillet E, Gould VC, Deglon N, de Almeida LP (2008) Striatal and nigral pathology in a lentiviral rat model of Machado-Joseph disease. *Human molecular genetics* **17:** 2071-2083

Aranda-Orgilles B, Rutschow D, Zeller R, Karagiannidis AI, Kohler A, Chen C, Wilson T, Krause S, Roepcke S, Lilley D, Schneider R, Schweiger S (2011) Protein phosphatase 2A (PP2A)-specific ubiquitin ligase MID1 is a sequence-dependent regulator of translation efficiency controlling 3-phosphoinositide-dependent protein kinase-1 (PDPK-1). *The Journal of biological chemistry* **286:** 39945-39957

Aranda-Orgilles B, Trockenbacher A, Winter J, Aigner J, Kohler A, Jastrzebska E, Stahl J, Muller EC, Otto A, Wanker EE, Schneider R, Schweiger S (2008) The Opitz syndrome gene product MID1 assembles a microtubule-associated ribonucleoprotein complex. *Human genetics* **123:** 163-176

Arigoni M, Barutello G, Riccardo F, Ercole E, Cantarella D, Orso F, Conti L, Lanzardo S, Taverna D, Merighi I, Calogero RA, Cavallo F, Quaglino E (2013) miR-135b coordinates progression of ErbB2-driven mammary carcinomas through suppression of MID1 and MTCH2. *The American journal of pathology* **182:** 2058-2070

Arrasate M, Mitra S, Schweitzer ES, Segal MR, Finkbeiner S (2004) Inclusion body formation reduces levels of mutant huntingtin and the risk of neuronal death. *Nature* **431:** 805-810

Bailey CK, Andriola IF, Kampinga HH, Merry DE (2002) Molecular chaperones enhance the degradation of expanded polyglutamine repeat androgen receptor in a cellular model of spinal and bulbar muscular atrophy. *Human molecular genetics* **11:** 515-523

Bardwell JC, Craig EA (1984) Major heat shock gene of Drosophila and the Escherichia coli heat-inducible dnaK gene are homologous. *Proceedings of the National Academy of Sciences of the United States of America* **81:** 848-852

Bernstein E, Caudy AA, Hammond SM, Hannon GJ (2001) Role for a bidentate ribonuclease in the initiation step of RNA interference. *Nature* **409:** 363-366

Betel D, Koppal A, Agius P, Sander C, Leslie C (2010) Comprehensive modeling of microRNA targets predicts functional non-conserved and non-canonical sites. *Genome biology* **11:** R90

Betel D, Wilson M, Gabow A, Marks DS, Sander C (2008) The microRNA.org resource: targets and expression. *Nucleic acids research* **36:** D149-153

Bichelmeier U, Schmidt T, Hubener J, Boy J, Ruttiger L, Habig K, Poths S, Bonin M, Knipper M, Schmidt WJ, Wilbertz J, Wolburg H, Laccone F, Riess O (2007) Nuclear localization of ataxin-3 is required for the manifestation of symptoms in SCA3: in vivo evidence. *The Journal of neuroscience : the official journal of the Society for Neuroscience* **27:** 7418-7428

Bilen J, Liu N, Burnett BG, Pittman RN, Bonini NM (2006) MicroRNA pathways modulate polyglutamine-induced neurodegeneration. *Molecular cell* **24:** 157-163

Boy J, Schmidt T, Wolburg H, Mack A, Nuber S, Bottcher M, Schmitt I, Holzmann C, Zimmermann F, Servadio A, Riess O (2009) Reversibility of symptoms in a conditional mouse model of spinocerebellar ataxia type 3. *Human molecular genetics* **18:** 4282-4295

Burnett B, Li F, Pittman RN (2003) The polyglutamine neurodegenerative protein ataxin-3 binds polyubiquitylated proteins and has ubiquitin protease activity. *Human molecular genetics* **12:** 3195-3205

Camnasio S, Delli Carri A, Lombardo A, Grad I, Mariotti C, Castucci A, Rozell B, Lo Riso P, Castiglioni V, Zuccato C, Rochon C, Takashima Y, Diaferia G, Biunno I, Gellera C, Jaconi M, Smith A, Hovatta O, Naldini L, Di Donato S, Feki A, Cattaneo E (2012) The first reported generation of several induced pluripotent stem cell lines from homozygous and heterozygous Huntington's disease patients demonstrates mutation related enhanced lysosomal activity. *Neurobiology of disease* **46:** 41-51

Cemal CK, Carroll CJ, Lawrence L, Lowrie MB, Ruddle P, Al-Mahdawi S, King RH, Pook MA, Huxley C, Chamberlain S (2002) YAC transgenic mice carrying pathological alleles of the MJD1 locus exhibit a mild and slowly progressive cerebellar deficit. *Human molecular genetics* **11:** 1075-1094

Chai Y, Berke SS, Cohen RE, Paulson HL (2004) Poly-ubiquitin binding by the polyglutamine disease protein ataxin-3 links its normal function to protein surveillance pathways. *The Journal of biological chemistry* **279:** 3605-3611

Chai Y, Koppenhafer SL, Bonini NM, Paulson HL (1999a) Analysis of the role of heat shock protein (Hsp) molecular chaperones in polyglutamine disease. *The Journal of neuroscience : the official journal of the Society for Neuroscience* **19:** 10338-10347

Chai Y, Koppenhafer SL, Shoesmith SJ, Perez MK, Paulson HL (1999b) Evidence for proteasome involvement in polyglutamine disease: localization to nuclear inclusions in SCA3/MJD and suppression of polyglutamine aggregation in vitro. *Human molecular genetics* **8:** 673-682

Chen CZ, Li L, Lodish HF, Bartel DP (2004) MicroRNAs modulate hematopoietic lineage differentiation. *Science* **303:** 83-86

Chen J, Bardes EE, Aronow BJ, Jegga AG (2009) ToppGene Suite for gene list enrichment analysis and candidate gene prioritization. *Nucleic acids research* **37:** W305-311

Chou AH, Yeh TH, Ouyang P, Chen YL, Chen SY, Wang HL (2008) Polyglutamine-expanded ataxin-3 causes cerebellar dysfunction of SCA3 transgenic mice by inducing transcriptional dysregulation. *Neurobiology of disease* **31:** 89-101

Chow MK, Mackay JP, Whisstock JC, Scanlon MJ, Bottomley SP (2004) Structural and functional analysis of the Josephin domain of the polyglutamine protein ataxin-3. *Biochemical and biophysical research communications* **322:** 387-394

Cummings CJ, Mancini MA, Antalffy B, DeFranco DB, Orr HT, Zoghbi HY (1998) Chaperone suppression of aggregation and altered subcellular proteasome localization imply protein misfolding in SCA1. *Nature genetics* **19:** 148-154

Davies SW, Beardsall K, Turmaine M, DiFiglia M, Aronin N, Bates GP (1998) Are neuronal intranuclear inclusions the common neuropathology of triplet-repeat disorders with polyglutamine-repeat expansions? *Lancet* **351:** 131-133

Davis S, Lollo B, Freier S, Esau C (2006) Improved targeting of miRNA with antisense oligonucleotides. *Nucleic acids research* **34:** 2294-2304

Donaldson KM, Li W, Ching KA, Batalov S, Tsai CC, Joazeiro CA (2003) Ubiquitin-mediated sequestration of normal cellular proteins into polyglutamine aggregates. *Proceedings of the National Academy of Sciences of the United States of America* **100:** 8892-8897

Doss-Pepe EW, Stenroos ES, Johnson WG, Madura K (2003) Ataxin-3 interactions with rad23 and valosin-containing protein and its associations with ubiquitin chains and the proteasome are consistent with a role in ubiquitin-mediated proteolysis. *Mol Cell Biol* **23:** 6469-6483

Durr A, Stevanin G, Cancel G, Duyckaerts C, Abbas N, Didierjean O, Chneiweiss H, Benomar A, Lyon-Caen O, Julien J, Serdaru M, Penet C, Agid Y, Brice A (1996) Spinocerebellar ataxia 3 and Machado-Joseph disease: clinical, molecular, and neuropathological features. *Annals of neurology* **39:** 490-499

Duursma AM, Kedde M, Schrier M, le Sage C, Agami R (2008) miR-148 targets human DNMT3b protein coding region. *Rna* **14:** 872-877

Ebert MS, Neilson JR, Sharp PA (2007) MicroRNA sponges: competitive inhibitors of small RNAs in mammalian cells. *Nature methods* **4:** 721-726

Elbashir SM, Lendeckel W, Tuschl T (2001) RNA interference is mediated by 21- and 22-nucleotide RNAs. *Genes & development* **15:** 188-200

Ellis RJ, Hemmingsen SM (1989) Molecular chaperones: proteins essential for the biogenesis of some macromolecular structures. *Trends in biochemical sciences* **14:** 339-342

Evert BO, Araujo J, Vieira-Saecker AM, de Vos RA, Harendza S, Klockgether T, Wullner U (2006) Ataxin-3 represses transcription via chromatin binding, interaction with histone deacetylase 3, and histone deacetylation. *The Journal of neuroscience : the official journal of the Society for Neuroscience* **26:** 11474-11486

Evert BO, Vogt IR, Kindermann C, Ozimek L, de Vos RA, Brunt ER, Schmitt I, Klockgether T, Wullner U (2001) Inflammatory genes are upregulated in expanded ataxin-3-expressing cell lines and spinocerebellar ataxia type 3 brains. *The Journal of neuroscience : the official journal of the Society for Neuroscience* **21:** 5389-5396

Evert BO, Vogt IR, Vieira-Saecker AM, Ozimek L, de Vos RA, Brunt ER, Klockgether T, Wullner U (2003) Gene expression profiling in ataxin-3 expressing cell lines reveals distinct effects of normal and mutant ataxin-3. *Journal of neuropathology and experimental neurology* **62:** 1006-1018

Fire A, Xu S, Montgomery MK, Kostas SA, Driver SE, Mello CC (1998) Potent and specific genetic interference by double-stranded RNA in Caenorhabditis elegans. *Nature* **391:** 806-811

Forman JJ, Legesse-Miller A, Coller HA (2008) A search for conserved sequences in coding regions reveals that the let-7 microRNA targets Dicer within its coding sequence. *Proceedings of the National Academy of Sciences of the United States of America* **105:** 14879-14884

Franceschini A, Szklarczyk D, Frankild S, Kuhn M, Simonovic M, Roth A, Lin J, Minguez P, Bork P, von Mering C, Jensen LJ (2013) STRING v9.1: protein-protein interaction networks, with increased coverage and integration. *Nucleic acids research* **41:** D808-815

Freeman BC, Morimoto RI (1996) The human cytosolic molecular chaperones hsp90, hsp70 (hsc70) and hdj-1 have distinct roles in recognition of a non-native protein and protein refolding. *The EMBO journal* **15:** 2969-2979

Freeman BC, Myers MP, Schumacher R, Morimoto RI (1995) Identification of a regulatory motif in Hsp70 that affects ATPase activity, substrate binding and interaction with HDJ-1. *The EMBO journal* **14:** 2281-2292

Friedman RC, Farh KK, Burge CB, Bartel DP (2009) Most mammalian mRNAs are conserved targets of microRNAs. *Genome research* **19:** 92-105

Fu YH, Kuhl DP, Pizzuti A, Pieretti M, Sutcliffe JS, Richards S, Verkerk AJ, Holden JJ, Fenwick RG, Jr., Warren ST, et al. (1991) Variation of the CGG repeat at the fragile X site results in genetic instability: resolution of the Sherman paradox. *Cell* **67:** 1047-1058

Garcia DM, Baek D, Shin C, Bell GW, Grimson A, Bartel DP (2011) Weak seed-pairing stability and high target-site abundance decrease the proficiency of lsy-6 and other microRNAs. *Nature structural & molecular biology* **18:** 1139-1146

Grimson A, Farh KK, Johnston WK, Garrett-Engele P, Lim LP, Bartel DP (2007) MicroRNA targeting specificity in mammals: determinants beyond seed pairing. *Molecular cell* **27:** 91-105

Gunawardena S, Goldstein LS (2005) Polyglutamine diseases and transport problems: deadly traffic jams on neuronal highways. *Archives of neurology* **62:** 46-51

Haacke A, Broadley SA, Boteva R, Tzvetkov N, Hartl FU, Breuer P (2006) Proteolytic cleavage of polyglutamine-expanded ataxin-3 is critical for aggregation and sequestration of non-expanded ataxin-3. *Human molecular genetics* **15:** 555-568

Haacke A, Hartl FU, Breuer P (2007) Calpain inhibition is sufficient to suppress aggregation of polyglutamine-expanded ataxin-3. *The Journal of biological chemistry* **282:** 18851-18856

Hamilton AJ, Baulcombe DC (1999) A species of small antisense RNA in posttranscriptional gene silencing in plants. *Science* **286:** 950-952

Hammond SM, Bernstein E, Beach D, Hannon GJ (2000) An RNA-directed nuclease mediates post-transcriptional gene silencing in Drosophila cells. *Nature* **404:** 293-296

Haraguchi T, Ozaki Y, Iba H (2009) Vectors expressing efficient RNA decoys achieve the long-term suppression of specific microRNA activity in mammalian cells. *Nucleic acids research* **37:** e43

Hattori H, Liu YC, Tohnai I, Ueda M, Kaneda T, Kobayashi T, Tanabe K, Ohtsuka K (1992) Intracellular localization and partial amino acid sequence of a stress-inducible 40-kDa protein in HeLa cells. *Cell structure and function* **17:** 77-86

Hay DG, Sathasivam K, Tobaben S, Stahl B, Marber M, Mestril R, Mahal A, Smith DL, Woodman B, Bates GP (2004) Progressive decrease in chaperone protein levels in a mouse model of Huntington's disease and induction of stress proteins as a therapeutic approach. *Human molecular genetics* **13:** 1389-1405

Holz MK, Ballif BA, Gygi SP, Blenis J (2005) mTOR and S6K1 mediate assembly of the translation preinitiation complex through dynamic protein interchange and ordered phosphorylation events. *Cell* **123:** 569-580

Houbaviy HB, Murray MF, Sharp PA (2003) Embryonic stem cell-specific MicroRNAs. *Developmental cell* **5:** 351-358

Huang F, Zhang L, Long Z, Chen Z, Hou X, Wang C, Peng H, Wang J, Li J, Duan R, Xia K, Chuang DM, Tang B, Jiang H (2014) miR-25 alleviates polyQ-mediated cytotoxicity by silencing ATXN3. *FEBS letters* **588:** 4791-4798

Hutvagner G, Zamore PD (2002) A microRNA in a multiple-turnover RNAi enzyme complex. *Science* **297:** 2056-2060

Ichikawa Y, Goto J, Hattori M, Toyoda A, Ishii K, Jeong SY, Hashida H, Masuda N, Ogata K, Kasai F, Hirai M, Maciel P, Rouleau GA, Sakaki Y, Kanazawa I (2001) The genomic structure and expression of MJD, the Machado-Joseph disease gene. *Journal of human genetics* **46:** 413-422

Ikeda H, Yamaguchi M, Sugai S, Aze Y, Narumiya S, Kakizuka A (1996) Expanded polyglutamine in the Machado-Joseph disease protein induces cell death in vitro and in vivo. *Nature genetics* **13:** 196-202

Ingolia TD, Craig EA (1982) Drosophila gene related to the major heat shock-induced gene is transcribed at normal temperatures and not induced by heat shock. *Proceedings of the National Academy of Sciences of the United States of America* **79:** 525-529

Jana NR, Tanaka M, Wang G, Nukina N (2000) Polyglutamine length-dependent interaction of Hsp40 and Hsp70 family chaperones with truncated N-terminal huntingtin: their role in suppression of aggregation and cellular toxicity. *Human molecular genetics* **9:** 2009-2018

Janssen HL, Reesink HW, Lawitz EJ, Zeuzem S, Rodriguez-Torres M, Patel K, van der Meer AJ, Patick AK, Chen A, Zhou Y, Persson R, King BD, Kauppinen S, Levin AA, Hodges MR (2013) Treatment of HCV infection by targeting microRNA. *The New England journal of medicine* **368:** 1685-1694

Jin J, Cheng Y, Zhang Y, Wood W, Peng Q, Hutchison E, Mattson MP, Becker KG, Duan W (2012) Interrogation of brain miRNA and mRNA expression profiles reveals a molecular regulatory network that is perturbed by mutant huntingtin. *Journal of neurochemistry* **123:** 477-490

Johnson R, Zuccato C, Belyaev ND, Guest DJ, Cattaneo E, Buckley NJ (2008) A microRNA-based gene dysregulation pathway in Huntington's disease. *Neurobiology of disease* **29:** 438-445

Karres JS, Hilgers V, Carrera I, Treisman J, Cohen SM (2007) The conserved microRNA miR-8 tunes atrophin levels to prevent neurodegeneration in Drosophila. *Cell* **131:** 136-145

Kawaguchi Y, Okamoto T, Taniwaki M, Aizawa M, Inoue M, Katayama S, Kawakami H, Nakamura S, Nishimura M, Akiguchi I, et al. (1994) CAG expansions in a novel gene for Machado-Joseph disease at chromosome 14q32.1. *Nature genetics* **8:** 221-228

Kocerha J, Xu Y, Prucha MS, Zhao D, Chan AW (2014) microRNA-128a dysregulation in transgenic Huntington's disease monkeys. *Molecular brain* **7:** 46

Koch P, Breuer P, Peitz M, Jungverdorben J, Kesavan J, Poppe D, Doerr J, Ladewig J, Mertens J, Tuting T, Hoffmann P, Klockgether T, Evert BO, Wullner U, Brustle O (2011) Excitation-induced ataxin-3 aggregation in neurons from patients with Machado-Joseph disease. *Nature* **480:** 543-546

Kohler A, Demir U, Kickstein E, Krauss S, Aigner J, Aranda-Orgilles B, Karagiannidis AI, Achmuller C, Bu H, Wunderlich A, Schweiger MR, Schaefer G, Schweiger S, Klocker H, Schneider R (2014) A hormone-dependent feedback-loop controls androgen receptor levels by limiting MID1, a novel translation enhancer and promoter of oncogenic signaling. *Molecular cancer* **13:** 146

Krauss S, Griesche N, Jastrzebska E, Chen C, Rutschow D, Achmuller C, Dorn S, Boesch SM, Lalowski M, Wanker E, Schneider R, Schweiger S (2013) Translation of HTT mRNA with expanded CAG repeats is regulated by the MID1-PP2A protein complex. *Nature communications* **4:** 1511

Krench M, Littleton JT (2013) Modeling Huntington disease in Drosophila: Insights into axonal transport defects and modifiers of toxicity. *Fly* **7:** 229-236

Krichevsky AM, King KS, Donahue CP, Khrapko K, Kosik KS (2003) A microRNA array reveals extensive regulation of microRNAs during brain development. *Rna* **9:** 1274-1281

La Spada AR, Paulson HL, Fischbeck KH (1994) Trinucleotide repeat expansion in neurological disease. *Annals of neurology* **36:** 814-822

Laemmli UK (1970) Cleavage of structural proteins during the assembly of the head of bacteriophage T4. *Nature* **227:** 680-685

Lagos-Quintana M, Rauhut R, Lendeckel W, Tuschl T (2001) Identification of novel genes coding for small expressed RNAs. *Science* **294:** 853-858

Lagos-Quintana M, Rauhut R, Yalcin A, Meyer J, Lendeckel W, Tuschl T (2002) Identification of tissue-specific microRNAs from mouse. *Current biology : CB* **12:** 735-739

Lai EC (2002) Micro RNAs are complementary to 3' UTR sequence motifs that mediate negative post-transcriptional regulation. *Nature genetics* **30:** 363-364

Lajoie P, Snapp EL (2010) Formation and toxicity of soluble polyglutamine oligomers in living cells. *PloS one* **5:** e15245

Lanks KW (1986) Modulators of the eukaryotic heat shock response. *Experimental cell research* **165:** 1-10

Lau NC, Lim LP, Weinstein EG, Bartel DP (2001) An abundant class of tiny RNAs with probable regulatory roles in Caenorhabditis elegans. *Science* **294:** 858-862

Lee RC, Ambros V (2001) An extensive class of small RNAs in Caenorhabditis elegans. *Science* **294:** 862-864

Lee ST, Chu K, Im WS, Yoon HJ, Im JY, Park JE, Park KH, Jung KH, Lee SK, Kim M, Roh JK (2011) Altered microRNA regulation in Huntington's disease models. *Experimental neurology* **227:** 172-179

Lee Y, Ahn C, Han J, Choi H, Kim J, Yim J, Lee J, Provost P, Radmark O, Kim S, Kim VN (2003) The nuclear RNase III Drosha initiates microRNA processing. *Nature* **425:** 415-419

Lee Y, Jeon K, Lee JT, Kim S, Kim VN (2002) MicroRNA maturation: stepwise processing and subcellular localization. *The EMBO journal* **21:** 4663-4670

Lee Y, Samaco RC, Gatchel JR, Thaller C, Orr HT, Zoghbi HY (2008) miR-19, miR-101 and miR-130 co-regulate ATXN1 levels to potentially modulate SCA1 pathogenesis. *Nature neuroscience* **11:** 1137-1139

Lehmann SM, Kruger C, Park B, Derkow K, Rosenberger K, Baumgart J, Trimbuch T, Eom G, Hinz M, Kaul D, Habbel P, Kalin R, Franzoni E, Rybak A, Nguyen D, Veh R, Ninnemann O, Peters O, Nitsch R, Heppner FL, Golenbock D, Schott E, Ploegh HL, Wulczyn FG, Lehnardt S (2012) An unconventional role for miRNA: let-7 activates Toll-like receptor 7 and causes neurodegeneration. *Nature neuroscience* **15:** 827-835

Leitman J, Ulrich Hartl F, Lederkremer GZ (2013) Soluble forms of polyQ-expanded huntingtin rather than large aggregates cause endoplasmic reticulum stress. *Nature communications* **4:** 2753

Lewis BP, Burge CB, Bartel DP (2005) Conserved seed pairing, often flanked by adenosines, indicates that thousands of human genes are microRNA targets. *Cell* **120:** 15-20

Li F, Macfarlan T, Pittman RN, Chakravarti D (2002) Ataxin-3 is a histone-binding protein with two independent transcriptional corepressor activities. *The Journal of biological chemistry* **277:** 45004-45012

Li H, Li SH, Yu ZX, Shelbourne P, Li XJ (2001) Huntingtin aggregate-associated axonal degeneration is an early pathological event in Huntington's disease mice. *The Journal of neuroscience : the official journal of the Society for Neuroscience* **21:** 8473-8481

Lim LP, Lau NC, Weinstein EG, Abdelhakim A, Yekta S, Rhoades MW, Burge CB, Bartel DP (2003) The microRNAs of Caenorhabditis elegans. *Genes & development* **17:** 991-1008

Lindquist S (1986) The heat-shock response. *Annual review of biochemistry* **55:** 1151-1191

Liu E, Knutzen CA, Krauss S, Schweiger S, Chiang GG (2011) Control of mTORC1 signaling by the Opitz syndrome protein MID1. *Proceedings of the National Academy of Sciences of the United States of America* **108:** 8680-8685

Liu J, Prickett TD, Elliott E, Meroni G, Brautigan DL (2001) Phosphorylation and microtubule association of the Opitz syndrome protein mid-1 is regulated by protein phosphatase 2A via binding to the regulatory subunit alpha 4. *Proceedings of the National Academy of Sciences of the United States of America* **98:** 6650-6655

Liu N, Landreh M, Cao K, Abe M, Hendriks GJ, Kennerdell JR, Zhu Y, Wang LS, Bonini NM (2012) The microRNA miR-34 modulates ageing and neurodegeneration in Drosophila. *Nature* **482:** 519-523

Lotz GP, Legleiter J, Aron R, Mitchell EJ, Huang SY, Ng C, Glabe C, Thompson LM, Muchowski PJ (2010) Hsp70 and Hsp40 functionally interact with soluble mutant huntingtin oligomers in a classic ATP-dependent reaction cycle. *The Journal of biological chemistry* **285:** 38183-38193

Lu T, Chen R, Cox TC, Moldrich RX, Kurniawan N, Tan G, Perry JK, Ashworth A, Bartlett PF, Xu L, Zhang J, Lu B, Wu M, Shen Q, Liu Y, Richards LJ, Xiong Z (2013) X-linked microtubule-associated protein, Mid1, regulates axon development. *Proceedings of the National Academy of Sciences of the United States of America* **110:** 19131-19136

Lu TP, Lee CY, Tsai MH, Chiu YC, Hsiao CK, Lai LC, Chuang EY (2012) miRSystem: an integrated system for characterizing enriched functions and pathways of microRNA targets. *PloS one* **7:** e42390

Lund E, Guttinger S, Calado A, Dahlberg JE, Kutay U (2004) Nuclear export of microRNA precursors. *Science* **303:** 95-98

Lytle JR, Yario TA, Steitz JA (2007) Target mRNAs are repressed as efficiently by microRNA-binding sites in the 5' UTR as in the 3' UTR. *Proceedings of the National Academy of Sciences of the United States of America* **104:** 9667-9672

Mahishi LH, Hart RP, Lynch DR, Ratan RR (2012) miR-886-3p levels are elevated in Friedreich ataxia. *The Journal of neuroscience : the official journal of the Society for Neuroscience* **32:** 9369-9373

Mankodi A, Takahashi MP, Jiang H, Beck CL, Bowers WJ, Moxley RT, Cannon SC, Thornton CA (2002) Expanded CUG repeats trigger aberrant splicing of ClC-1 chloride channel pre-mRNA and hyperexcitability of skeletal muscle in myotonic dystrophy. *Molecular cell* **10:** 35-44

Marti E, Pantano L, Banez-Coronel M, Llorens F, Minones-Moyano E, Porta S, Sumoy L, Ferrer I, Estivill X (2010) A myriad of miRNA variants in control and Huntington's disease brain regions detected by massively parallel sequencing. *Nucleic acids research* **38:** 7219-7235

Masino L, Musi V, Menon RP, Fusi P, Kelly G, Frenkiel TA, Trottier Y, Pastore A (2003) Domain architecture of the polyglutamine protein ataxin-3: a globular domain followed by a flexible tail. *FEBS letters* **549:** 21-25

McCampbell A, Taylor JP, Taye AA, Robitschek J, Li M, Walcott J, Merry D, Chai Y, Paulson H, Sobue G, Fischbeck KH (2000) CREB-binding protein sequestration by expanded polyglutamine. *Human molecular genetics* **9:** 2197-2202

Menzies FM, Huebener J, Renna M, Bonin M, Riess O, Rubinsztein DC (2010) Autophagy induction reduces mutant ataxin-3 levels and toxicity in a mouse model of spinocerebellar ataxia type 3. *Brain* **133:** 93-104

Michels AA, Kanon B, Bensaude O, Kampinga HH (1999) Heat shock protein (Hsp) 40 mutants inhibit Hsp70 in mammalian cells. *The Journal of biological chemistry* **274:** 36757-36763

Michels AA, Kanon B, Konings AW, Ohtsuka K, Bensaude O, Kampinga HH (1997) Hsp70 and Hsp40 chaperone activities in the cytoplasm and the nucleus of mammalian cells. *The Journal of biological chemistry* **272:** 33283-33289

Muchowski PJ, Schaffar G, Sittler A, Wanker EE, Hayer-Hartl MK, Hartl FU (2000) Hsp70 and hsp40 chaperones can inhibit self-assembly of polyglutamine proteins into amyloid-like fibrils. *Proceedings of the National Academy of Sciences of the United States of America* **97:** 7841-7846

Nascimento-Ferreira I, Santos-Ferreira T, Sousa-Ferreira L, Auregan G, Onofre I, Alves S, Dufour N, Colomer Gould VF, Koeppen A, Deglon N, Pereira de Almeida L (2011) Overexpression of the autophagic beclin-1 protein clears mutant ataxin-3 and alleviates Machado-Joseph disease. *Brain* **134:** 1400-1415

Nguyen HN, Byers B, Cord B, Shcheglovitov A, Byrne J, Gujar P, Kee K, Schule B, Dolmetsch RE, Langston W, Palmer TD, Pera RR (2011) LRRK2 mutant iPSC-derived DA neurons demonstrate increased susceptibility to oxidative stress. *Cell stem cell* **8:** 267-280

Nicastro G, Masino L, Esposito V, Menon RP, De Simone A, Fraternali F, Pastore A (2009) Josephin domain of ataxin-3 contains two distinct ubiquitin-binding sites. *Biopolymers* **91:** 1203-1214

Nicastro G, Menon RP, Masino L, Knowles PP, McDonald NQ, Pastore A (2005) The solution structure of the Josephin domain of ataxin-3: structural determinants for molecular recognition. *Proceedings of the National Academy of Sciences of the United States of America* **102:** 10493-10498

Nobrega C, Nascimento-Ferreira I, Onofre I, Albuquerque D, Conceicao M, Deglon N, de Almeida LP (2013) Overexpression of mutant ataxin-3 in mouse cerebellum induces ataxia and cerebellar neuropathology. *Cerebellum* **12:** 441-455

Ohtsuka K (1993) Cloning of a cDNA for heat-shock protein hsp40, a human homologue of bacterial DnaJ. *Biochemical and biophysical research communications* **197:** 235-240

Ohtsuka K, Masuda A, Nakai A, Nagata K (1990) A novel 40-kDa protein induced by heat shock and other stresses in mammalian and avian cells. *Biochemical and biophysical research communications* **166:** 642-647

Okano H, Yamanaka S (2014) iPS cell technologies: significance and applications to CNS regeneration and disease. *Molecular brain* **7:** 22

Orr HT, Zoghbi HY (2007) Trinucleotide repeat disorders. *Annual review of neuroscience* **30:** 575-621

Packer AN, Xing Y, Harper SQ, Jones L, Davidson BL (2008) The bifunctional microRNA miR-9/miR-9* regulates REST and CoREST and is downregulated in Huntington's disease. *The Journal of neuroscience : the official journal of the Society for Neuroscience* **28:** 14341-14346

Palatnik JF, Allen E, Wu X, Schommer C, Schwab R, Carrington JC, Weigel D (2003) Control of leaf morphogenesis by microRNAs. *Nature* **425:** 257-263

Park IH, Arora N, Huo H, Maherali N, Ahfeldt T, Shimamura A, Lensch MW, Cowan C, Hochedlinger K, Daley GQ (2008) Disease-specific induced pluripotent stem cells. *Cell* **134:** 877-886

Park SH, Kukushkin Y, Gupta R, Chen T, Konagai A, Hipp MS, Hayer-Hartl M, Hartl FU (2013) PolyQ proteins interfere with nuclear degradation of cytosolic proteins by sequestering the Sis1p chaperone. *Cell* **154:** 134-145

Pasquinelli AE, Ruvkun G (2002) Control of developmental timing by micrornas and their targets. *Annual review of cell and developmental biology* **18:** 495-513

Paulson HL, Das SS, Crino PB, Perez MK, Patel SC, Gotsdiner D, Fischbeck KH, Pittman RN (1997a) Machado-Joseph disease gene product is a cytoplasmic protein widely expressed in brain. *Annals of neurology* **41:** 453-462

Paulson HL, Perez MK, Trottier Y, Trojanowski JQ, Subramony SH, Das SS, Vig P, Mandel JL, Fischbeck KH, Pittman RN (1997b) Intranuclear inclusions of expanded polyglutamine protein in spinocerebellar ataxia type 3. *Neuron* **19:** 333-344

Perez MK, Paulson HL, Pendse SJ, Saionz SJ, Bonini NM, Pittman RN (1998) Recruitment and the role of nuclear localization in polyglutamine-mediated aggregation. *J Cell Biol* **143:** 1457-1470

Persengiev S, Kondova I, Otting N, Koeppen AH, Bontrop RE (2011) Genome-wide analysis of miRNA expression reveals a potential role for miR-144 in brain aging and spinocerebellar ataxia pathogenesis. *Neurobiology of aging* **32:** 2316 e2317-2327

Piccioni F, Pinton P, Simeoni S, Pozzi P, Fascio U, Vismara G, Martini L, Rizzuto R, Poletti A (2002) Androgen receptor with elongated polyglutamine tract forms aggregates that alter axonal trafficking and mitochondrial distribution in motor neuronal processes. *FASEB journal : official publication of the Federation of American Societies for Experimental Biology* **16:** 1418-1420

Pieretti M, Zhang FP, Fu YH, Warren ST, Oostra BA, Caskey CT, Nelson DL (1991) Absence of expression of the FMR-1 gene in fragile X syndrome. *Cell* **66:** 817-822

Quaderi NA, Schweiger S, Gaudenz K, Franco B, Rugarli EI, Berger W, Feldman GJ, Volta M, Andolfi G, Gilgenkrantz S, Marion RW, Hennekam RC, Opitz JM, Muenke M, Ropers HH, Ballabio A (1997) Opitz G/BBB syndrome, a defect of midline development, is due to mutations in a new RING finger gene on Xp22. *Nature genetics* **17:** 285-291

Raabe T, Manley JL (1991) A human homologue of the Escherichia coli DnaJ heat-shock protein. *Nucleic acids research* **19:** 6645

Reinhart BJ, Weinstein EG, Rhoades MW, Bartel B, Bartel DP (2002) MicroRNAs in plants. *Genes & development* **16:** 1616-1626

Renart J, Reiser J, Stark GR (1979) Transfer of proteins from gels to diazobenzyloxymethyl-paper and detection with antisera: a method for studying antibody specificity and antigen structure. *Proceedings of the National Academy of Sciences of the United States of America* **76:** 3116-3120

Riess O, Rub U, Pastore A, Bauer P, Schols L (2008) SCA3: neurological features, pathogenesis and animal models. *Cerebellum* **7:** 125-137

Rodriguez-Lebron E, Liu G, Keiser M, Behlke MA, Davidson BL (2013) Altered Purkinje cell miRNA expression and SCA1 pathogenesis. *Neurobiology of disease* **54:** 456-463

Ross CA (1997) Intranuclear neuronal inclusions: a common pathogenic mechanism for glutamine-repeat neurodegenerative diseases? *Neuron* **19:** 1147-1150

Rub U, Hentschel M, Stratmann K, Brunt E, Heinsen H, Seidel K, Bouzrou M, Auburger G, Paulson H, Vonsattel JP, Lange H, Korf HW, den Dunnen W (2014) Huntington's disease (HD): degeneration of select nuclei, widespread occurrence of neuronal nuclear and axonal inclusions in the brainstem. *Brain pathology* **24:** 247-260

Rub U, Schols L, Paulson H, Auburger G, Kermer P, Jen JC, Seidel K, Korf HW, Deller T (2013) Clinical features, neurogenetics and neuropathology of the polyglutamine spinocerebellar ataxias type 1, 2, 3, 6 and 7. *Progress in neurobiology* **104:** 38-66

Rubinsztein DC, Wyttenbach A, Rankin J (1999) Intracellular inclusions, pathological markers in diseases caused by expanded polyglutamine tracts? *Journal of medical genetics* **36:** 265-270

Rujano MA, Kampinga HH, Salomons FA (2007) Modulation of polyglutamine inclusion formation by the Hsp70 chaperone machine. *Experimental cell research* **313:** 3568-3578

Schaefer A, O'Carroll D, Tan CL, Hillman D, Sugimori M, Llinas R, Greengard P (2007) Cerebellar neurodegeneration in the absence of microRNAs. *The Journal of experimental medicine* **204:** 1553-1558

Schmidt T, Landwehrmeyer GB, Schmitt I, Trottier Y, Auburger G, Laccone F, Klockgether T, Volpel M, Epplen JT, Schols L, Riess O (1998) An isoform of ataxin-3 accumulates in the nucleus of neuronal cells in affected brain regions of SCA3 patients. *Brain pathology* **8:** 669-679

Schmitt I, Linden M, Khazneh H, Evert BO, Breuer P, Klockgether T, Wuellner U (2007) Inactivation of the mouse Atxn3 (ataxin-3) gene increases protein ubiquitination. *Biochemical and biophysical research communications* **362:** 734-739

Schols L, Amoiridis G, Epplen JT, Langkafel M, Przuntek H, Riess O (1996) Relations between genotype and phenotype in German patients with the Machado-Joseph disease mutation. *Journal of neurology, neurosurgery, and psychiatry* **61:** 466-470

Schwarz DS, Hutvagner G, Du T, Xu Z, Aronin N, Zamore PD (2003) Asymmetry in the assembly of the RNAi enzyme complex. *Cell* **115:** 199-208

Schweiger S, Foerster J, Lehmann T, Suckow V, Muller YA, Walter G, Davies T, Porter H, van Bokhoven H, Lunt PW, Traub P, Ropers HH (1999) The Opitz syndrome gene product, MID1, associates with microtubules. *Proceedings of the National Academy of Sciences of the United States of America* **96:** 2794-2799

Seidel K, den Dunnen WF, Schultz C, Paulson H, Frank S, de Vos RA, Brunt ER, Deller T, Kampinga HH, Rub U (2010) Axonal inclusions in spinocerebellar ataxia type 3. *Acta neuropathologica* **120:** 449-460

Seidel K, Meister M, Dugbartey GJ, Zijlstra MP, Vinet J, Brunt ER, van Leeuwen FW, Rub U, Kampinga HH, den Dunnen WF (2012a) Cellular protein quality control and the evolution of aggregates in spinocerebellar ataxia type 3 (SCA3). *Neuropathology and applied neurobiology* **38:** 548-558

Seidel K, Siswanto S, Brunt ER, den Dunnen W, Korf HW, Rub U (2012b) Brain pathology of spinocerebellar ataxias. *Acta neuropathologica* **124:** 1-21

Sempere LF, Freemantle S, Pitha-Rowe I, Moss E, Dmitrovsky E, Ambros V (2004) Expression profiling of mammalian microRNAs uncovers a subset of brain-expressed microRNAs with possible roles in murine and human neuronal differentiation. *Genome biology* **5:** R13

Shapiro AL, Vinuela E, Maizel JV, Jr. (1967) Molecular weight estimation of polypeptide chains by electrophoresis in SDS-polyacrylamide gels. *Biochemical and biophysical research communications* **28:** 815-820

Soldner F, Hockemeyer D, Beard C, Gao Q, Bell GW, Cook EG, Hargus G, Blak A, Cooper O, Mitalipova M, Isacson O, Jaenisch R (2009) Parkinson's disease patient-derived induced pluripotent stem cells free of viral reprogramming factors. *Cell* **136:** 964-977

Soong B, Cheng C, Liu R, Shan D (1997) Machado-Joseph disease: clinical, molecular, and metabolic characterization in Chinese kindreds. *Annals of neurology* **41:** 446-452

Stevanin G, Le Guern E, Ravise N, Chneiweiss H, Durr A, Cancel G, Vignal A, Boch AL, Ruberg M, Penet C, et al. (1994) A third locus for autosomal dominant cerebellar ataxia type I maps to chromosome 14q24.3-qter: evidence for the existence of a fourth locus. *American journal of human genetics* **54:** 11-20

Sugito K, Yamane M, Hattori H, Hayashi Y, Tohnai I, Ueda M, Tsuchida N, Ohtsuka K (1995) Interaction between hsp70 and hsp40, eukaryotic homologues of DnaK and DnaJ, in human cells expressing mutant-type p53. *FEBS letters* **358:** 161-164

Switonski PM, Fiszer A, Kazmierska K, Kurpisz M, Krzyzosiak WJ, Figiel M (2011) Mouse ataxin-3 functional knock-out model. *Neuromolecular medicine* **13:** 54-65

Szebenyi G, Morfini GA, Babcock A, Gould M, Selkoe K, Stenoien DL, Young M, Faber PW, MacDonald ME, McPhaul MJ, Brady ST (2003) Neuropathogenic forms of huntingtin and androgen receptor inhibit fast axonal transport. *Neuron* **40:** 41-52

Takeuchi H, Kobayashi Y, Yoshihara T, Niwa J, Doyu M, Ohtsuka K, Sobue G (2002) Hsp70 and Hsp40 improve neurite outgrowth and suppress intracytoplasmic aggregate formation in cultured neuronal cells expressing mutant SOD1. *Brain research* **949:** 11-22

Takiyama Y, Igarashi S, Rogaeva EA, Endo K, Rogaev EI, Tanaka H, Sherrington R, Sanpei K, Liang Y, Saito M, et al. (1995) Evidence for inter-generational instability in the CAG repeat in the MJD1 gene and for conserved haplotypes at flanking markers amongst Japanese and Caucasian subjects with Machado-Joseph disease. *Human molecular genetics* **4:** 1137-1146

Tan H, Poidevin M, Li H, Chen D, Jin P (2012) MicroRNA-277 modulates the neurodegeneration caused by Fragile X premutation rCGG repeats. *PLoS genetics* **8:** e1002681

Teixeira-Castro A, Ailion M, Jalles A, Brignull HR, Vilaca JL, Dias N, Rodrigues P, Oliveira JF, Neves-Carvalho A, Morimoto RI, Maciel P (2011) Neuron-specific proteotoxicity of mutant ataxin-3 in C. elegans: rescue by the DAF-16 and HSF-1 pathways. *Human molecular genetics* **20:** 2996-3009

Tessier-Lavigne M, Goodman CS (1996) The molecular biology of axon guidance. *Science* **274:** 1123-1133

Todd PK, Paulson HL (2010) RNA-mediated neurodegeneration in repeat expansion disorders. *Annals of neurology* **67:** 291-300

Tominaga N, Kosaka N, Ono M, Katsuda T, Yoshioka Y, Tamura K, Lotvall J, Nakagama H, Ochiya T (2015) Brain metastatic cancer cells release microRNA-181c-containing extracellular vesicles capable of destructing blood-brain barrier. *Nature communications* **6:** 6716

Towbin H, Staehelin T, Gordon J (1979) Electrophoretic transfer of proteins from polyacrylamide gels to nitrocellulose sheets: procedure and some applications. *Proceedings of the National Academy of Sciences of the United States of America* **76:** 4350-4354

Trockenbacher A, Suckow V, Foerster J, Winter J, Krauss S, Ropers HH, Schneider R, Schweiger S (2001) MID1, mutated in Opitz syndrome, encodes an ubiquitin ligase that targets phosphatase 2A for degradation. *Nature genetics* **29:** 287-294

Trott A, Jardim LB, Ludwig HT, Saute JA, Artigalas O, Kieling C, Wanderley HY, Rieder CR, Monte TL, Socal M, Alonso I, Ferro A, Carvalho T, do Ceu Moreira M, Mendonca P, Ferreirinha F, Silveira I, Sequeiros J, Giugliani R, Saraiva-Pereira ML (2006)

Spinocerebellar ataxias in 114 Brazilian families: clinical and molecular findings. *Clinical genetics* **70:** 173-176

Trottier Y, Cancel G, An-Gourfinkel I, Lutz Y, Weber C, Brice A, Hirsch E, Mandel JL (1998) Heterogeneous intracellular localization and expression of ataxin-3. *Neurobiology of disease* **5:** 335-347

Tsai HF, Tsai HJ, Hsieh M (2004) Full-length expanded ataxin-3 enhances mitochondrial-mediated cell death and decreases Bcl-2 expression in human neuroblastoma cells. *Biochemical and biophysical research communications* **324:** 1274-1282

Tuschl T, Zamore PD, Lehmann R, Bartel DP, Sharp PA (1999) Targeted mRNA degradation by double-stranded RNA in vitro. *Genes & development* **13:** 3191-3197

Twist EC, Casaubon LK, Ruttledge MH, Rao VS, Macleod PM, Radvany J, Zhao Z, Rosenberg RN, Farrer LA, Rouleau GA (1995) Machado Joseph disease maps to the same region of chromosome 14 as the spinocerebellar ataxia type 3 locus. *Journal of medical genetics* **32:** 25-31

Varela-Echavarria A, Guthrie S (1997) Molecules making waves in axon guidance. *Genes & development* **11:** 545-557

Vo NK, Dalton RP, Liu N, Olson EN, Goodman RH (2010) Affinity purification of microRNA-133a with the cardiac transcription factor, Hand2. *Proceedings of the National Academy of Sciences of the United States of America* **107:** 19231-19236

Wang G, Sawai N, Kotliarova S, Kanazawa I, Nukina N (2000) Ataxin-3, the MJD1 gene product, interacts with the two human homologs of yeast DNA repair protein RAD23, HHR23A and HHR23B. *Human molecular genetics* **9:** 1795-1803

Warrick JM, Paulson HL, Gray-Board GL, Bui QT, Fischbeck KH, Pittman RN, Bonini NM (1998) Expanded polyglutamine protein forms nuclear inclusions and causes neural degeneration in Drosophila. *Cell* **93:** 939-949

Watanabe H, Tanaka F, Matsumoto M, Doyu M, Ando T, Mitsuma T, Sobue G (1998) Frequency analysis of autosomal dominant cerebellar ataxias in Japanese patients and clinical characterization of spinocerebellar ataxia type 6. *Clinical genetics* **53:** 13-19

Weber JJ, Sowa AS, Binder T, Hubener J (2014) From Pathways to Targets: Understanding the Mechanisms behind Polyglutamine Disease. *BioMed research international* **2014:** 701758

Wellington CL, Ellerby LM, Hackam AS, Margolis RL, Trifiro MA, Singaraja R, McCutcheon K, Salvesen GS, Propp SS, Bromm M, Rowland KJ, Zhang T, Rasper D, Roy S, Thornberry N, Pinsky L, Kakizuka A, Ross CA, Nicholson DW, Bredesen DE, Hayden MR (1998) Caspase cleavage of gene products associated with triplet expansion disorders generates truncated fragments containing the polyglutamine tract. *The Journal of biological chemistry* **273:** 9158-9167

Whelan SA, Hightower LE (1985) Differential induction of glucose-regulated and heat shock proteins: effects of pH and sulfhydryl-reducing agents on chicken embryo cells. *Journal of cellular physiology* **125:** 251-258

Winborn BJ, Travis SM, Todi SV, Scaglione KM, Xu P, Williams AJ, Cohen RE, Peng J, Paulson HL (2008) The deubiquitinating enzyme ataxin-3, a polyglutamine disease protein, edits Lys63 linkages in mixed linkage ubiquitin chains. *The Journal of biological chemistry* **283:** 26436-26443

Wong HK, Veremeyko T, Patel N, Lemere CA, Walsh DM, Esau C, Vanderburg C, Krichevsky AM (2013) De-repression of FOXO3a death axis by microRNA-132 and -212 causes neuronal apoptosis in Alzheimer's disease. *Human molecular genetics* **22:** 3077-3092

Wu S, Huang S, Ding J, Zhao Y, Liang L, Liu T, Zhan R, He X (2010) Multiple microRNAs modulate p21Cip1/Waf1 expression by directly targeting its 3' untranslated region. *Oncogene* **29:** 2302-2308

Wu W, Yang J, Feng X, Wang H, Ye S, Yang P, Tan W, Wei G, Zhou Y (2013) MicroRNA-32 (miR-32) regulates phosphatase and tensin homologue (PTEN) expression and promotes growth, migration, and invasion in colorectal carcinoma cells. *Molecular cancer* **12:** 30

Wu Z, Sun H, Zeng W, He J, Mao X (2012) Upregulation of MircoRNA-370 induces proliferation in human prostate cancer cells by downregulating the transcription factor FOXO1. *PloS one* **7:** e45825

Xu P, Vernooy SY, Guo M, Hay BA (2003) The Drosophila microRNA Mir-14 suppresses cell death and is required for normal fat metabolism. *Current biology : CB* **13:** 790-795

Yagi T, Ito D, Okada Y, Akamatsu W, Nihei Y, Yoshizaki T, Yamanaka S, Okano H, Suzuki N (2011) Modeling familial Alzheimer's disease with induced pluripotent stem cells. *Human molecular genetics* **20:** 4530-4539

Yi R, Qin Y, Macara IG, Cullen BR (2003) Exportin-5 mediates the nuclear export of pre-microRNAs and short hairpin RNAs. *Genes & development* **17:** 3011-3016

Yu L, Zhou L, Cheng Y, Sun L, Fan J, Liang J, Guo M, Liu N, Zhu L (2014) MicroRNA-543 acts as an oncogene by targeting PAQR3 in hepatocellular carcinoma. *American journal of cancer research* **4:** 897-906

Yu YC, Kuo CL, Cheng WL, Liu CS, Hsieh M (2009) Decreased antioxidant enzyme activity and increased mitochondrial DNA damage in cellular models of Machado-Joseph disease. *J Neurosci Res* **87:** 1884-1891

Zamore PD, Tuschl T, Sharp PA, Bartel DP (2000) RNAi: double-stranded RNA directs the ATP-dependent cleavage of mRNA at 21 to 23 nucleotide intervals. *Cell* **101:** 25-33

Zijlstra MP, Rujano MA, Van Waarde MA, Vis E, Brunt ER, Kampinga HH (2010) Levels of DNAJB family members (HSP40) correlate with disease onset in patients with spinocerebellar ataxia type 3. *The European journal of neuroscience* **32:** 760-770

Zoghbi HY, Orr HT (2000) Glutamine repeats and neurodegeneration. *Annual review of neuroscience* **23:** 217-247

Zongaro S, Hukema R, D'Antoni S, Davidovic L, Barbry P, Catania MV, Willemsen R, Mari B, Bardoni B (2013) The 3' UTR of FMR1 mRNA is a target of miR-101, miR-129-5p and miR-221: implications for the molecular pathology of FXTAS at the synapse. *Human molecular genetics* **22:** 1971-1982